Abstract

Title of document: EFFECT OF NOBLE METAL NANOPARTICLES ON ENDOGENOUS AND DIETARY ANTIOXIDANTS AND THEIR COMBINED INTERACTION WITH REACTIVE OXYGEN SPECIES

Yuting Zhou, Doctor of Philosophy, 2013

Directed By: Y. Martin Lo, Ph.D., Department of Nutrition and Food Science, University of Maryland, College Park

In the last decade, nanotechnology has been extensively exploited in a variety of areas because nanoscaled materials provide a wide range of benefits that bulk materials do not possess. In spite of its advent, when applied to consumer related products, the new technology inevitably brings about side effect especially to biological or environment systems. Many have already determined that the damaging effect of nanomaterials in cell lines is caused by oxidative stress as a result of overproduction of reactive oxygen species (ROS). The present study aims at evaluating the role of noble metal nanomaterials in the generation and scavenging of ROS. It is noteworthy that the behavior of silver nanoparticles (Ag NPs) in the presence of hydrogen peroxide, a continuously generated component in biological systems, is adjusted by the mimetic microenvironment. These Ag NPs were found to be capable of inducing production of ROS hydroxyl radicals and oxygen in acidic and alkaline environments, respectively. The Ag NPs were oxidized to ions at pH 4.6 while they have been found to participate in Ag^0-Ag^1-Ag^0 cyclic reaction at pH 11. As a promising antimicrobial agent, Ag NPs alone barely scavenge free radicals, but they are found to moderate the scavenging capability of thiol-based antioxidants, essential endogenous antioxidants, due to their formation of Ag-S bond. In addition, Platinum nanoparticles (Pt NPs) have been mostly used as catalysts in many chemical reactions. While recent reports suggest antioxidant activity of Pt

NPs due to their peroxidase-like activity, there are limitations in the use of Pt NPs as an antioxidant in scavenging hydroxyl radicals. Alternatively, owing to their ascorbate oxidase-like activity, Pt NPs reduce the antioxidant ability of ascorbic acid, an important antioxidant participating in many biological reactions. In addition, they exert tyrosinase-like activity in catalyzing the oxidation of (-)-Epicatechin, caffeic acid, and resveratrol to form pigment compounds. Therefore, Pt NPs vary in their effect on the antioxidant activity of phenolics against various radicals (DPPH radicals > hydroxyl radicals >superoxide radicals). Our study may provide insights for finding new applications for noble metal nanoparticles and for risk assessment.

EFFECT OF NOBLE METAL NANOPARTICLES ON ENDOGENOUS AND DIETARY ANTIOXIDANTS AND THEIR COMBINED INTERACTION WITH REACTIVE OXYGEN SPECIES

By

Yuting Zhou

Dissertation submitted to the Faculty of the Graduate School of the

University of Maryland, College Park, in partial fulfillment

of the requirements for the degree of

Doctor of Philosophy

2013

Advisory Committee:
Dr. Y. Martin Lo, Chair
Dr. Thomas W. Castonguay
Dr. Wen-Hsing Cheng
Dr. William J. Kenworthy
Dr. Jun-Jie Yin

Acknowledgements

My great appreciation is sent to Dr. Y. Martin Lo, who admitted me to Food Science program in 2010, so that I can have the opportunity to experience such an unforgettable and wonderful Ph.D. life at University of Maryland. He is always thoughtful and caring for students, brilliant in research and teaching, and dedicated to his extension work. I would like to express my heartfelt gratefulness to Dr. Lo for his continual support and guidance throughout my graduate career. I am also very thankful for the research guidance on my entire nano research project provided by Dr. Jun-Jie Yin at CFSAN, FDA. His dedication to research has made him an excellent role model for me. I really appreciate great help from our visiting scientist Dr. Weiwei He to move my project forward. I would also like to thank Dr. Wayne Warmer for his helpful discussion in research and advice in scientific writing. In addition, I am thankful to Dr. John Callahan who has provided everything to support me working at CFSAN. Many thanks are given to my dissertation committee members Dr. Thomas Castonguay, Dr. Wen-Hsing Cheng, and Dr. William J. Kenworthy for their advice and direction. I also appreciate the assistance of Dr. Wen-An Chiou and Dr. Pan-Ju Shang from NISP laboratory at Maryland Nanocenter in Nanoscale imaging.

I want to thank all my labmates for being patient with me and being always encouraging to me: Melody Ge, Dr. Pavan Kumar Soma, Dr. Patrick Williams, Elizabeth Beck, Meng Li, Tong Liu, Maho Zeno, Maryam Ganjavi, Armin Norouzi, Setareh Shiroodi, Ana Aguado, Michael Wiederobder, Dr. Eirene Yossa. I want to especially thank my parents for their patience, encouragement, and support during my Ph.D career and for their unconditional love that they have given to my entire life.

My work was partially supported by a regulatory science grant under the FDA Nanotechnology CORES Program and by the Office of Cosmetics and Colors, CFSAN/FDA.

Table of Contents

List of Tables

List of Figures

(d), 0.05 (e), and 0.1 (f) mg/mL. (B) Dependence of ·OH generation on the concentration of Ag NPs as indicated in A. (C) Effect of H_2O_2 on the generation of ·OH from samples containing 50 mM DMPO, 0.1 mg/mL 75 nm citrate coated Ag NPs, 10 mM HAc/NaAc buffer (pH 3.6), and H_2O_2 at different concentrations; inset shows the spectra obtained from samples without H_2O_2 (upper) and with 0.5 mM H_2O_2 (lower). (D) Effect of Ag^+ on the generation of hydroxyl radicals induced by Ag NPs. Solutions included 10 mM HAc/NaAc buffer (pH 3.6), 50 mM DMPO, 0.5 mM H_2O_2, and a), none; b), 5 mM Ag^+; c), 0.1 mg/mL 75 nm citrate coated Ag NPs; d), 5 mM Ag^+ and 0.1 mg/mL 75 nm citrate coated Ag NPs. All the spectra were obtained 6 min after mixing.

Figure 3-6(A) ESR spectra of hydroxyl radicals generated in absence and presence of Ag nanoparticles with different pH buffer solutions containing 0.1 mg/mL 75 nm Ag NPs, 10 mM buffer, 50 mM DMPO, and 0.5 mM H_2O_2. (B) ESR signal intensity vs buffer pH from (A). Samples contained 50 mM DMPO, 0.5 mM H_2O_2; all of the spectra were obtained after 6 min of incubation.

Figure 3-7 Generation of hydroxyl radicals in artificial perspiration and cosmetic emulsion induced by Ag NPs (0.1 mg/mL 75 nm citrate coated Ag NPs). Samples contained 50 mM DMPO, 0.5 mM H_2O_2, 5% artificial perspiration (pH 4.5) or cosmetic emulsion. All of the spectra were obtained at 6 min of incubation.

Figure 3-8 (Left) ESR spectra of hydroxyl radicals spin adducts generated in absence (a) and presence of Ag nanoparticles with different sizes of 10 nm (b), 30 nm (c), 50 nm (d), 75 nm (e) and 100 nm (f). (Right) ESR signal intensity vs Ag nanoparticles size. Sample solutions contained 10 mM HAc/NaAc buffer (pH 3.6), 0.1 mg/mL citrate coated Ag NPs of different sizes, 50 mM DMPO, and 0.5 mM H_2O_2. Spectra were recorded 6 min after sample mixing.

Figure 3-9 Evolution of UV-VIS spectra for 0.01 mg/ml citrate coated Ag NPs having different sizes: 10 nm (A), 30 nm (B) and 75 nm (C) in the presence of 0.5 mM hydrogen peroxide at pH 3.6. (D) Corresponding relative absorbance variation (A_0-A_t, where A_0 is initial absorbance, A_t represents the absorbance at reaction time t) was dependent on Ag NPs size over time. The absorbance was measured at the SPR peak maximum wavelength.

Figure 3-10 Generation of O_2 induced by Ag NPs in different circumstances. (A) Photographs of sample solutions containing 0.1 mM CTPO, and (a) 10 mM buffer (pH 11.0) and 10 mM H_2O_2, and 0.2 mg/mL citrate coated 10 nm Ag NPs. (B) ESR spectra of 0.1 mM CTPO in 10 mM buffers of different pHs in presence of 25 mM H_2O_2 and 0.2 mg/mL 75 nm citrate coated Ag NPs. (C) pH dependence of oxygen generation obtained from data depicted in (B). Sample solutions were purged with nitrogen for 15 min prior to mixing.

Figure 3-11 Generation of O_2 induced by Ag NPs having different sizes. (A) ESR spectra of CTPO in presence of H_2O_2 and Ag NPs having different sizes at pH 11.0. (B) Dependence of oxygen generation on Ag NPs size at pH 11.0 and 7.4. Conditions: 0.1 mg/mL CTPO + 5 mM H_2O_2+10 mM pH 11.0 (or 7.4) buffer + 0.025 mg/mL citrate coated Ag NPs at pH 11.0 (0.05 mg/mL citrate coated Ag NPs at pH 7.4). ESR spectra were recorded at 0.5 min and all sample solutions were purged with nitrogen for 15 min prior to mixing.

Figure 5-3 (A) Ascorbyl radical production is dependent on the concentration of Au@Pt nanorods and Pt NPs. Samples contained 5 mM AA and Au@Pt nanorods or Pt NPs at variable concentrations in 50 mM PBS (pH 7.4).The inset shows the ESR spectrum of the ascorbyl radical. The ESR signal intensity was measured as the peak-to-peak value of the first line of the spectrum. (B) Oxygen consumption during the oxidation of ascorbic acid catalyzed by Pt NPs. Samples contained 5 mM AA, 0.14mM CTPO, 0.05 mM Pt NPs, and 50 mM PBS buffer (pH 7.4). The Inset shows the ESR spectrum change of CTPO. (C) UV-Vis spectra evolution of 0.1 mM AA in presence of 5 μM Pt NPs in 50 mM PBS buffer (pH 7.4) during 30 min. Arrow shows decrease in absorbance. The concentration of nanoparticles refers to atomic concentration.

Figure 5-4 Thermal stability of AAO and Au@Pt nanorods. 0.9 nM AAO and 0.5 nM Au@Pt nanorods were preincubated at 23, 40, or 70 ^{o}C for 0, 3, and 6 hrs prior to oxidation reaction of 5 mM AA in 50 mM PBS (pH 7.4). Inset represents ESR spectrum of ascorbyl radical. The signal intensity was measured as the peak-to-peak value of the first line of the spectrum. ESR spectra were collected at 1 min after sample mixing.

Figure 5-5 Evolution of ESR spectrum of the spin label CTPO during the oxidation of AA catalyzed by Au@Pt nanorods. Sample solutions contained 0.1 mM CTPO, 5 mM AA, 50 mM PBS (pH 7.4), in the absence (control) and in the presence of 0.5 nM Au@Pt nanorods. ESR spectra were obtained at 0.5, 1.5, and 3 min after addition of Au@Pt nanorods.

Figure 5-6 Ability of AAO and Au@Pt nanorods in catalyzing AA oxidation determined by initial O_2 consumption over a wide pH range. Sample solutions included 0.1 mM CTPO, 5 mM AA, and 50 mM buffers at different pHs.

Figure 5-7 Effect of Au@Pt nanorods on hydroxyl radicals generated through the Fenton reaction. Reaction mixtures contained 10 mM PBS buffer (pH 7.4), 10mM DEPMPO, 1 mM H_2O_2, 0.2 mM Au@Pt nanorods or 1 mM AA, and 0.5 mM Fe^{2+} (this order was followed in preparing the control (a), AA added to the control sample (b), and Au@Pt added to the control sample (c-f)). For time premixing, the Au@Pt nanorods were first mixed with A (d-f) H_2O_2 or B (d-f) Fe^{2+} for 1, 5, and 10 min and then Fe^{2+} (panel A) or H_2O_2 (panel B) was added before adding the spin trap. ESR conditions: power 20 mW, field modulation 1G, scan width 100 G. Pt nanodots concentration was used for Au@Pt nanorods.

Figure 5-8 The effect of Au@Pt nanorods on hydroxyl radical levels and their combined effect with ascorbic acid to scavenge hydroxyl radicals generated during irradiation of metal oxides. (A) Sample solutions containing 0.1 mg/ml P25 (TiO_2) and 50 mM DMPO were exposed to UV radiation (340nm). Samples in A and B contained Au@Pt nanorods, AA, or their combination. ESR spectra were collected at 1 min after UV light was turned on. Pt nanodots concentration was used for Au@Pt nanorods.

Figure 5-9 Effects of Au@Pt nanorods on the antioxidant ability of ascorbic acid. Control sample in (A) contained 0.1 mM DPPH•, 10% (v/v) ethanol, and 10 mM PBS buffer (pH 7.4); samples containing AA, Au@Pt nanorods, or a mixture of these were kept at room temperature for 24 hr. Control sample in (B) was a Fenton reaction system consisting of 50 mM DMPO, 10 mM PBS buffer (pH 7.4), 0.1 mM Fe^{2+}, and 1 mM H_2O_2; AA, Au@Pt nanorods, or a mixture of these were kept at room temperature for 48 hr. Control sample in (C) included 25 mM BMPO, 10 mM PBS buffer (pH 7.4), 1 mM xanthine, and 0.2 U/ml

Chapter 1: Introduction

1.1 Introduction

According to National Nanotechnology Initiative, there already exist over 800 everyday commercial products that rely on nanoscale materials and processes (*1*). Those products are among all categories related to human life: nanoscale additives in polymer composite materials for badminton rackets and luggage or surface treatments of fabric; nanoscale thin film on eyeglasses and electronics displays; nanoscale materials in cosmetic products to provide antioxidant property or greater clarity or coverage, nano-engineered materials in food industry including nanocomposites in food containers and nanosensors; nano-engineered materials in automotive products; nano-engineered materials that make superior household products; nanoparticles are used increasingly in catalysis to boost chemical reactions. Applications of nanomaterials in medical and health have real potential to revolutionize a wide array of medical and biotechnology tools and procedures. Nanotechnology has been used in early diagnosis of atherosclerosis that is the build-up of plaque in arteries, Alzheimer's disease, and rare molecular signals associated with malignancy. Also, nanoparticles serve as a vehicle in multifunctional therapeutics to facilitate its specific targeting to cancer cells and delivery of a potent treatment. Many studies are ongoing such as usage of nanotechnology to spur the growth of nerve cells.

With the advent of nanotechnology, one should consider the potential consequences to human health and the environment associated with the new technology. The first strategy for Nanotechnology-related environmental, health, and safety (EHS) research was published in 2008 and updated in 2011 (*2*). The strategy provides guidance to Federal agencies as they develop their agency-specific nanotechnology EHS research so as to

protect public health and the environment at the same time supporting the beneficial use of nanotechnology. The impact of nanomaterials on biological systems is a major aspect in addressing the health concerns of nanotechnology. Noble metal nanomaterials are of great interest in therapeutic and biomedical devices. Therefore, the potential side effects of those nanoscaled noble metals on biological systems are of tremendous significance and the underlying mechanism study is critical in order to advance future research.

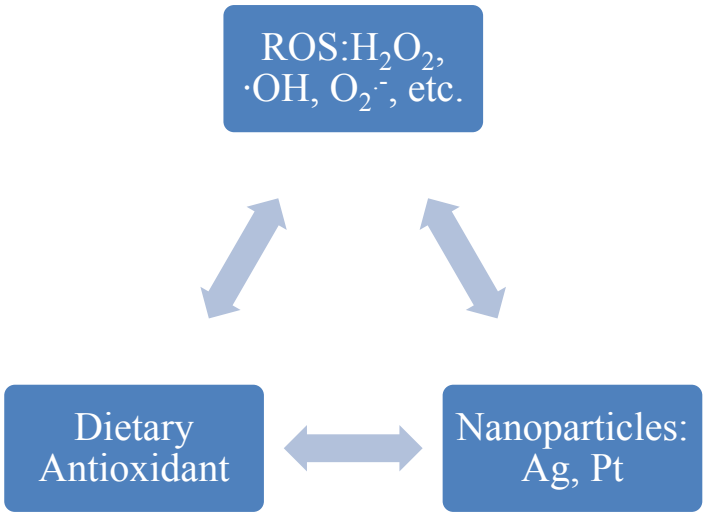

Scheme 1-1 Schematic illustration of present study.

1.2 Research objectives

The ultimate goal of the proposed research is to study the effect of noble metal nanomaterials in biologically relevant conditions due to their increasing application in consumer-related products. Reactive oxygen species (ROS) are the main cause of cell damage or apoptosis and in turn various diseases and aging. In addition to their intrinsic properties the behavior of noble metal nanoparticles is influenced by many factors in a biological system, such as environment conditions and other related chemicals. In the current study, silver and platinum nanomaterials are selected to investigate their potential effect from the aspect of ROS via their interaction with biological relevant reagents,

including hydrogen peroxide, endogenous and dietary antioxidants. In order to achieve this goal, there were four specific objectives, where the subsequent chapters following the literature review are presented as separate manuscripts:

Objective #1: Examine the behavior of silver nanoparticles under conditions mimicking different biological microenvironments.

Objective #2: Study the influence of silver nanomaterials on thiol-based antioxidants with respect to various free radicals.

Objective #3: Investigate the enzyme-mimetic effects of gold@platinum nanorods on the antioxidant activity of ascorbic acid.

Objective #4: Investigate the enzyme-mimetic effects of gold@platinum nanorods on the antioxidant activity of phenolics.

Chapter 2: Literature review

2.1 Reactive Oxygen Species

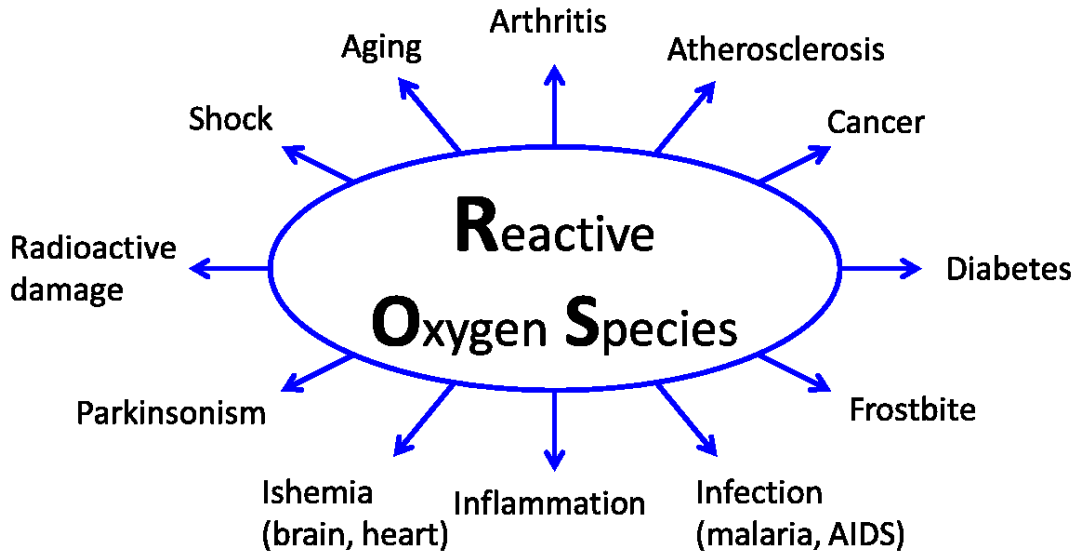

Figure 2-1 Diseases and damages caused by reactive oxygen species (ROS).

Reactive oxygen species are a group of molecules that are by-products of cellular oxidative metabolism, which mainly occurs in mitochondria of cells (*3, 4*). They have been of great interest to researchers for a long time because they have been considered to be associated with many diseases (Figure 2-1). They include hydroxyl radical (·OH), superoxide radical ($O_2^{\cdot-}$), hydrogen peroxide (H_2O_2), peroxyl radical (·OOR), and singlet oxygen ($^1O_2$). Molecular O_2 proceeds univalent reduction to form superoxide radical mediated by NADPH oxidase and xanthine oxidase or other redox-reactive compounds of the mitochondrial electron transport chain (*5*). Superoxide radical may be converted to hydrogen peroxide by superoxide oxidase (*6*) or to singlet oxygen non-enzymatically (*7*). Otherwise, hydrogen peroxide may be converted to water by catalase or glutathione peroxidase. Glutathione (GSH) is oxidized to glutathione disulfide (GSSG), which can be converted back to GSH by glutathione reductase in an NADPH-consuming process (*8*). The hydroxyl radical possesses the highest one-electron reduction potential among all the

physiologically relevant ROS and it is extremely reactive with almost every type of biomolecule (*9, 10*). In the presence of transition metal ions, such as iron, copper, and chromium, superoxide radical and hydrogen peroxide may be converted to hydroxyl radical, which could initiate a radical chain reaction leading to extensive lipid and organic peroxide formation. The presence of hydroxyl radical in vivo has been demonstrated to directly attack proteins and nucleic acids (*11, 12*). Hydroxyl radical is not only highly reactive but also cannot be detoxified by known enzymatic reaction. As a result, hydroxyl radical may serve as an excellent target to investigate the potential of antioxidants to react or quench free radicals and protect important biomolecules from radical-mediated damage.

ROS can have contrasting effects on living systems, being either beneficial or deleterious. At low to moderate concentrations, ROS plays beneficial physiological roles in cellular signaling systems (*13*) and induction of mitogenic response (*14*). The involvement of these free radicals in stimulating signal transduction has been shown to induce several biological processes, including cell growth, apoptosis, and cell adhesion (*15*).

The deleterious effects of the by-products of oxygen metabolism were first inferred by Gerschman's free radical theory of oxygen toxicity that identified the partially reduced form of oxygen was responsible for its toxicity (*16*). A couple of years later, Harman put forward his famous theory that free radical was associated with the process of aging (*17*). The free radical theory of aging reveals that oxygen-centered radicals produced in vivo during aerobic respiration cause cumulative oxidative damage to cellular systems, which leads to aging and death (*17, 18*). The role of ROS in human pathology has since been of great interest in the area of health promotion and disease prevention because ROS has been recognized as mediators of tissue injury and disease (*19*). Over-production of ROS, termed

as oxidative stress, has been associated with damage in biological system, resulting in aging and degenerative diseases (*5, 20-22*). The damage in vivo is related to numerous degenerative conditions of major public health concerns, including cardiovascular disease (*23*), inflammation (*24*), Alzheimer's disease (*25*), Parkinson's disease (*26*), diabetes (*27*), and carcinogenesis (*28*). The mechanisms underlying the involvement of ROS and oxidative stress in disease development may include oxidation of proteins (*20, 29*) and lipids (*30*), DNA strand breaks and modification to nucleic acids (*11*), modulation of gene expression through activation of redox-sensitive transcription factors (*31*), and modulation of inflammatory responses through signal transduction (*24*).

Exposure of animals or cell cultures to various conditions of oxidative stress results in an increase in the levels of protein carbonyls. The accumulation of oxidized protein has been associated with many diseases and aging (*20*). Also, the unsaturated fatty acids in cell membranes and other cellular constituents are especially susceptible to excessive ROS. The oxidation product of these fatty acids, peroxyl radical, is eventually formed to malondialdehyde (MDA), which is believed to damage DNA (*32*). MDA reacts with DNA to form adducts that are mutagenic in bacterial and mammalian cells and carcinogenic in rats (*33, 34*). In addition, hydroxyl radical could react and in turn damage both purine and pyrimidine bases, as well as the deoxyribose backbone of DNA, resulting in mutagenesis, carcinogenesis, and aging (*9*).

2.2 Antioxidants

2.2.1 Inherent defense system against ROS

The strict regulation of ROS levels is essential to the survival of all aerobic organisms. Cells, tissues, organs, and organisms inherently utilize multiple layers of antioxidant

defenses and damage removal, and replacement or repair systems in order to manage the remaining stress and damage caused by oxygen (*35*). Cellular enzymes are a group of protectors to cope with the situation caused by detrimental biological oxidants. Superoxide dismutase (SOD), peroxidase, and catalase are extensively studied antioxidative enzymes. For example, SOD catalyzes the dismutation of superoxide to hydrogen peroxide, which in turn decomposes to water via catalase.

In human cells, the most important H_2O_2-removing enzyme is glutathione peroxidase, which catalyzed the oxidation of reduced glutathione (GSH) to oxidized glutathione (GSSG). Glutathione reductase regenerates GSH from GSSH with NADPH as a source of reducing power (*4*). The redox reactions occur through the reversible oxidation of its active thiol group from its cysteinyl moiety. That is the reason why GSH is very important in maintaining cellular redox status and the depletion of GSH is considered a marker of oxidative stress (*36*). GSH has an intracellular concentration between 0.5 and 10 mM, accounting for 99% of glutathione in unstressed cells (*37*). In addition, GSH is required for the maintenance of the thiol redox status of the cell, protection against oxidative damage, detoxification of endogenous and exogenous reactive species, storage and transport of cysteine, protein and DNA synthesis, cell cycle regulation, and cell differentiation (*38*). Glutathione also aids in the storage and transfer of cysteine. With the ability of thiols to undergo redox reactions, cysteine exhibits antioxidant properties by hydrogen donation and forms cystine, which produces toxic oxygen radicals. To avoid this, most of nonprotein cysteine is stored in glutathione (*39*).

In addition, glutathione is an excellent scavenger of lipid peroxidation products that have been found to bind proteins inhibiting their activities (*40, 41*). Glutathione also reacts with

saturated reactive carbon atoms, unsaturated carbon atoms, and aromatic carbon atoms to detoxify the nucleophilic attack from the electrophilic carbon on these compounds (*42*). Moreover, glutathione forms metal complexes via nonezymatic reactions to terminate Fenton or Fenton-like reactions (*37, 38, 42*).

In healthy individuals, oxidants and radicals are generally neutralized by antioxidant enzymes. However, with age and for individuals with certain ailments, the endogenous antioxidants may require exogenous assistance from dietary antioxidants in order to maintain the integrity of cell membranes.

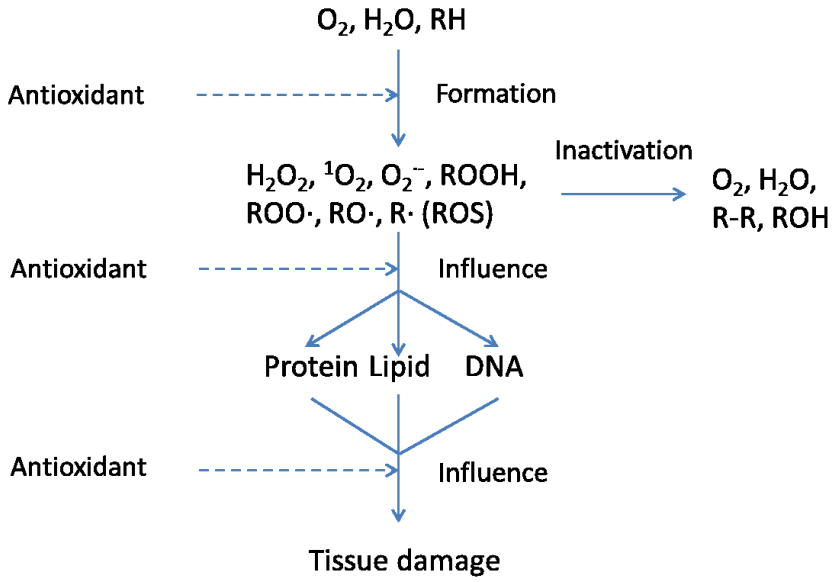

Figure 2-2 Consequences of reactive oxygen species in diseases and the preventive role of antioxidants.

2.2.2 Dietary antioxidants

Food-grade antioxidants have been used in food manufacturing to prevent food products from deterioration. Moreover, antioxidants have been of interest to health professionals because they help the body to protect itself against damage caused by ROS associated with degenerative disease (*43*), when the endogenous ROS defense system is not sufficient.

Therefore, more and more natural or synthesized antioxidants are used in food products, dietary supplements, and skin care products to relieve the oxidative stress.

Antioxidants are essentially reducing agents and they participate in redox reactions by donating electrons or hydrogen atoms. There are some biologically important antioxidants but they can only be derived from diet. For example, Vitamin C (ascorbic acid or ascorbate) can neutralize free radicals by donating a hydrogen atom, forming ascorbyl radical, which readily reacts with NADH or NADPH-dependent reductases to regenerate ascorbate (*44*). The path way of Vitamin C as an antioxidant is similar to that of GSH aforementioned. Other dietary antioxidants of biological significance include Vitamin E (tocopherol), Vitamin A (carotenoids), green tea polyphenols (epicatechin, epicathechin-3-gallate, epigallocatechin, epigallocatechin-3-gallate), isoflavones (genistein, daidzein), caffeic acid, and resveratrol. (*45*).

Alternatively, other antioxidants may reduce free radical formation by inducing the production and release of antioxidant enzymes like SOD or catalase (*46*), or by chelating redox-active metal ions (Cu^{+}, Fe^{2+}) and making them unavailable to participate in Fenton-type reactions that generate free radicals (*22*).

2.2.2.1 Ascorbic acid

Ascorbic acid was discovered by James Lind in 1753 as an essential nutrient in humans by its capability of preventing scurvy in individuals deficient in ascorbic acid. This is due to its function in hydroxylation reactions of procollagen (*47*) and its regulation of collagen synthesis independent of hydroxylation (*48*). Besides its key function in connective tissue protein post-translational hydroxylation and carnitine synthesis (*49, 50*), ascorbic acid has been shown to facilitate iron absorption (*51*), inhibit mutagenesis and carcinogenesis (*52*-

54), and strengthen immune system (*55, 56*). Ascorbic acid also appears to be effective in inhibition of LDL oxidation and inhibition of leukocyte adhesion to the endothelium and vascular endothelial dysfunction, which are the possible mechanisms of atherosclerosis (*57*). Moreover, ascorbic acid plays a role in prevention and treatment of cancer (*58, 59*), regulation of aging and inhibition of aging-related pathologies (*60, 61*), cardiovascular disease prevention and hypertension treatment (*62-64*), and lowering of side-effect toxicity of cancer treatment (*65, 66*).

When encountered with free radicals, ascorbic acid is oxidized to ascorbate radical. It serves as a good antioxidant because the reduction potential of ascorbate radical/ascorbate thermodynamic couple is lower than that of hydroxyl radical, superoxide radical, glutathione radical, α-tocopherol radical, and alkyl peroxyl radical (*67*). As a versatile scavenger, ascorbate has also been evidenced by its high reactivity with free radical in body fluids (*68*). However, ascorbic acid oxidation has been demonstrated to exhibit crossover effect depending on its level due to a metal-catalyzed oxidation under a variety of conditions. Ascorbic acid barely chelates metal ions but it participates in the redox cycling of iron at a low concentration, resulting in generation of radical species (*10, 69*).

In addition to its individual antioxidant effect, ascorbic acid functions in a collaboration with other compounds. Vitamin C in living organisms could regenerate primary lipid antioxidant vitamin E by reducing the tocopherol radical that is produced when vitamin E scavenges a peroxyl radical (*70, 71*). One potential mechanism for the damage of gastrointestinal (GI) tract caused by aspirin has been associated with oxygen radical-dependent microvascular injury. But vitamin C has been reported to moderate the adverse effect resulted from aspirin (*72*).

2.2.2.2 Phenolics

Phenolics are a group of substances possessing an aromatic ring bearing one or more hydroxyl groups, including their functional derivatives. They generally originate from plants and are essential for their growth and reproduction. Phenolics can also act as antifeedants and antipathogens (*73*). In addition, they contribute to the pigmentation of plant foods and serve as antibiotics, natural pesticides, and protective agents against UV light. Intake of phenolics at high levels could cause a decrease in food palatability and fiber and protein digestibility, growth rate or feed conversion (*74*), inhibition of enzymes (*75*), and lower egg production (*76*). However, food-grade antioxidants of a phenolic nature have been widely used by food manufacturers to prevent quality deterioration of products and to maintain their nutritional value (*77*). Phenolics serve as excellent antioxidants because they can terminate radical chain reactions and form relatively stable radical intermediates due to resonance delocalization and lack of suitable sites for attack by molecular oxygen (*78, 79*). However, polyphenol oxidase (PPO), also rich in plants, is a major concern to food processors and researchers for the sake of enzymatic oxidation of phenolics catalyzed by PPO, mainly tyrosinase (*80*). The reaction does not only result in degradation of antioxidant phenolics, but the oxidation product quinone also causes subsequent reaction with proteins and enzymes and in turn brings about formation of brown pigments and affects sensory properties (*81*).

The flavonols (-)-Epicatechin, (-)-Epicatechin gallate, (-)-Epigallocatechin, and (-)-Epigallocatechin gallate, mainly sourced from tea, possess antioxidant activity due to the *o*-dihydroxylation of the B-ring (Figure 2-2) (*82*). Therefore, green tea extract has been extensively studied in various diseases associated with ROS. Epidemiological and animal model studies have shown antiangiogenic (prevention of tumor blood vessel growth),

antimutagenic, antidiabetic, antibacterial, antiaging, and anti-inflammatory activity. They also showed a protection effect against cancer such as skin, breast, prostate, and lung cancer (*83*). Phenolic acids are another group of phenolics largely existing in plants but they are present mainly in their glycosides and esters. It has been demonstrated that two or three neighboring phenolic hydroxyl groups and a carbonyl group are the essential molecular features required to achieve a high level of antioxidant activity (*82*). Among them, caffeic acid and its derivatives are believed to be associated with prevention of heart disease (*84*), against cancer (*85*) and even against toxicity induced by chemotherapy and radiotherapy (*86*). Resveratrol is a trihydroxystilbene found in grape and berry skins (*87*). Since resveratrol has a hydrophobic part, it is involved in lipid oxidation and thus has shown inhibitory effect on low-density lipoproteins (LDL) oxidation (*88, 89*), which has been suggested to contribute to the beneficial effect on coronary heart disease of red wine (*90*). Resveratrol also prevents cell proliferation in tumor cell lines in vitro (*91*) and decreases tumor growth in a rat tumor model (*92*).

The most widely used method to determine total amount of phenolics is the Folin-Denis assay, in which phenolic compounds are able to reduce phosphomolybdic-phos-photungstic acid (Folis-Denis) reagent to a blue-colored complex in an alkaline solution (*93*). For identification of individual groups of phenolics, UV spectrophotometric assay is used because of their characteristic UV absorption bands (Table 2-1).

Table 2-1 UV Absorption Patterns of Various Phenolic Compounds. Adapted from Macheix et al (*94*).

Class of Compounds	UV Absorption, λ_{max}
Benzoic acids	270-280
Hydroxycinnamic acid	290-300[a]; 305-330
Anthocyanic pigments	270-280; 315-325[b]
Flavonols	250-270; 330[b]; 350-380
Flavan-3-ols	270-280
Coumarins	220-230; 310-350
Flavones	250-270; 330-350
Flavanones, Flavanonols	270-295; 300-330[a]
Chalcones	220-270; 300-320; 340-390
Aurones	240-270
Isoflavones	245-270; 300-350

Note: solvent is methanol, except for anthocyanin pigments in which methanol containing HCl 0.01% is used.
[a] Shoulder.
[b] In the case of acylation by hydroxycinnamic acids

2.2.2.3 Alpha-lipoic acid (ALA)

Alpha-lipoic acid (ALA) has an oxidized form (disulfide) and a reduced form (dihydrolipoic acid, DHLA), both of which show antioxidant properties. DHLA is the predominant form that quenches ROS, but the oxidized form of ALA can also inactivate free radicals (*95*). ALA is an endogenous source of thiols found in mitochondria, acting as the coenzyme for pyruvate dehydrogenase and α–ketoglutarate dehydrogenase (*96*), but

only a small amount is synthesized in the human body. Therefore, dietary administration of ALA is necessary (*97*).

ALA exhibits preventive or ameliorative effects in both Type I and Type II diabetes A (*96*). Clinic studies have also showed that ALA is a good candidate as an antioxidant agent in neurodegenerative diseases (*98-100*), which are partially caused by byproducts, free radicals, from mitochondria. DHLA prevents ischemia-reperfusion induced changes in fluidity and polarity of rat heart mitochondria (*101-103*). ALA, rather than DHLA, protected against radiation injury to hematopoietic tissues in mice (*104*).

The ALA/DHLA is a redox couple that ALA from diet is converted to DHLA in many tissues (*105, 106*). One or both of them effectively quench various free radicals in lipid and aqueous phases (*96*). ALA has been generally identified as an antioxidant due to its scavenging ability of hydroxyl radicals (*107, 108*), hypochlorous acid (*108, 109*), and singlet oxygen (*110, 111*), and its chelating effect on transition metals (*112*). ALA also causes an increase in intracellular glutathione (*113*). On the other side, DHLA scavenges hypochlorous acid (*108, 109*), and peroxyl radicals (*114*) and probably scavenges hydroxyl radicals (*107*). DHLA acts synergistically with other antioxidants because it regenerates other antioxidants from their radical or inactive forms (*115, 116*). However, DHLA may also serve as a pro-oxidant due to its reducing power on transition metals (*117, 118*).

2.3 Nanomaterials

2.3.1 Introduction

The concept of nanoscience and technology has been put forward in the middle 20th century, and since then the discipline has developed at a fast pace. As a matter of fact, nanoscience and technology is an interdisciplinary and significant technical revolution in

the modern world. Nano is a unit of length that 1 nm = 10^{-9} m. As a comparison, a human hair is around 100,000 nm. Nanomaterials are defined as an object that has at least one of three dimensions between 1-100 nm. They are different from either bulk materials or atoms and molecules. Several atoms or molecules are put together in well-defined ways to form an object in nanometer scale with novel and characteristic properties, which are different from bulk materials and individual atoms or molecules.

Back to Greco-Roman times, ancient Egyptian used PbS nanocrystal based formula to dye hairs (*119*). However, people did not realize the existence of the nanomaterials until Dr. Richard Feynman's speech "There is plenty of room at the bottom" at the annual meeting of the American Physical Society at the California Institute of Technology on December 29, 1959. He put forward "Why cannot we write the entire 24 volumes of the *Encyclopedia Britannica* on the head of a pin?" and "What would happen if we could arrange the atoms one by one the way we want them?" (*120*). The speech by this Nobel Prize winner has inspired scientists all over the world. In 1999, a direct-write nanolithography has been developed that is writing alkanethiols with 30 nm linewidth resolution on a gold thin film (*121*). In the early 1980's the scanning tunneling microscope was invented at IBM-Zurich by Drs. Gerd Bining and Heinrich Rohrer in Switzerland. This is the first instrument that was able to "see" atoms. A few years later, the Atomic Force Microscope was invented, expanding the capabilities and types of materials that could be investigated. Since then, research and development has resulted in tremendous advances in nanoscience and technology.

Why materials in bulk could behave completely different than those at nanoscale? There are two basic size-dependent effects of materials: smoothly scalable effects that are related

to the fraction of atoms at the surface and quantum effects that show discontinuous behavior due to completion of shells in systems with delocalized electrons (*122*). Owing to the characteristic properties of nanomaterials, nanotechnology has been studied cross-disciplinarity, including physics, chemistry, material science, biomedicine, electronics, biology, and processing. When faced with strategic problems, such as spread of disease, environmental pollution, and energy deficiency, people give much expectation to nanotechnology.

2.3.2 Application

Nanomaterials have been involved with more than 500 consumer products and it is estimated that the value of products with nanotechnology applications is $1 trillion on the world market (*123*). A variety of nanomaterials have been synthesized and applied depending on their end use, some of which are designed for direct use while some have been developed as delivery systems. Currently, the United States Environmental Protection Agency is assessing types of nanomaterials that are widely used in products or have been recognized for their potential to be used, including carbon nanotubes, nano silver, micronized copper, cerium oxide, titanium dioxide, and iron in nano-scale (*123*). Herein, we are introducing some nanomaterials of great importance in consumer products.

2.3.2.1 Carbon nanotubes

Carbon nanotubes (CNTs) are long cylinders of covalently bonded carbon atoms. There are two basic types of CNTs: single-wall carbon nanotubes (SWCNTs) that are in fundamental cylindrical structure and multi-wall carbon nanotubes (MWCNTs) that are made of coaxial cylinders (Figure 2-3) (*124*). Due to their remarkable mechanical properties (*125*), CNTs have also been utilized as promising nanofiller for polymer composites through being added to enhance polymer performance. In addition, the

extraordinary electrical properties of CNTs (*126*) make them a good candidate in the application of biosensors (*127, 128*).

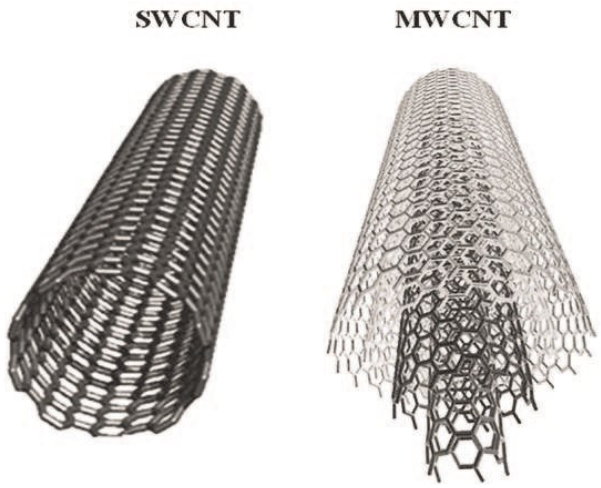

Figure 2-3 Schematic diagrams of single-wall carbon nanotube (SWCNT) and multi-wall carbon nanotube (MWCNT). Adapted from Choudhary and Gupta's work (*124*).

2.3.2.2 Metal oxide

Both zinc oxide (ZnO) and titanium dioxide (TiO_2) nanoparticles have been studied in sunscreen applications because they could attenuate ultraviolet light, a known carcinogen, by adsorption and scattering depending on their size (*129*). Nevertheless, exposure of these metal oxides also causes formation of free radicals, termed as phototoxicity, which may further results in cytotoxicity and genotoxicity (*130*). Therefore, the dermal penetration of those nanoparticles is an important issue related to the usage of ZnO and TiO_2 nanoparticles (*131*). Nanostructured TiO_2 has also been developed for dye-sensitized solar cells because it provides large surface area, which allows a larger amount of dye to be attached to the TiO_2 surface (*132, 133*). Moreover, TiO_2 nanoparticles have demonstrated antibacterial activity (*134*) and they could potentially decrease pasteurization temperature for orange juice when incorporated in food packaging (*135*). Private industry has developed an approach to decrease the amount of particulate matter in air using cerium oxide (CeO_2)

nanoparticles (*136*). Likewise, CeO_2 nanoparticles find their usage in treatment of medical disorders caused by ROS on account of their radical scavenging effect (*137*). However, some reported contrary observation that ROS generation was induced by CeO_2 nanoparticles (*138*). Xue et al later found out the oxidant/antioxidant property of CeO_2 nanoparticles was related to the presence of environmental anions (*139*).

2.3.2.3 Transition metal nanoparticles (Fe, Cu)

As an essential element present in food, copper exists in the form of ions or salts, exerting antimicrobial activity. The activity has also been extensively exploited in nanostructured copper generated in the form of element or oxide, which then were embedded in polyethylene (*140*), impregnated with cotton fabrics (*141*), or immobilized on chitosan (*142*). CuO nanoparticles were demonstrated to control oral biofilm due to their activity against a range of bacterial pathogens (*143*). Iron nanoparticles are a group of nanomaterials providing opportunities in biology and biomedicine because of the superparamagnetism and its response to a magnetic field (*144*). Since iron nanoparticles could be easily manipulated through external magnetic force, they have been explored as a perfect application in magnetic separation. For example, ferrofluids have been utilized as a highly sensitive technique to select rare tumor cells (*145*). In addition, the magnetic moment of iron nanoparticles enhances the signal of nearby protons, which allows them to act as a Magnetic resonance imaging (MRI) contrast agent. Also, the size of iron oxide nanoparticles significantly affects the imaging result due to different tissues uptake (*146-148*). Furthermore, since Gilchrist et al realized that iron nanoparticles have potential to treat cancer via hyperthermia in that the nanoparticles generate heat when an external magnetic field is applied (*149*), many studies have been conducted to further investigate its feasibility (*150*).

2.3.2.4 Gold nanoparticles

Currently, the preciousness of noble metals extends their application in the form of nanoparticles or colloids in the context of emerging nanoscience and nanotechnology. As a matter of fact, noble metal nanoparticles have already existed in ancient products. For example, the Lycurgus Cup that was manufactured in the 5th to 4th century B.C. is ruby red in transmitted light and green in reflected light due to the presence of gold colloids (*151*), as shown in Figure 2-4. People at that time did not realize it was caused by the surface plasmon resonance (SPR) property of gold nanoparticles. The plasmon resonance can either radiate light (Mie scattering), a process that finds great utility in optical and imaging fields, or be rapidly converted to heat (absorption) (*152*). The SPR property of Au nanoparticles is strongly associated with their size, shape, and dielectric environment, thus Au NPs can be tuned according to practical need. Using UV-vis spectrophotometer, Au nanosphere 10 nm has a strong absorption around 520 nm, while the SPR red shifts to 530 nm for the nanospheres @ 40 nm. Due to the strongly enhanced SPR, Au NPs scatter light intensely at the SPR frequency, making them excellent candidates for optical imaging and labeling of biological systems (*153, 154*). Since the dielectric constant of the medium surrounding nanoparticles attributes to the surface plasmon oscillation frequency, the environment change could be sensed by monitoring SPR red-shift (*155, 156*). In addition, in contrast to the inert nature of bulk gold, Au NPs were found to exhibit an enhanced catalytic activity, especially for the low-temperature oxidation of CO (*157-159*).

Figure 2-4 Lycurgus Cup is now present in British museum. The Cup was captured in visible light (left) and flash without light coming through the glass (right). Adapted from http://en.wikipedia.org/wiki/Lycurgus_Cup.

2.3.2.5 Silver nanoparticles

Silver has been used for at least six millennia to prevent microbial infections and it was the most important antimicrobial agent before the introduction of antibiotics (*160*). In recent decades, the availability of silver nanomaterials enables silver to regain great interests due to their enhanced physicochemical and biological properties and activities compared to their bulk parent materials (*161*). Silver nanoparticles (Ag NPs) have been found to be antimicrobial in a broad spectrum, such as *Escherichia coli*, *Staphylococcus aureus*, *E. coli* K12, *Pseudomonas mendocina* KR1, MS2 *bacteriophage (162-165)*, as well as fungus pathogenic Candida species (*166*). Also, Ag NPs were confirmed to exert anti-HIV activity at an early stage of viral replication (*167*). Owing to their antimicrobial properties, Ag NPs have been used as anti-inflammatory dressing (*168-170*), anti-angiogenic (*171, 172*) and

antineoplastic (*173, 174*) agents as well as gynecology and reproductive medicine (*175, 176*) in surgery and wound therapy. Ag NPs have also been incorporated with other polymers to form antimicrobial packaging for food and other consumer products (*177, 178*). The antibacterial mechanism is still in discussion. Some believe it is the silver ions converted from Ag NPs that kill pathogens; while others think it is the direct contact of Ag NPs which causes the breakdown of bacterial membrane or other necessary proteins and their effect is dependent on their shapes with the same surface area.

2.3.2.6 Platinum nanoparticles

In contradiction of the inertness of platinum in bulk form, Pt nanomaterials showed extraordinary catalytic activity on oxidation of methanol (*179*) and hydrogenation of ethylene (*180*). Controlling the catalytic activity of Pt NPs could be achieved through changing their shape and facet (*181*). In biomedical field, Pt NPs have been applied in biosensor due to their peroxidase-like properties (*182-184*). Among all the Pt NPs, those in alloy structure could greatly enhance their catalysis performance. For example, during the catalysis of methanol oxidation, the catalytic ability of pure Pt NPs was reduced significantly due to their absorption of the reaction intermediate.. However, Pt alloyed with other metal elements obviously overcame the catalyst deactivation (*185-187*). Besides the catalytic activity, Pt NPs have been reported as antioxidants to scavenge ROS (*188, 189*) and in turn reduce oxidative stress on cells (*190*). In clinical study, Platinum nanomaterials have been utilized as anticancer drugs after modification with recognition molecules (*191*).

2.4 Concerns

The possible effects on human health and ecosystem health come along with the wide application of nanomaterials. The unique properties of nanomaterials could cause their enhanced performance in both positive and negative ways. For example, Su et al found that

the bactericidal effect of Ag NPs was due to their sorption to the negatively charged bacterial cell wall, deactivation of cellular enzymes, and disruption of membrane permeability (*192*). However, another study reported that the silver ions released by Ag NPs could result in complete deenergization and probably cell death of normal cells (*193*). Therefore, the topics on toxicity induced by noble metal nanoparticles including cytotoxicity and genotoxicity are still in discussion due to the speculation of all possible underlying mechanisms. However, it is thought that the major effect of noble metal nanoparticles on biological systems is the generation of ROS and accordingly induced oxidative stress.

2.4.1 Noble metal nanoparticles with ROS

Numerous studies have been conducted to evaluate cytotoxicity and genotoxicity of silver nanoparticles in various cell lines including human normal cell (*194*), human carcinemia cell (*195, 196*), rat cell (*197*), and murine macrophages (*198*). They all believe that the mitochondrial damage, viability or apoptosis of cells has been associated with ROS generation induced by silver nanoparticles. Also, It is also reported that cell damage caused by Ag NPs has been related to their inhibition on GSH (*199*). Lim et al investigated the toxicity induced by Ag NPs in *Caenorhabditis elegans* and found it to be related to formation of ROS (*200*). Platinum nanoparticles have been claimed as ROS scavengers, and in turn showed anti-inflammatory effects on lipopolysaccharide-induced macrophages (*201, 202*), neuroprotective effect in ischemic mouse brains (*203*), inhibitive effects on the apoptosis of human breast cell line induced by oxidant (*204*), and protective effect on the apoptosis of HeCaT keratinocytes cell lines induced by UV-light (*205*). Because of the specific property against ROS, Pt NPs have been commercialized in many consumer products and claimed as antioxidant ingredients.

Major studies have found gold nanoparticles play an important role in production of ROS. Au NPs could enhance formation of ROS in human breast cancer cells under light irradiation (*206*) and in human epithelia cancer cells when exposed to a low power laser light (*207*). Furthermore, Misawa and Takahashi have confirmed the generation of hydroxyl radical and superoxide anion induced by Au NPs under x-ray and UV irradiations (*208*). Nevertheless, the scavenging effect of Au NPs on DPPH radical, a non-biological existing radical, was examined to support their antioxidative property (*209*). In addition, Au NPs supported by ceria were demonstrated to reduce ROS in human cell lines due to their peroxidase-like activity (*210*).

Overall, the relationship between ROS and noble metal nanoparticles is different and each type of noble metal nanoparticles showed various influence on ROS. Notwithstanding, most of studies attribute the impact of noble metal nanoparticles on biological system to their behavior to intracellular ROS.

2.4.2 Experimental approaches

Currently, the commonly used method to detect ROS is fluorescence spectrometry. This indirect method is however limited in sensitivity and identification of specific ROS. Electron spin resonance (ESR) spectroscopy is a non-destructive method that could quantitatively and definitively detect and identify unpaired electrons. Three distinct ESR approaches are: 1) straight detection of long-lived paramagnetic species; 2) detection of unstable species trapped by spin traps that are ESR silent; and 3) investigation of specific molecules, such as oxygen, through synthetic stable paramagnetic species, spin labels (*211*).

Ascorbyl radical is ESR detectable, which enables ESR feasible to monitor ascorbic acid oxidation. Since ascorbic acid is highly sensitive to the oxidative status of biological system, ascorbyl radical is the most exploited endogenous marker of oxidative status (*10, 212*).

Since most ROS are short-lived free radicals that are highly reactive, ESR is an excellent tool for ROS determination with the help of spin traps. Spin traps are autologous ESR silent but they physically interact with free radicals and form stable spin adducts that are ESR detectable with specific characteristics. Figure 2-5 shows the principle of formation of DEPMPO spin adduct.

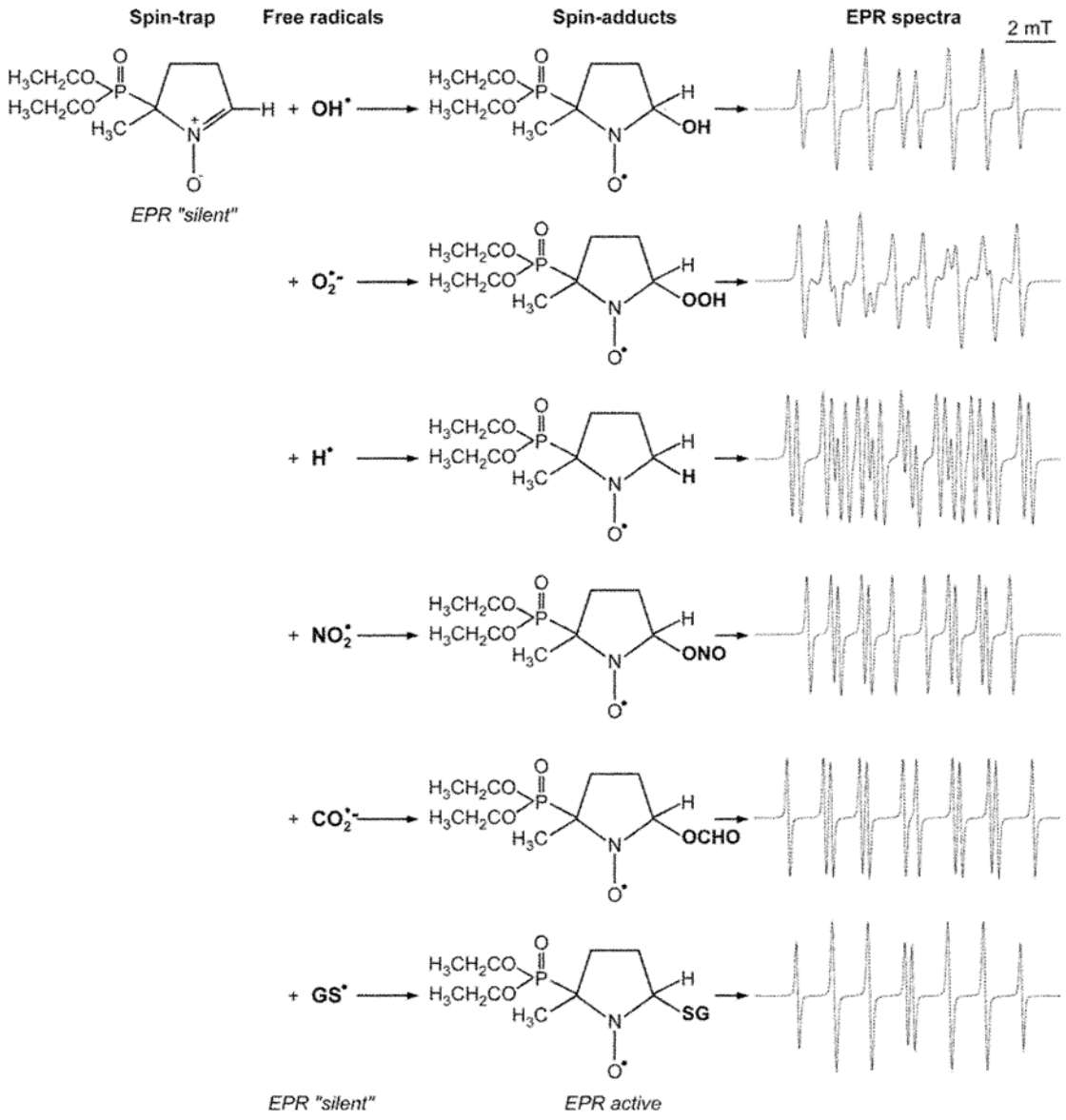

Figure 2-5 The basic principles of ESR spin-trapping method, shown on the example of spin-trap DEPMPO and a variety of physiologically most relevant free radicals-hydroxyl radical, superoxide anion radical, hydrogen atom, nitrogen dioxide radical, carbon dioxide radical, and glutathione thiyl radical. EPR represents ESR. Adapted from Spasojevic's review (*211*).

As an important participant in redox reactions, oxygen could be quantitatively measured by monitoring the ESR signal of a spin label that is a stable nitroxide free radical. In ESR oximetry, commonly used water-soluble spin labels are ^{14}N-containing nitroxide, 3-carbamoyl-2,2,5,5-tetramethyl-3-pyrroline-1-yloxyl (CTPO) and ^{15}N-containing nitroxide

perdeutero, ^{15}N-2,2,6, 6-tetramethyle-4-piperidone-1-oxyl (^{15}N-PDT) (*213*). Their ESR spectra shapes are dependent on the amount of O_2 molecule interacting with the spin labels, which means the dissolved oxygen content in reaction system (Figure 2-6).

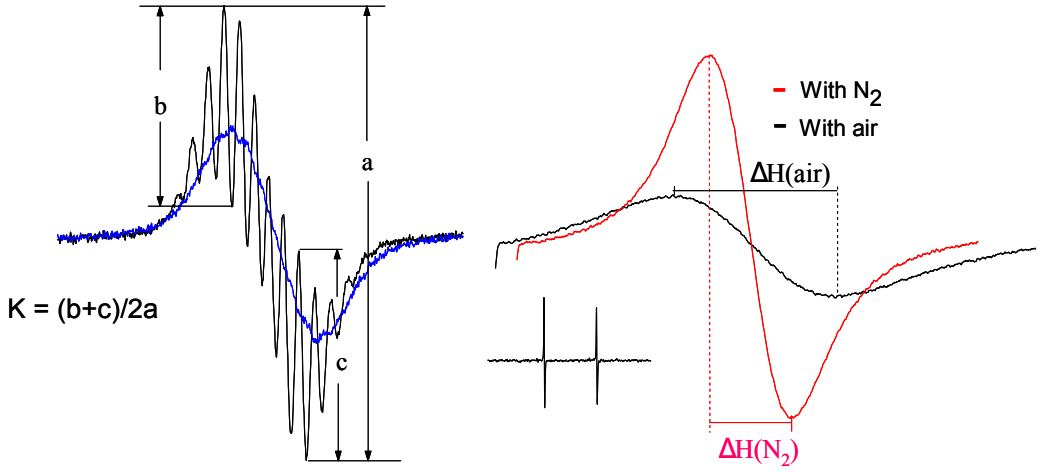

Figure 2-6 Left: The superhyperfine structure of the center field line from ESR spectra of CTPO in nitrogen-saturated (black) and air-saturated (blue) aqueous solution. The *K* parameter is used to determine oxygen concentration and is calculated by the equation *K* = (b+c)/2a. Right: The hyperfine structure of the low field line from the ESR spectra of ^{15}N-PDT in a nitrogen atmosphere (red line) or air-saturated (black line) aqueous solutions.

2.5 Significance of current work

In vitro and in vivo investigations have provided strong evidence on the benefit of antioxidants, whereas intervention studies have produced extremely contrasting results that no evidence of benefits is reported, and in some instances, even an enhancement of the mortality rates has been recorded (*214-216*). We have also revealed crossover activity of selected antioxidants in the presence of copper (*217*). Consequently, studies focusing only on single compound without any information on the efficiency of the network may underestimate the impact of antioxidants in oxidative stress prevention (*218*). The impact of noble metal nanoparticles on ROS has been extensively studied in model systems or cells, but information related to each individual ROS is lacking. Moreover, in biological or other matrix, the nanoparticles may not only exert direct but also indirect effects on ROS

due to the complicated environment. For example, they could influence antioxidants and in turn affect ROS. The combination of nanoparticles and antioxidant could result in duplicate effects, synergetic, or even antagonistic effects.

Chapter 3: Mechanisms of the pH dependent generation of hydroxyl radicals and oxygen induced by Ag nanoparticles

Adapted from He, W. W.*; Zhou, Y. T.*; Wamer, W. G.; Boudreau, M. D.; Yin, J. J., Mechanisms of the pH dependent generation of hydroxyl radicals and oxygen induced by Ag nanoparticles. *Biomaterials* **2012,** *33*, 7547-7555.

3.1 Introduction

Silver has been used in medical applications for hundreds years because of its antibacterial properties. Advances in nanotechnology have further increased the availability of silver nanoparticles (Ag NPs) with a wide range of physiochemical properties. The increased availability and reported superior and size-dependent antibacterial activity of Ag NPs have resulted in their widespread use in clothing, cosmetics, electronics, food packaging, medical devices, textiles, and various household products (*219-222*). The widespread use of Ag NPs inevitably results in their release into the environment. Currently, there are concerns that the distinctive physicochemical properties of nanomaterials may lead to adverse biological and environmental effects. Investigators have reported that Ag NPs are highly toxic to *Chlamydomonas reinhardtii* (*223*), freshwater alga *Ochromonas danica* (*224*), some beneficial microbial communities (*225*), and human cells (*226*). However, generally, the short- and long-term risks associated with uses of Ag NPs are incompletely understood. Among the previously reported mechanisms (*199, 226-232*), the generation of ROS and the dissolution of Ag NPs have been proposed as the two dominant hypotheses for toxicity induced by Ag NPs (*199, 227-230, 232*). Overproduction of ROS, including superoxide, hydroxyl radicals, singlet oxygen, and hydrogen peroxide (H_2O_2), can induce oxidative stress and result in significant damage to cellular components. To understand the toxicity of Ag NPs, it is important to identify the types of ROS generated because ROS differ in their oxidizing/reducing activities. In most available studies, the production of

ROS has been determined by indirect spectroscopic methods (*192, 233-235*). However, definitive identification of ROS with these methods is difficult since ROS are short-lived and can be quickly scavenged by endogenous reductants or scavengers. In addition, the toxicity may be associated with concomitant release of Ag^+ due to dissolution under physiological conditions, as reported previously (*236-240*). One study pointed out that Ag^+ was released from Ag NPs, causing cytotoxicity and bacterial death (*236*). The detailed underlying mechanism for toxicity, however, was not determined since the oxidation of Ag NPs proceeded through complex processes and was affected by the particle size, surface coating, medium pH and concentration, dissolved oxygen and ligand molecules (*241-243*).

In the current study, we have used electron spin resonance (ESR) spectroscopy to examine the effects of Ag NPs on generation of ROS. ESR spectroscopy with spin trapping is the most reliable and direct method for identification and quantification of short-lived free radicals (*217, 244-246*). To assess the role of Ag NPs in environmentally and biologically relevant redox reactions, we have examined the effects of Ag NPs on the decomposition of H_2O_2 over a range of pHs.

Because hydrogen peroxide is continuously formed at micromolar levels and participates in redox homeostasis in cells and tissues (*245, 247-249*), it is meaningful to study the interaction between H_2O_2 and Ag NPs. Up to now, little mechanistic information is available for the effects of Ag NPs on the oxidation/reduction of H_2O_2, especially over a wide pH range. Herein, we examine the effects of Ag NPs upon generation of ROS and oxygen over a physiologically relevant pH range.

3.2 Materials and methods

3.2.1 Materials

Ag nanoparticles (10, 20, 30, 40, 50, 60, 75,100 nm) with a spherical morphology and coated with polyvinylpyrrolidone (PVP), citrate or tannic acid were purchased from nanoComposix, Inc. (San Diego, CA) and used as received. Ag nanoparticles (75 nm) coated with polystyrenesulfonate (PSS) were a gift from X.C.Wu at National Center for Nanoscience and Technology, China. The spin traps, 5, 5-dimethyl N-oxide pyrroline (DMPO) and 5-(diethoxyphosphoryl)-5-methyl-1-pyrroline-N-oxide (DEPMPO), were purchased from Radical Vision (Marseille, France) and 5-tertbutoxycarbonyl 5-methyl-1-pyrroline N-oxide (BMPO) was from Bioanalytical Labs (Sarasota, FL). The spin label 3-carbamoyl-2,5-dihydro-2,2,5,5-tetramethyl-1H-pyrrol-1-yloxyl (CTPO), spin trap a-(4-pyridyl-1-oxide)-N-tert-butylnitrone (4-POBN), $AgNO_3$, Ag wire with diameter of 0.5 mm, 3 mm Ag powder, 30% H_2O_2, dimethyl sulfoxide (DMSO), ethanol, and standard buffer solutions were all purchased from Sigma-Aldrich (St. Louis, MO). Each buffer stock solution (pH 1.2 HCl/KCl, pH 3.6 HAc/NaAc, pH 4.6 HAc/NaAc, pH 5.5 HAc/NaAc, pH 6.5 HAc/NaAc, pH 7.4 PBS, pH 9.5 borax and pH 11.0 borax) was 0.1 M. Before use, each buffer was treated with Chelex®100 molecular biology grade resin from Bio-Rad Laboratories (Hercules, CA) to remove trace metal ions. Milli-Q water (18 MΩ cm) was used for all solution preparations. Artificial perspiration was obtained from Pickering Laboratories (Mountain View, CA) and contained lactic acid, uric acid, urea, minerals and amino acids, pH 4.5. A cosmetic emulsion, formulated as a representative skin care cream, was made according to Kraeling and Bronaugh's study (*250*) using phosphate-sodium hydroxide buffer (pH 7).

3.2.2 Characterization

Transmission electron microscopy (TEM) images were captured on a JEM 2100 FEG (JEOL) transmission electron microscope at an accelerating voltage of 200 kV located at the NanoCenter, University of Maryland, College Park, MD. To observe the morphological evolution of the nanoparticles after oxidation, 0.2 mg/mL Ag NPs and 5mM H_2O_2 were mixed in 0.5 mL 10mM pH 11.0 borax buffer solution for 30 min and twice centrifuged (12,000 rpm, 5 min). After the supernatants were decanted, 20 mL water was added to redisperse the precipitates. The samples for TEM analysis were prepared by adding drops of the redispersed colloidal solutions onto standard holey carbon-coated copper grids, which were then air dried at room temperature.

UV-vis absorption spectra were obtained using a Varian Cary 300 spectrophotometer. The oxidation of Ag NPs by H_2O_2 in buffers at different pHs was performed as follows: H_2O_2 (freshly prepared) was mixed with different pH buffers and made up with H_2O to a final concentration of 5mM and 10mM, respectively. Then, Ag NPs (10 mL, 1.0 mg/mL) having different sizes were added into the above mixture. To monitor the progress of the reaction, absorption spectra were collected at 1 min intervals using the scanning kinetics mode of the spectrophotometer.

3.2.3 Electron spin resonance (ESR)

All ESR measurements were carried out using a Bruker EMX ESR spectrometer (Billerica, MA) at ambient temperature. Fifty microliter aliquots of control or sample solutions were put in glass capillary tubes with internal diameters of 1 mm and sealed. The capillary tubes were inserted in the ESR cavity, and the spectra were recorded at selected times. Other settings were as follows: 1 G field modulation, 100 G scan range, and 20 mW microwave power for detection of spin adducts using spin traps and 0.04 G field modulation, 5 G scan

range, and 1 mW microwave power for ESR oximetry using the spin label CTPO. The spin traps DMPO, BMPO, DEPMPO, and POBN were employed to verify the formation of hydroxyl radicals (·OH) during the degradation of H_2O_2 enhanced by Ag NPs under various conditions. DMPO was used in experiments designed to quantitatively estimate the formation of hydroxyl radicals. In these experiments, the intensity of the ESR signal was measured as the peak-to-peak height of the second line of ESR spectrum of the hydroxyl radical spin adduct with DMPO (DMPO/·OH).

Hydrogen peroxide solution was mixed with DMPO in buffers of different pHs and the reaction was initiated by addition of Ag NPs. ESR spin label oximetry in conjunction with the water soluble spin label CTPO was used to investigate oxygen generation since the super hyperfine structure change in the ESR spectrum of CTPO is a sensitive measure of changes in O_2 concentration. The detailed method for calculating O_2 concentrations, based on the ESR spectrum of CTPO has been described in a previous review (*213*). The sample mixture, containing CTPO, H_2O_2, buffer, with or without Ag NPs, was deoxygenated by aerating with N_2. The final concentration of each component is described in each figure caption.

3.3 Results and discussion

3.3.1 Generation of hydroxyl radicals induced by Ag NPs

Hydroxyl radicals (·OH) cannot be detected directly by ESR because of their short lifetime. However, they readily react with diamagnetic nitrone spin traps, forming a stable free radical (spin adduct) that can be identified from the magnetic parameters of the ESR spectrum (*244*). To verify the generation of hydroxyl radicals induced by Ag NPs, we chose four spin traps that are often used to capture hydroxyl radicals, DMPO, DEPMPO, BMPO

and POBN. Figure 3-1 shows the ESR spectra obtained for solutions at pH 3.6 containing different spin traps without or with Ag NPs. For samples containing only H_2O_2 and a spin trap (Figure 3-1A), characteristic ESR spectra for spin adducts attributable to hydroxyl radical were absent. However, ESR spectra characteristic for the hydroxyl radical spin adduct for each spin trap appeared upon the reaction of H_2O_2 with 0.1 mg/mL Ag NPs for 2 min (Figure 3-1B). In the sample containing DMPO, we observed a four-line spectrum with relative intensities of 1:2:2:1, and hyperfine splitting parameters of $\alpha_N = \alpha_H = 14.9$ G. This ESR spectrum is characteristic for the spin adduct between DMPO and the hydroxyl radical (DMPO/·OH) (*251*). Use of DEPMPO resulted in the ESR spectrum expected for the DEPMPO/·OH adduct, having eight lines with intensity ratios of 1:2:2:1:1:2:2:1 and hyperfine splitting parameters of $\alpha_P = 47.3$ G, $\alpha_H = 13.2$ G, $\alpha_N = 14.0$ G (*252*). An ESR spectrum characteristic for the BMPO/·OH spin adduct (four lines with relative intensities of 1:2:2:1 and hyperfine splitting parameters of $\alpha_N = 13.56$, $\alpha^{\beta}_H = 12.30$, $\alpha^{\gamma}_H = 0.66$) was observed when BMPO was the added spin trap (*251*). Spin trap POBN was dissolved in 170 mM ethanol rather than water. Addition of Ag NPs yielded a six-line ESR spectrum representative of POBN/·$CH(OH)CH_3$ adduct. The ·$CH(OH)CH_3$ radicals are formed in the reaction between ethanol and ·OH (*253*). All of these results support the conclusion that hydroxyl radicals are generated when decomposition of hydrogen peroxide is assisted by Ag NPs under acidic conditions. Moreover, the addition of 5% DMSO, a commonly recognized hydroxyl radical scavenger (*254*), greatly reduced the DMPO/·OH ESR signal intensity. This result provides additional evidence for the generation of ·OH in the presence of Ag NPs (Figure 3-2). It should be noted that no spin adducts attributable to superoxide radical anion were observed. In contrast, other investigators have reported superoxide

radical anion formation during Ag NP-assisted H_2O_2 decomposition (*234, 255*). Detection of the formation of superoxide radical anion by ESR has been reported for decomposition of H_2O_2 assisted by Ag NPs on an alumina support in 1.0 M KOH (*255*). These experimental conditions differ dramatically both from our experimental conditions and those expected in environmental and biological systems. Other studies reporting superoxide radical anion formation during decomposition of H_2O_2 in the presence of Ag NPs have used indirect methods for detecting this radical (*234*).

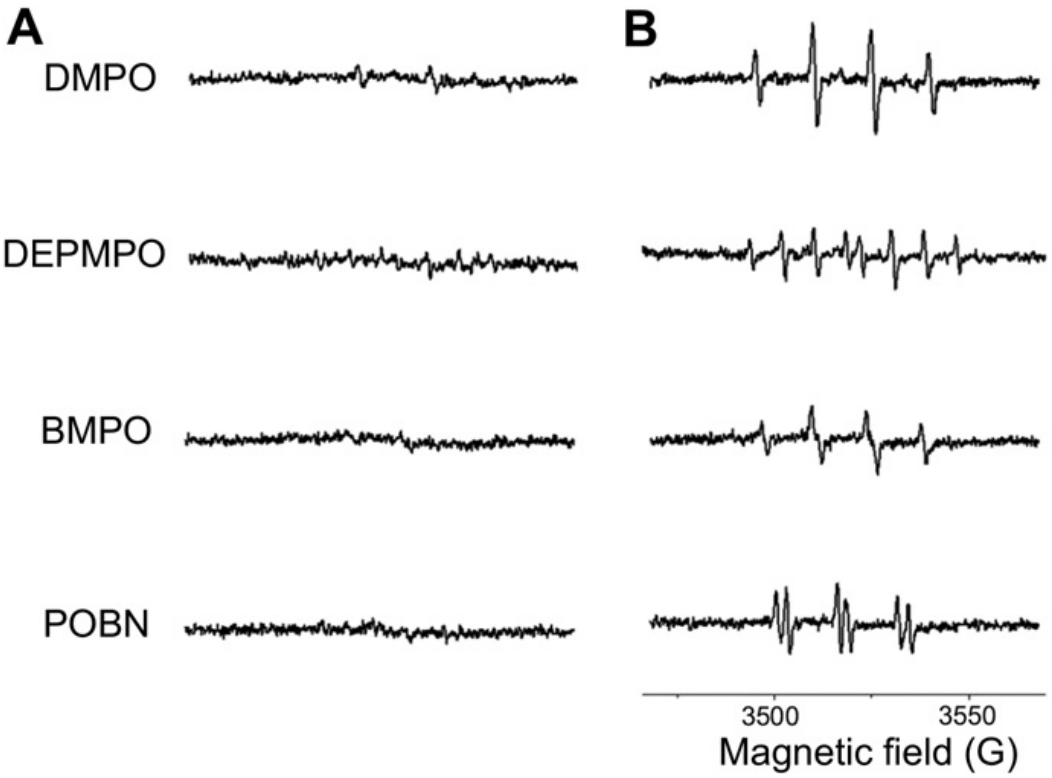

Figure 3-1 Demonstration of hydroxyl radicals generated by Ag NPs in presence of hydrogen peroxide at pH 3.6 (10 mM HAc/NaAc buffer) using different spin traps. The sample solutions contained 0.5 mM H_2O_2 and different spin traps (50 mM DMPO, 28 mM DEPMPO, 25 mM BMPO, or 50 mM POBN) in absence of Ag NPs (spectra in column A) or in presence of 0.1 mg/mL citrate coated Ag NPs (75 nm) (spectra in column B). Spectra were recorded 2 min after sample mixing.

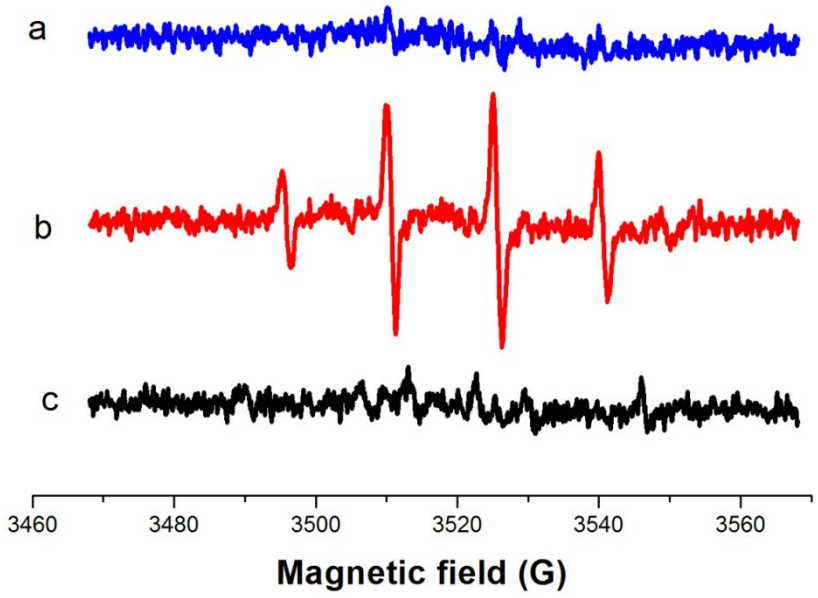

Figure 3-2 ESR spectra of hydroxyl radical in the absence (a) and presence (b) of 0.1 mg/mL citrate coated Ag NPs. Addition of 5% DMSO suppresses the formation of the spin adduct (c). Conditions: 0.1 mg/mL 75 nm citrate coated Ag NPs + 10 mM pH 3.6 HAc/NaAc buffer + 50 mM DMPO+ 0.5 mM H_2O_2, obtained after 6 min incubation.

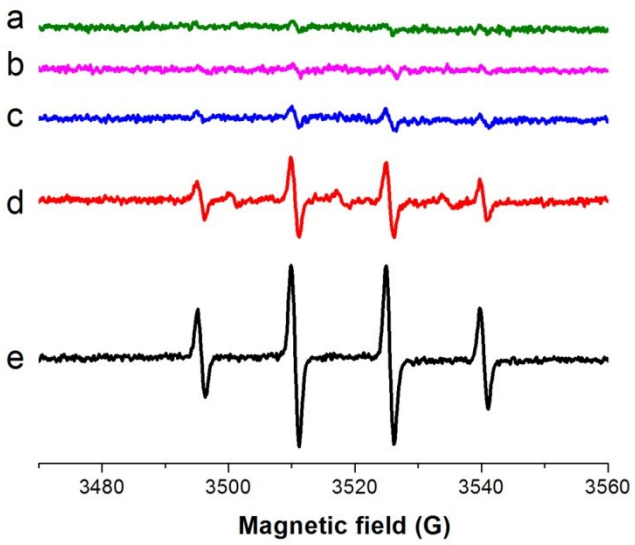

Figure 3-3 Generation of hydroxyl radicals induced by silver in different forms. Sample solutions included 50 mM DMPO, 0.5 mM H_2O_2, 10 mM HAc/NaAc buffer (pH 3.6), and (a) no silver; (b) 0.54 mg/mL Ag^+; (c) 4 mg Ag wire (OD 500 µm; in 50 µl); (d) 0.2 mg/mL 3 µm Ag powder; (e) 0.1 mg/mL 75 nm citrate coated Ag NPs. Spectra were obtained after 7 min of mixing.

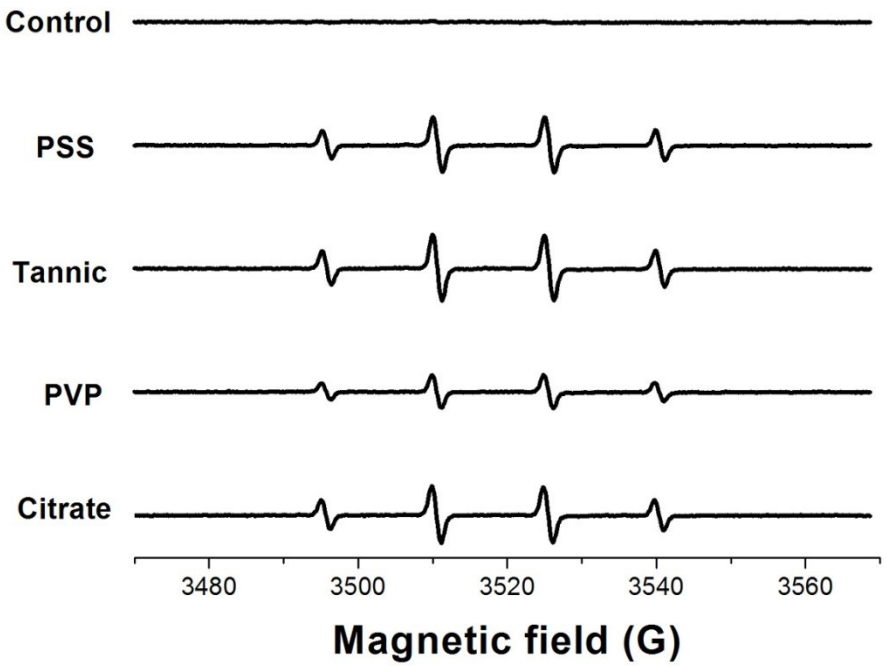

Figure 3-4 Effect of surface coating of Ag NPs on generation of hydroxyl radicals. Conditions: 0.1 mg/mL 75 nm Ag NPs with different coatings + 10 mM pH 3.6 HAc-NaAc buffer + 50 mM DMPO + 0.5 mM H_2O_2, incubation time 6 min.

Two sets of experiments were performed to determine whether Ag NPs differ from other forms of silver in their ability to elicit hydroxyl radicals during decomposition of hydrogen peroxide.

First, generation of hydroxyl radicals from H_2O_2 was studied in the presence of Ag^+, bulk Ag wire (with diameter 0.5 mm), 3-5 mm Ag micro particles, or 75 nm Ag NPs (Figure 3-3). Similar to control sample (no silver), little hydroxyl radical was generated in the presence of 0.54 mg/mL $AgNO_3$. Even after 30 min of incubation and at concentrations up to 500 mg/mL $AgNO_3$, Ag^+ had no discernible effect on the ESR signal observed for the hydroxyl radical spin adduct (data not shown). These results demonstrate that Ag^+ had no significant activity for generating hydroxyl radicals in the presence of H_2O_2. In comparison with bulk silver and microscaled silver powder, higher levels of hydroxyl radical were

observed using 75 nm Ag NPs coated with citrate. This effect may be attributed to the large surface area to mass ratio of nanoparticles. Next, we investigated the effect of surface coating on the capability of Ag NPs to produce hydroxyl radicals from H_2O_2. Ag NP with four coatings, including polyvinylpyrrolidone (PVP), citrate, tannic acid and polystyrenesulfonate (PSS), all efficiently assisted in generating hydroxyl radicals (Figure 3-4). Among these coatings, Ag NPs coated with PVP were less efficient than Ag NPs with the other three coatings. This observation is consistent with a previous report that PVP coated Ag NPs were less toxic than citrate coated Ag NPs and may reflect the ease with which citrate is displaced from Ag NPs compared to other coatings (*256*).

3.3.2 Ag NPs generating hydroxyl radicals based on Fenton-like activity

Hydrogen peroxide has been found to produce hydroxyl radicals in two ways: they are formed by UV irradiation, reaction (1), and Fenton or Fenton-like reactions involving transition metal ions such as Fe^{2+} and Cu^{2+}, reaction (2) (*257*).

$$H_2O_2 + h\nu \rightarrow 2{\bullet}OH \qquad (1)$$

$$H_2O_2 + M^{n+} \rightarrow M^{n+1} + {\bullet}OH + OH^- \qquad (2)$$

Currently, mechanistic studies on the ability of metal nanoparticles (such as Ag NPs) to induce ·OH generation in presence of H_2O_2 are largely lacking. Does Ag NP act as a catalyst or is it involved in a Fenton-like pathway to produce ·OH? Theoretically, elemental silver (($\varphi Ag^+/Ag$ = +0.7996 V, reaction (3)) can be oxidized to Ag^+ by dissolved oxygen having a reduction potential of 1.2 V or by hydrogen peroxide having a reduction potential of 1.77 V, reaction (4).The oxidative dissolution of Ag NPs has been demonstrated in several kinetic and mechanistic studies (*237-240*). In the current study, the oxidation of Ag

NPs was evidenced by the visible color change from original yellow to colorless and gradual decrease of the surface plasmon resonance (SPR) peak, centered near 400 nm, during the incubation with hydrogen peroxide. Therefore, the possibility of Ag NPs acting catalytically can be excluded since dissolution of Ag NPs to form Ag^+ accompanied the decomposition of hydrogen peroxide under conditions leading to the formation of hydroxyl radicals.

$Ag^+ + e^- = Ag$ ($\varphi = +0.7996$ V) (3)

$H_2O_2 + 2H^+ + 2e^- = 2H_2O$ ($\varphi = +1.77$ V) (4)

The formation of hydroxyl radicals may go through a process similar to the Fenton reaction where Ag NPs act as a Fenton-like reagent:

$Ag + H_2O_2 + H^+ = Ag^+ + \cdot OH + H_2O$ (5)

The valence of Ag changes from zero to one, thus Ag NPs may be viewed as "Fenton nanoparticles", and the concentration dependence should be predicted by reaction (5). That is, the production of hydroxyl radicals will be accelerated by increasing the Ag NPs or hydrogen peroxide concentration, or decreasing the pH of the buffer. In addition, production of ·OH will be inhibited by addition of Ag^+ or increasing the pH of the buffer. To test the hypothesis that Ag NPs are involved in a Fenton-like reaction, the effect of reactant/product concentrations and pH on hydroxyl radical production was determined.

The influence of Ag NPs concentration, hydrogen peroxide concentration and Ag^+ concentration on the generation of hydroxyl radicals has been studied as shown in Figure 3-5. In the absence of Ag NPs, the DMPO/·OH ESR signal was barely observed (Figure 3-

5A, a) and the signal intensity increased as more Ag NPs were added (Figure 3-5A, b-f). As shown in Figure 3-5B, the production of ·OH was quasi-linearly proportional to the concentration of Ag NPs from 4 μg/mL to 0.1 mg/mL. Also a direct correlation between DMPO/·OH signal intensity and H_2O_2 concentration was found (Figure 3-5C). At lower H_2O_2 concentrations (≤1.0 mM), a linear relationship was observed (Figure 3-5C, red dashed line). At concentrations of H_2O_2 above 1 mM, generation of hydroxyl radicals no longer increased indicating a saturation of the reactivity of Ag NPs. When added without Ag NPs, Ag^+ induced a negligible ESR signal for the hydroxyl radical spin adduct (Figure 3-5D, spectrum b). In the presence of Ag NPs, Ag^+ suppressed the generation of hydroxyl radical (Figure 3-5D, spectrum d compared to spectrum c). This result is consistent with the proposed Fenton-like reaction (5) between Ag NPs and H_2O_2 to form hydroxyl radicals.

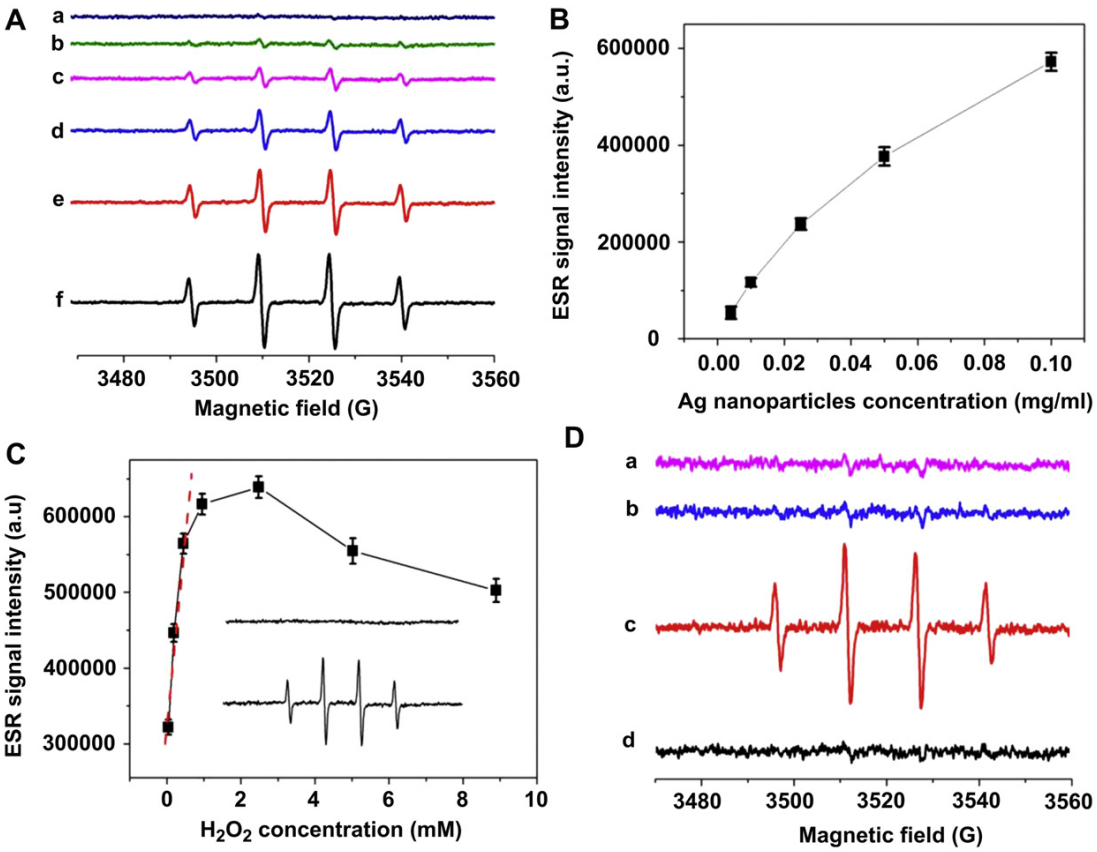

Figure 3-5 (A) ESR spectra of DMPO/·OH generated from a sample solution containing 50 mM DMPO, 0.5 mM H_2O_2 and 10 mM pH 3.6 HAc/NaAc buffer in the absence (a) and presence of 75 nm citrate coated Ag NPs with concentration of 0.004 (b), 0.01 (c), 0.025 (d), 0.05 (e), and 0.1 (f) mg/mL. (B) Dependence of ·OH generation on the concentration of Ag NPs as indicated in A. (C) Effect of H_2O_2 on the generation of ·OH from samples containing 50 mM DMPO, 0.1 mg/mL 75 nm citrate coated Ag NPs, 10 mM HAc/NaAc buffer (pH 3.6), and H_2O_2 at different concentrations; inset shows the spectra obtained from samples without H_2O_2 (upper) and with 0.5 mM H_2O_2 (lower). (D) Effect of Ag^+ on the generation of hydroxyl radicals induced by Ag NPs. Solutions included 10 mM HAc/NaAc buffer (pH 3.6), 50 mM DMPO, 0.5 mM H_2O_2, and a), none; b), 5 mM Ag^+; c), 0.1 mg/mL 75 nm citrate coated Ag NPs; d), 5 mM Ag^+ and 0.1 mg/mL 75 nm citrate coated Ag NPs. All the spectra were obtained 6 min after mixing.

3.3.3 pH dependent hydroxyl radicals generation

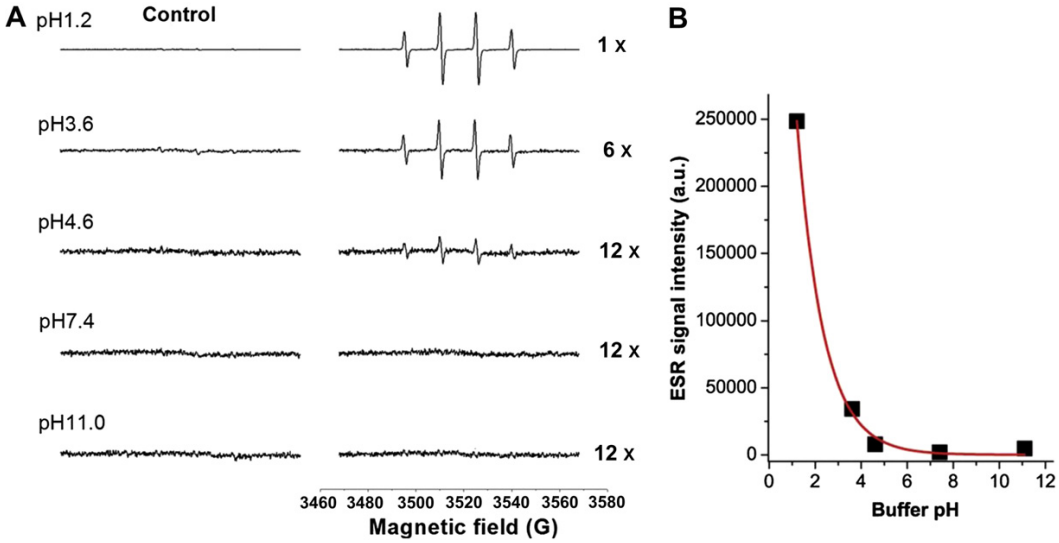

Figure 3-6(A) ESR spectra of hydroxyl radicals generated in absence and presence of Ag nanoparticles with different pH buffer solutions containing 0.1 mg/mL 75 nm Ag NPs, 10 mM buffer, 50 mM DMPO, and 0.5 mM H_2O_2. (B) ESR signal intensity vs buffer pH from (A). Samples contained 50 mM DMPO, 0.5 mM H_2O_2; all of the spectra were obtained after 6 min of incubation.

In control solutions (no Ag NPs) with pH ranging from 1.2 to 11.0, no apparent signal of ·OH was detected (Figure 3-6A). With addition of Ag NPs, the ESR data collected for samples having a pH 1.2, 3.6 and 4.6 showed the spectrum characteristic of the DMPO/·OH adduct. The ·OH was generated most efficiently at pH 1.2 and its production decreased dramatically in the buffers with pH increasing from 1.2 to 4.6 (Figure 3-6B). Above pH 7.4, the ESR spectra were comparable to that of the control sample where the signal for the spin adduct DMPO/·OH was negligible. These results indicate that the generation of hydroxyl radicals induced by Ag NPs is strongly dependent on the chemical environment and that more ·OH is formed at a lower pH. The concentration and pH dependences we have observed are consistent with the proposed Fenton-like mechanism.

It is well established that hydroxyl radicals are extremely reactive and can cause oxidative damage leading to toxicity in biological systems (*257*). The pH dependence of ·OH induced

by Ag NPs suggests that Ag NPs may be more toxic in an environment having a lower pH, such as the stomach with a pH about 1.2 and sweat glands with a pH of 3-5. Because of their antifungal and antibacterial activities, Ag NPs are currently found in commercial products such as wound dressings and cosmetics. We have examined the effects of Ag NPs on hydroxyl radical generation under conditions that represent topical exposure. We determined that Ag NPs increased the formation of hydroxyl radicals when added to a representative cosmetic formulation or when added to artificial perspiration (Figure 3-7). These results suggest that the safety of topical exposure to Ag NPs warrant further investigation.

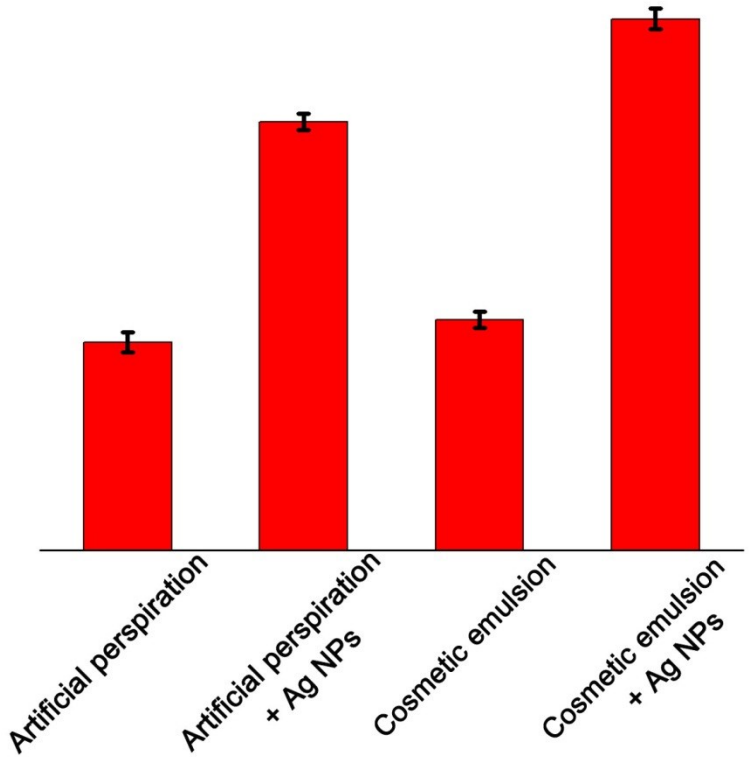

Figure 3-7 Generation of hydroxyl radicals in artificial perspiration and cosmetic emulsion induced by Ag NPs (0.1 mg/mL 75 nm citrate coated Ag NPs). Samples contained 50 mM DMPO, 0.5 mM H_2O_2, 5% artificial perspiration (pH 4.5) or cosmetic emulsion. All of the spectra were obtained at 6 min of incubation.

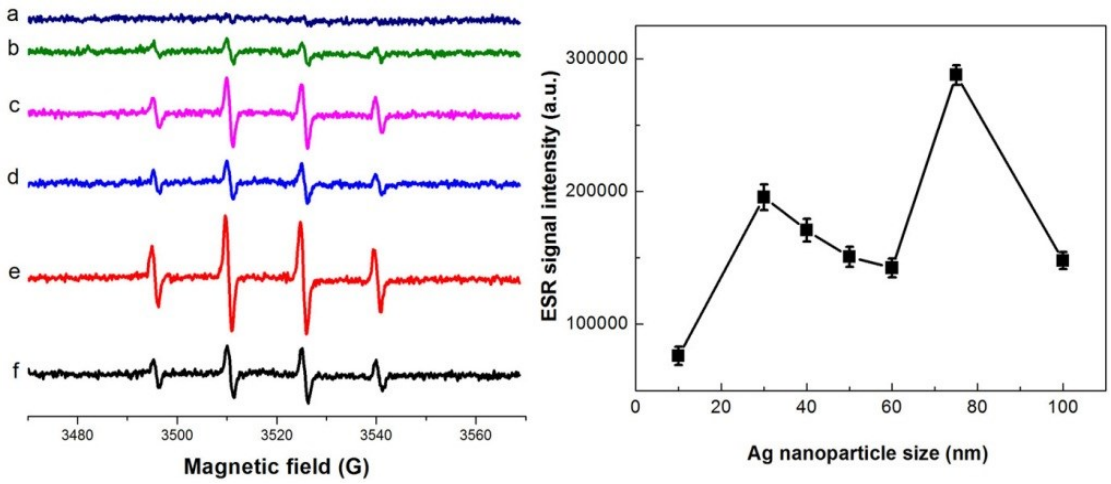

Figure 3-8 (Left) ESR spectra of hydroxyl radicals spin adducts generated in absence (a) and presence of Ag nanoparticles with different sizes of 10 nm (b), 30 nm (c), 50 nm (d), 75 nm (e) and 100 nm (f). (Right) ESR signal intensity vs Ag nanoparticles size. Sample solutions contained 10 mM HAc/NaAc buffer (pH 3.6), 0.1 mg/mL citrate coated Ag NPs of different sizes, 50 mM DMPO, and 0.5 mM H_2O_2. Spectra were recorded 6 min after sample mixing.

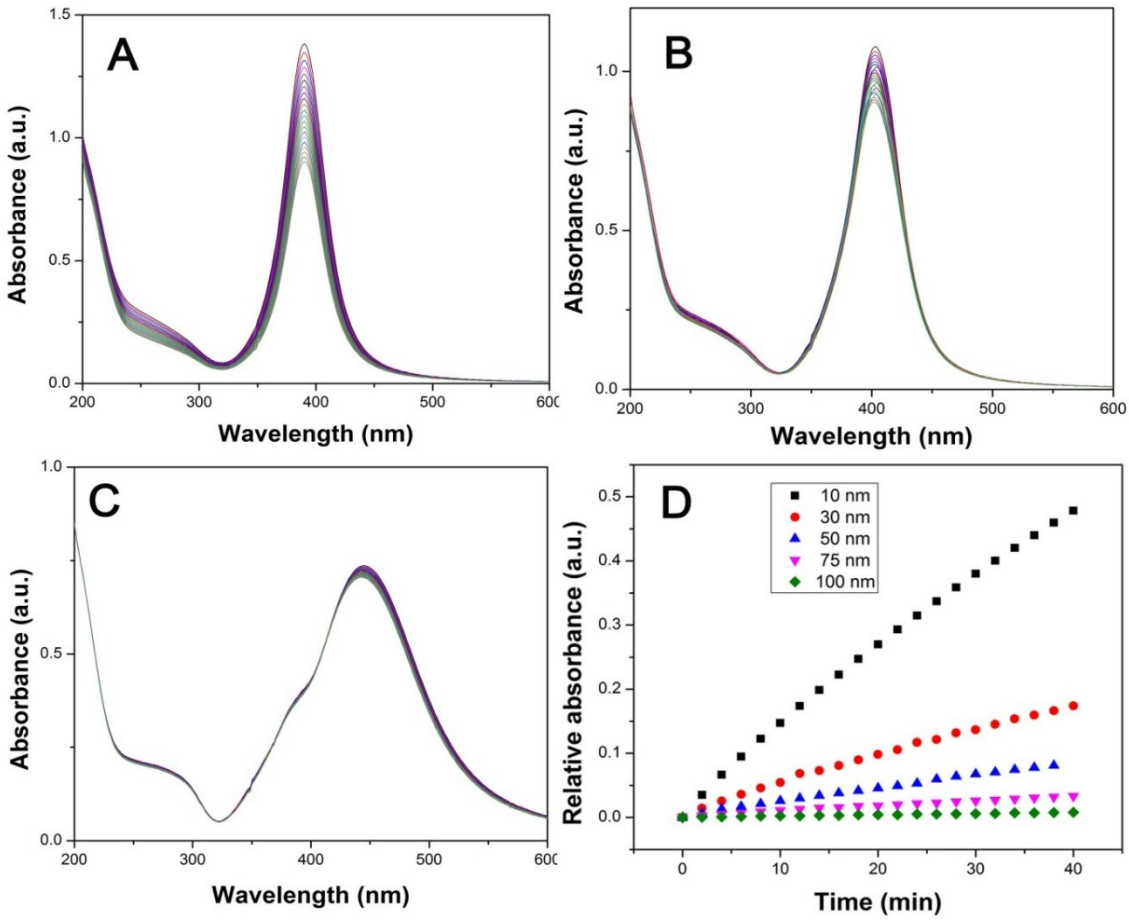

Figure 3-9 Evolution of UV-VIS spectra for 0.01 mg/ml citrate coated Ag NPs having different sizes: 10 nm (A), 30 nm (B) and 75 nm (C) in the presence of 0.5 mM hydrogen peroxide at pH 3.6. (D) Corresponding relative absorbance variation (A_0-A_t, where A_0 is initial absorbance, A_t represents the absorbance at reaction time t) was dependent on Ag NPs size over time. The absorbance was measured at the SPR peak maximum wavelength.

As described in reaction (5), the generation of hydroxyl radicals, proceeds concomitantly with dissolution of Ag NPs and release of Ag^+. We examined the role that nanoparticle size, ranging from 10 nm to 100 nm, plays in generation of hydroxyl radicals (Figure 3-8). Hydroxyl radicals were generated in the presence of all of the Ag NPs and 0.5 mM H_2O_2. However, the expected increase in generation of hydroxyl radicals with decreasing particle size was not observed. Instead, addition of 75 nm Ag NPs resulted in the highest level of ·OH formation, followed by 30 nm Ag NPs. In contrast, we determined that the dissolution of Ag NPs, in the presence of H_2O_2 at pH 3.6 was more rapid for smaller particle sizes

(Figure 3-9). This difference in the size-dependent behavior for generation of hydroxyl radicals and dissolution of Ag NPs indicates that, in addition to the described Fenton-like reaction, other redox reactions are occurring which involve H_2O_2 and lead to dissolution of Ag NPs. Other redox reactions that may contribute to dissolution of Ag NPs include:

$H_2O_2 + 2Ag + 2H^+ \rightarrow 2H_2O + 2Ag^+$ (in acidic medium) (6)

$½\ O_2 + 2Ag + 2H^+ \rightarrow 2Ag^+ + H_2O$ (7)

$H_2O_2 + 2Ag \rightarrow 2Ag^+ + 2OH^-$ (in basic medium) (8)

In these reactions, oxidation and dissolution of Ag NPs occurs, however hydroxyl radicals are not generated. When Ag NPs are in an environmental or biological system, ligands such as Cl^-, PO_4^{3-},S^{2-}, SH and NH_3 can form complexes or precipitates with Ag^+, with the potential to further enhance the dissolution of Ag NPs (*258*). Further studies are needed to understand the effects of a complex chemical environment on the formation of hydroxyl radicals by Ag NPs participating in environmentally and biologically relevant redox reactions. We are currently investigating whether chemical components of cells and tissues may broaden the pH range, over which hydroxyl radicals are formed during Ag NP-assisted decomposition of H_2O_2.

3.3.4 pH dependence for generation of O_2 during the Ag NP-assisted decomposition of H_2O_2

In addition to its oxidizing property, hydrogen peroxide can act as a reducing agent, especially in an alkaline environment. For example, H_2O_2 has been often used as a reductant for synthesis of nanoparticles (*259*). Therefore, the unique pH dependent oxidation reduction potential of H_2O_2 will cause different interactions with Ag NPs that

can be altered by adjusting the environment's pH (*248, 249*). As discussed above, Ag NPs did not induce the generation of hydroxyl radicals in alkaline medium. However, consistent with the reducing activity of H_2O_2 in alkaline medium, we observed generation of O_2. As shown in Figure 3-10A, evolution of O_2 was observed in neither the control sample without Ag NPs nor the sample without H_2O_2. However, clearly visible evolution of O_2 was noted from solutions containing H_2O_2 and 10 nm Ag NPs at pH 11.0. This result visually demonstrates the ability of Ag NPs in facilitating the decomposition of H_2O_2 under alkaline conditions.

We further investigated the effect of pH on the production of O_2 by using ESR oximetry in conjunction with spin label CTPO. ESR spectra of the spin label CTPO exhibit three lines due to the hyperfine interaction of the unpaired electron with the nitrogen nucleus. Each line is further split into another group of lines because of proton super hyperfine interactions. The resolution of the super hyperfine structure of the low-field line of the ESR spectrum of CTPO strongly depends on the O_2 concentration of the sample solution. Increasing oxygen concentrations result in the progressive diminution of the super hyperfine structure. In the current study, the first line of hyperfine structure of the CTPO line at 3500 Gauss was recorded. Oxygen production was calculated from a calibration curve relating the K parameter to oxygen concentration (*213*).

Production of O_2 induced by Ag NPs shows a strong dependence on pH. As seen in the left column of Figure 3-10B, when the pH was varied from 1.2 to 5.5, no appreciable change in the ESR spectrum was observed compared with control sample containing no Ag NPs. In contrast, the super hyperfine splitting clearly diminished for samples having a pH ranging from 5.5 to 11. It is noteworthy that in this pH range a time dependent flattening

of the intensity of CTPO's super hyperfine structure was observed (data not shown). This indicates prolonged generation of O_2 during Ag NP-assisted decomposition of H_2O_2 under alkaline conditions. A dramatic change was noted at pH 11 where the intensity of CTPO's super hyperfine splitting was negligible 1 min after sample mixing, indicating rapid formation of O_2. The quantitative results of the oxygen production are shown in Figure 3-10C, which clearly demonstrate the ability of Ag NPs to decompose H_2O_2 in an alkaline environment.

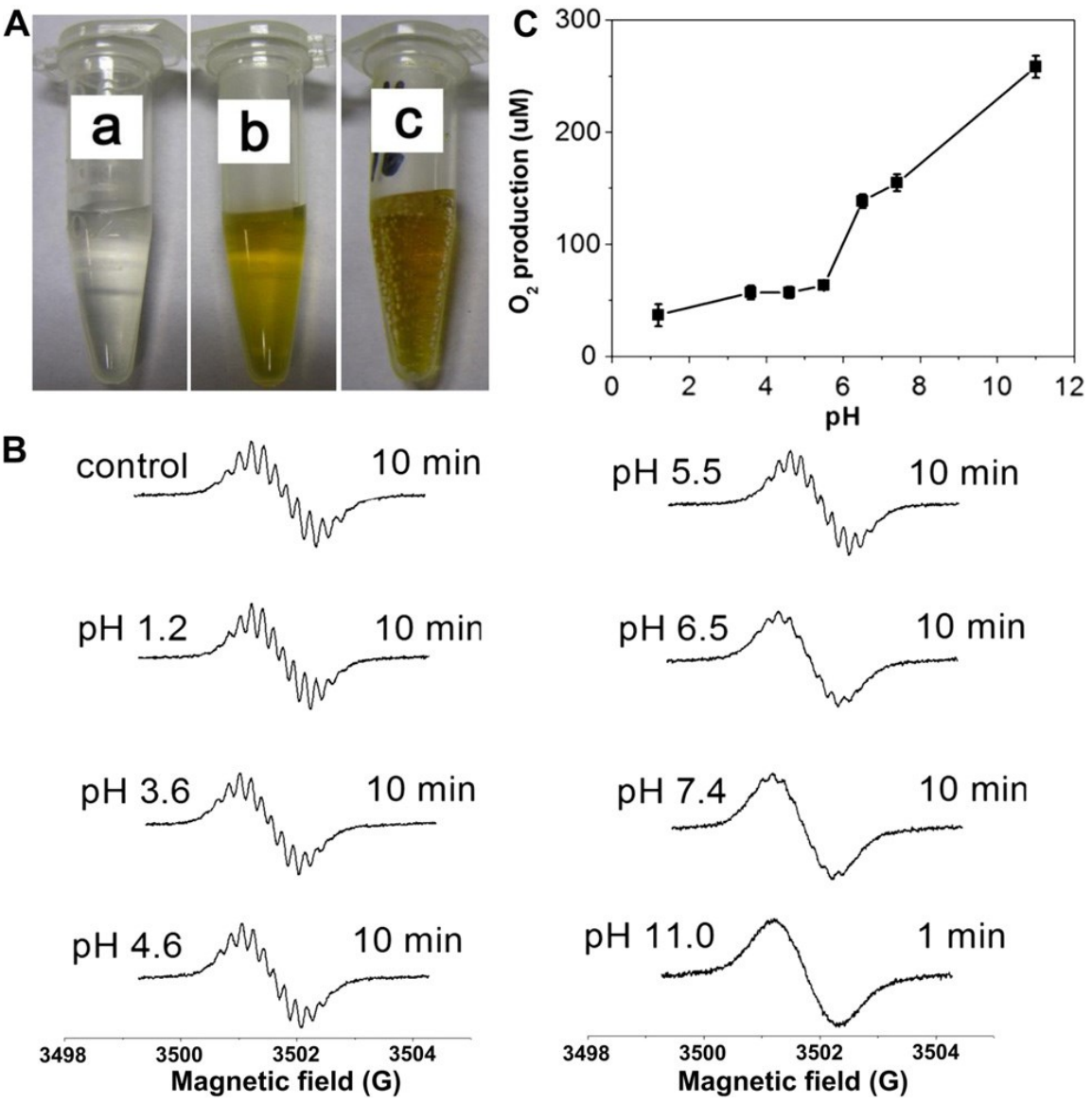

Figure 3-10 Generation of O_2 induced by Ag NPs in different circumstances. (A) Photographs of sample solutions containing 0.1 mM CTPO, and (a) 10 mM buffer (pH 11.0) and 10 mM H_2O_2, and 0.2 mg/mL citrate coated 10 nm Ag NPs. (B) ESR spectra of 0.1 mM CTPO in 10 mM buffers of different pHs in presence of 25 mM H_2O_2 and 0.2 mg/mL 75 nm citrate coated Ag NPs. (C) pH dependence of oxygen generation obtained from data depicted in (B). Sample solutions were purged with nitrogen for 15 min prior to mixing.

ESR oximetry was also employed to determine the correlation between O_2 production and the particle size of Ag NPs. At pH 11, all of the Ag NPs with diameter from 10 nm to 100 nm induced oxygen production during decomposition of H_2O_2 (Figure 3-11). The Ag NPs having diameters of 10 nm and 20 nm showed greater activity in generating O_2 as

evidenced by the disappearance of super hyperfine splitting and significant flattening of hyperfine splitting in the ESR spectrum of CTPO. As larger Ag NPs were used, O_2 production diminished. We have examined the effect of particle size on O_2 production at pH 11.0 and 7.4 (Figure 3-11). Similar correlations between size and O_2 production were observed at each pH except for the 10 nm Ag NPs which needs further investigation.

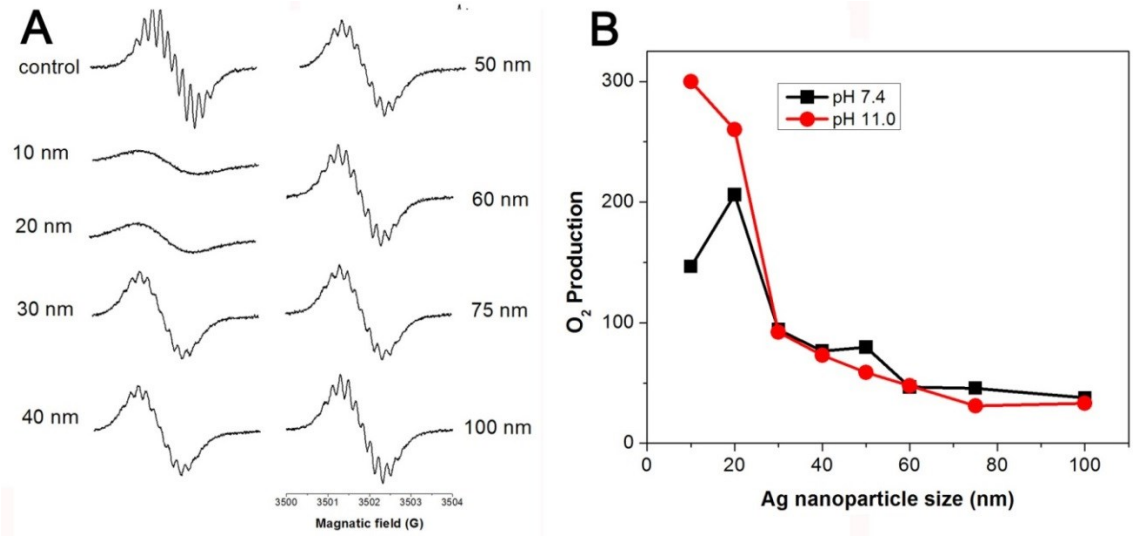

Figure 3-11 Generation of O_2 induced by Ag NPs having different sizes. (A) ESR spectra of CTPO in presence of H_2O_2 and Ag NPs having different sizes at pH 11.0. (B) Dependence of oxygen generation on Ag NPs size at pH 11.0 and 7.4. Conditions: 0.1 mg/mL CTPO + 5 mM H_2O_2+10 mM pH 11.0 (or 7.4) buffer + 0.025 mg/mL citrate coated Ag NPs at pH 11.0 (0.05 mg/mL citrate coated Ag NPs at pH 7.4). ESR spectra were recorded at 0.5 min and all sample solutions were purged with nitrogen for 15 min prior to mixing.

3.3.5 Reaction mechanism for the O_2 production

We examined the mechanism for O_2 generation to determine if net oxidation of Ag NPs occurred during decomposition of H_2O_2 or if Ag NPs had a catalase-like activity. First, we measured the oxidation kinetics of Ag NPs in buffers at different pHs. Ag NPs have a unique SPR absorbance band with a peak around 400 nm. The absorbance intensity of the SPR yields information about the particle concentration and the peak position of the SPR is representative of the particle size and shape (*260*). Accordingly, the oxidative dissolution of Ag NPs will be accompanied by a decrease in the intensity and wavelength shift of SPR,

which can be monitored by using UV-vis spectroscopy. Figure 3-12 shows the pH dependence for oxidative dissolution of Ag NPs. Dissolution of Ag NPs proceeded faster at higher pH in agreement with a previous study (*238*). H_2O_2 has a slightly lower standard reduction potential (0.88 V) in basic solutions. The increased oxidation rate with increasing pH might be due to the formation of an Ag^+ complex with OH^- at higher pH thus lowering the reduction potential of Ag^+/Ag (*261*). It is interesting that the similar pH dependence was noted for the dissolution rate of Ag NPs and generation of O_2 (Figure 3-10B). This similar pH dependence is consistent with a mechanistic link between oxygen production and dissolution of Ag NPs with release of Ag^+.

$O_2 + H_2O+2e^- \rightarrow HO_2^- + OH^-$ (φ = -0.076 V)

Serving as a strong reducing agent in alkaline environment, H_2O_2 may reduce Ag^+ to Ag and produce O_2 in an overall reaction as following:

$2Ag^+ + HO_2^- + OH^- \rightarrow 2Ag + O_2 + H_2O$

This reaction is preferred as the net standard redox potential is 0.8756 V (*261*). We have observed that Ag^+ can be reduced with concomitant generation of O_2 at pH 11.0 (data not shown). Therefore at higher pH, Ag NPs may participate in a cyclic reaction between elemental silver (i.e., Ag NPs) and Ag^+. This cyclic reaction was indirectly verified by an interesting observation that the sample solutions at pH 11.0 containing 10 or 20 nm Ag NPs remained the distinctive color of Ag NPs but the ones in lower pH buffer diminished to colorless during formation of oxygen. This observation may be attributed to the poor reducing ability of H_2O_2 in acidic solution resulting in very limited reduction of Ag^+ to Ag.

To further confirm the existence of a cyclic reaction, the spectra of sample solutions containing 10 nm Ag NPs were monitored using a UV-VIS spectrophotometer (Figure 3-13A and B). For samples at pH 4.6, the SPR intensity for 10 nm Ag NPs gradually decreased and the absorbance peak position showed little time dependence. In contrast, the SPR intensity of samples at pH 11.0 exhibited an initial reduction followed by an increase. These changes in SPR intensity were accompanied by a shift to longer wavelength for the SPR peak position (Figure 3-13B right inset). These results are consistent with concurrent oxidation of Ag NPs and reduction of Ag^+ by H_2O_2 at pH 11.0. The re-formed silver NPs may be different from original nanoparticles with respect to shape and size. In contrast, the oxidative dissolution of Ag NPs dominated at lower pHs due to the poor reducing ability of H_2O_2. This dynamic cyclic reaction may be expected to proceed until H_2O_2 is consumed. This expectation is confirmed by the declining intensity of the H_2O_2 spectrum (inset in Figure 3-13B left inset). Moreover, TEM was employed to examine the morphology of Ag NPs before and after reaction with hydrogen peroxide at different pHs. Compared with original 10 nm spherical and uniform Ag NPs (Figure 3-13C), larger and more irregular shaped nanoparticles were formed at pH 11.0 (Figure 3-13D). This observation is additionally consistent with re-formation Ag NPs at this pH. At pH 4.6, Ag NPs were oxidized and barely observed under TEM, ostensibly due to the low rate of Ag^+ reduction by H_2O_2 at this pH. Therefore, 10 nm Ag NPs at pH 11.0 can be viewed to have an activity similar to catalase, which catalyzes the H_2O_2 decomposition to O_2, because Ag NPs persist during generation of O_2. Our results demonstrate how the activity of Ag NPs is strongly controlled by the chemical environment. Two factors contributed to the interesting phenomena we observed: 1) the pH dependent redox behavior of H_2O_2 and 2)

behavior of Ag NPs in different chemical environments. Hydrogen peroxide is a weak acid (pK_a 11.6). Therefore, its physical and chemical properties, including ionization, dissociation and standard reduction potential, can be changed by adjusting pH. As a result, pH changes the oxidizing/reducing activity of $H_2O_2$and its reaction pathway (*248*). The effects of Ag NPs on pH dependent generation of hydroxyl radical and O_2 may be viewed as an expression of their general ability to facilitate electron transfer. As we have observed, the nature of the facilitated reactions is defined by factors such as pH. At low pH, hydroxyl radicals are formed during Ag NP-assisted decomposition of H_2O_2 accompanied by the dissolution of Ag NPs. At high pH, O_2 is formed via a cyclic process wherein Ag NPs increase in size, indicating of dissolution of smaller Ag NPs and formation of larger Ag NPs. These observations are illustrated in Scheme 3-1. Without Ag NPs, hydrogen peroxide alone can neither generate hydroxyl radicals at lower pH nor rapidly generate oxygen at higher pH. Here Ag NPs trigger and amplify the effects of pH on the redox activity of H_2O_2. In the presence of Ag NPs, one can switch between the generation hydroxyl radicals and oxygen during decomposition of H_2O_2 by adjusting the pH.

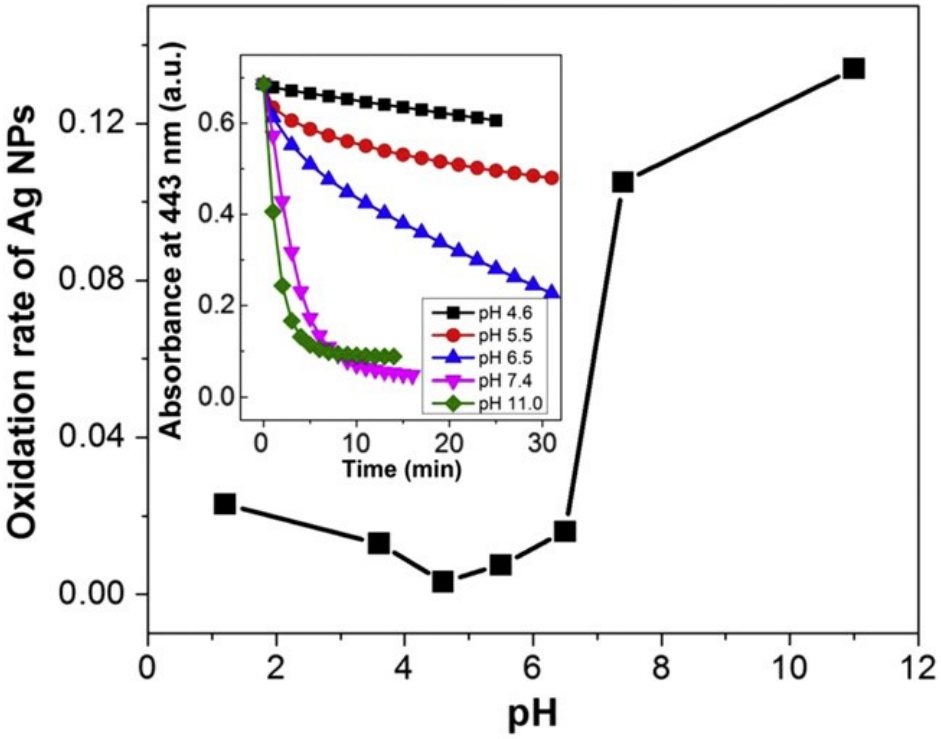

Figure 3-12 pH dependence for the oxidative dissolution of Ag NPs. Inset represents absorbance at 443 nm as a function of time after addition of Ag NPs at different pH (4.6, 5.5, 6.5, 7.4, and 11.0). Reaction conditions: 2.5 mM H_2O_2, 0.01 mg/mL 75 nm citrate coated Ag NPs, and 10 mM buffer at room temperature. Oxidation rate means the initial reaction rate calculated by measuring the absorbance variance along with time using UV-VIS spectroscopy scanning kinetics mode.

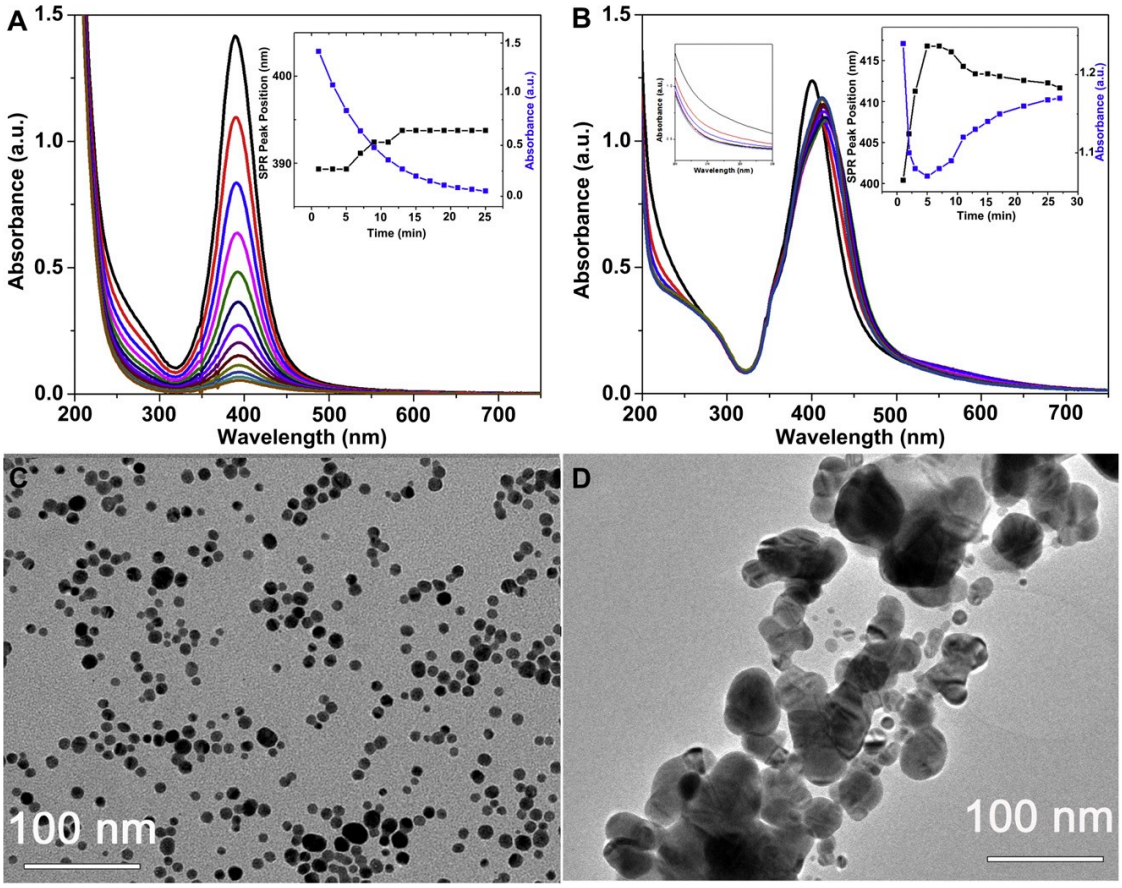

Figure 3-13 Evolution of UV-VIS spectra for 0.01 mg/ml 10 nm citrate coated Ag NPs in the presence of 5 mM hydrogen peroxide in pH (A) 4.6 and (B) 11.0. The right hand inset shows the corresponding SPR peak position and the SPR absorbance variation as a function of time. The left hand inset in (B) represents the spectrum of H_2O_2 at different times after mixing. TEM images of 10 nm Ag NPs before (C) and after (D) Reaction with H_2O_2 (pH 11.0). Conditions for TEM: 10 mM H_2O_2, 10 mM buffer, reaction time 30 min at room temperature.

3.4 Conclusion

In summary, by using ESR coupled with spin trapping and spin labeling, we have demonstrated that Ag NPs can induce ·OH and O_2 production in the presence of H_2O_2. This work identified ·OH as the ROS induced by Ag NPs. Generation of hydroxyl radicals and oxygen were strongly dependent on pH. The generation of hydroxyl radicals and oxygen was based on a Fenton-like reaction in an acidic environment and redox reaction in an alkaline environment, respectively. Our results indicate that alteration of the balance between hydroxyl radicals, oxygen and hydrogen peroxide should be considered when assessing the effects of Ag NPs.

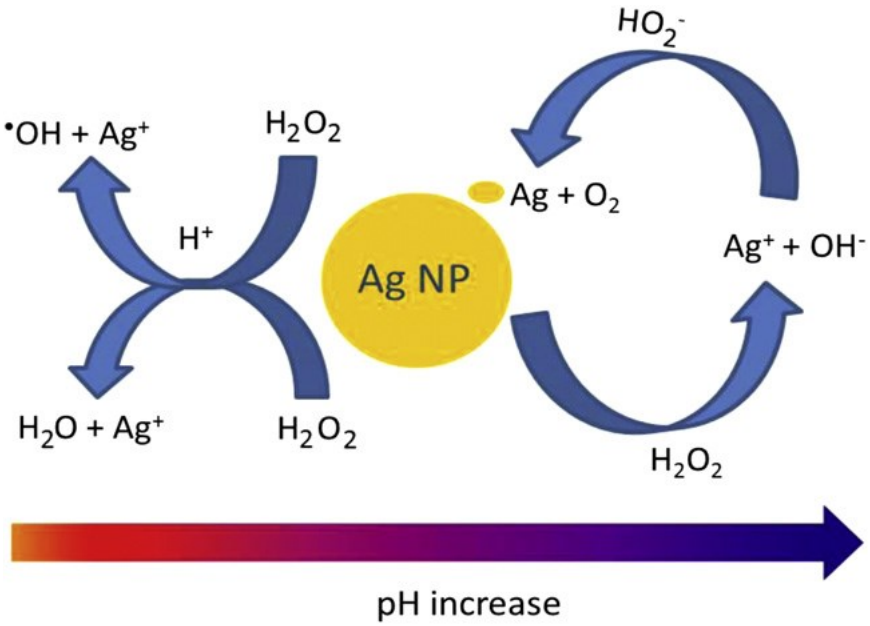

Scheme 3-1 Schematic presentation of Ag NPs triggering the generation of hydroxyl radicals and oxygen controlled by pH.

3.5 Acknowledgment

This article is not an official US Food and Drug Administration (FDA) guidance or policy statement. No official support or endorsement by the US FDA is intended or should be inferred. This work was supported by a regulatory science grant under the FY11 FDA Nanotechnology CORES Program. We thank Dr. John H. Callahan (CFSAN/FDA) for valuable suggestions and comments on the manuscript. We acknowledge the support of the Maryland Nano-Center and its NispLab. The NispLab is supported in part by the NSF as a MRSEC Shared Experimental Facility.

Chapter 4: Effect of silver nanomaterials on activity of thiol-containing antioxidants

4.1 Introduction

Reactive oxygen species (ROS) including hydrogen peroxide (H_2O_2), superoxide radical ($O_2^{\cdot -}$), and hydroxyl radical (·OH) can damage a variety of cellular targets. Oxidative damage caused by ROS has been implicated in a number of acute and chronic diseases. Antioxidants, such as ascorbic acid and glutathione, are important physiological defenses against oxidative damage. Glutathione, including reduced (GSH) and oxidized (GSSG), is synthesized in all mammalian cells. Glutathione has diverse physiological functions including detoxification, maintenance of essential thiol status, antioxidant activity, and regulation of growth and death (*8*). Dysregulation of GSH synthesis may cause aging (*262*) and many diseases (*263*), e.g. diabetes mellitus (*264*), cholestasis (*265*), endotoxemia (*266*), alcoholic liver disease (*267*), and cancer and drug-resistant tumors (*268*). Typically, ROS are reduced by cellular GSH, forming GSSG, which is in turn reduced back to GSH by GSH reductase. In this way, GSH can prevent oxidative damage elicited by ROS. A precursor of GSH, the amino acid cysteine is also believed to play an essential role in reversible redox reactions in cells to limit damage attributable to ROS (*269, 270*).

Silver usage in medical applications can be traced back for centuries and current nanotechnology enables more widely and sophisticated applications of nanoscale silver. In many cases, silver nanomaterials are used in food, health care and consumer products as an antimicrobial agent (*271*). Because of the increasing use of Ag nanomaterials, there is a need to thoroughly understand their bioactivity and safety under conditions of use. A number of investigators have examined cytotoxicity and genotoxicity resulting from exposure to Ag nanomaterials (*272*). We have previously investigated the interaction

between Ag nanoparticles and biologically relevant agents and predicted the mechanisms of potential toxicity due to generation of ROS in Chapter 3. To fully understand the bioactivity and potential toxicity of Ag nanomaterials, one must consider their interactions with components of biological systems. Because it is well established that Ag nanomaterials participate in redox reactions, it is important to understand the effects of Ag nanomaterials on cellular components involved in redox homeostasis. Antioxidants with sulfhydryl functional groups are among those for consideration. These antioxidants include the endogenous antioxidants glutathione (GSH), cysteine (Cys), and dietary antioxidants dihydrolipoic acid (DHLA) and N-acetyl-L-cysteine (NAC).

The results reported by Piao and coworkers suggest that Ag nanoparticles (NPs) can induce generation of ROS, reduce intracellular levels of GSH and sequentially lead to apoptosis of human liver cells (*199*). It has also been reported that in rat liver cells, exposure to Ag NPs resulted in decreased mitochondrial function accompanied by a reduction in intracellular GSH levels (*273*). Reduction in levels of GSH always accompanied the cytotoxicity resulting from exposure to Ag NPs. However, detailed knowledge about the interactions among ROS, GSH, and Ag NPs is lacking. Other thiol-containing antioxidants, NAC has been reported to protect both normal and tumor human cells from cytotoxicity induced by Ag NPs (*274, 275*). However, the underlying protective mechanism is still unclear.

The strength of the chemical bond between thiol groups and Ag has suggested many commercial applications and has important physiological implications. Sellers et al. have examined reactions between thiols and Ag as a method for producing self-assembling monolayers (*276*). In addition, the affinity of Ag for thiol groups may be exploited for

production of biosensors for detecting cysteine, homocysteine, and GSH (*277, 278*). Liu et al. have described the importance of interactions between Ag NPs and endogenous thiol-containing compounds during chemical transformations of Ag NP in physiological systems (*279*). In their studies, dissolution of Ag NPs during digestion to yield Ag^+ played an important role in formation of products between Ag and thiol-compounds.

We have investigated the effects of Ag nanomaterials on the antioxidant activity of physiologically and commercially important thiol-containing antioxidants. Antioxidant activity was assessed as the ability to quench radicals. In the present study, we examined quenching of four radicals: DPPH, azo radical, hydroxyl radical, and superoxide radical. Using DPPH, we examined the effects of silver nanoparticles on the scavenging capability of both hydrophilic and lipophilic thiol-containing antioxidants. DPPH was also used to study the temperature dependence for the interaction between silver nanorods and thiol-containing antioxidants. Finally, we examined the effects of silver nanorods on the ability of GSH and cysteine to quench the ROS, superoxide radical and hydroxyl radical.

4.2 Materials and Methods

4.2.1 Materials

Silver nanoparticles (50 nm) with a spherical morphology and coated with polyvinylpyrrolidone (PVP) or citrate were purchased from nanoComposix, Inc. (San Diego, CA) and used as received. Au@Ag nanorods with cetrimonium bromide (CTAB) (Au nanorods: ~60 nm in length and ~15 nm in width; Ag shell: ~10 nm in thickness) were gifted from Dr. X.C.Wu at National Center for Nanoscience and Technology, China. The detailed preparation of Au@Ag nanorods was previously described (*280*). The spin trap α-(4-pyridyl-1-oxide)-N-tert-butylnitrone (4-POBN), xanthine, ethanol, phosphate salts (Na_2HPO_4 and NaH_2PO_4), diethylenetriaminepentaacetic acid (DTPA), L-glutathione,

reduced (GSH), L-cysteine (Fluka™) were all purchased from Sigma-Aldrich (St. Louis, MO). 2,2'-Azobis[2-(2-imidazolin-2-yl)propane] dihydrochloride (AAPH) was purchased from Wako Chemicals (Richmond, VA). 1-Hydroxy-3-carboxy-2,2,5,5-tetramethylpyrrolidine·HCl (CP·H) was obtained from Enzo® Life Sciences (Farmingdale, NY). Dihydrolipoic acid (DHLA) was purchased from EMD Millipore (Billerica, MA). Zinc oxide nanoparticles aqueous dispersion (20 wt%, 30-40 nm) was purchased from US Research Nanomaterials, Inc (Houston, TX). Before use, phosphate buffer was treated with Chelex® 100 molecular biology grade resin from Bio-Rad Laboratories (Hercules, CA) to remove trace metal ions. Milli-Q water (18 MU cm) was used for all solution preparations.

4.2.2 Characterization

UV-vis spectroscopy was used to characterize changes in nanomaterials during reaction with glutathione. UV-vis absorption spectra were obtained using a Varian Cary 300 spectrophotometer. Silver nanoparticles coated with polyvinylpyrolidone (Ag(PVP)) or citrate (Ag(cit)) (0.01 mg/ml) were mixed with 1 mM GSH individually in water while Au@Ag nanorods with CTAB (0.1 nM) were mixed with 1 mM GSH in 0.1 mM CTAB to stabilized Ag nanorods. To monitor the progress of the reaction, absorption spectra were collected at 1 min intervals using the scanning kinetics mode of the spectrophotometer.

Nanomaterials were additionally characterized using transmission electron microscopy (TEM) images, captured on a JEM 2100 FEG (JEOL) transmission electron microscope at an accelerating voltage of 200 kV located at the NanoCenter, University of Maryland, College Park, MD. To observe the morphological evolution of the nanoparticles before and after incubation with GSH, 0.1 mg/mL Ag NPs and 0.1 nM Au@Ag NRs were mixed with 10 mM GSH for 10 min and twice centrifuged (12,000 rpm, 5 min). After the supernatants were decanted, 20 microliter water was added to redisperse the precipitates. The samples

for TEM analysis were prepared by adding drops of the redispersed colloidal solutions onto standard holey carbon-coated copper grids, which were then air dried at room temperature.

4.2.3 DPPH radical scavenging activity

The scavenging activity for DPPH, a stable radical, by antioxidants containing thiol groups was estimated as we previously described (*281*). Stock solutions of cysteine (Cys) and reduced glutathione (GSH) were prepared in water. Solution of dihydrolipoic acid (DHLA) was prepared in ethanol. The control solution contained 0.2 mM DPPH and 10% (20% for DHLA study) (v/v) ethanol in 0.1 mM pH 7.4 phosphate buffer. Ag nanomaterials or each of the three thiol containing antioxidants were added to DPPH control alone to evaluate their individual scavenging effect on DPPH radical. Then, Au@Ag NRs CTAB were pre-incubated with Cys, GSH, or DHLA at 37 ^{o}C for 10 min prior to addition to DPPH radical control.

To estimate the effect on GSH, three silver nanomaterials were used: were Ag(cit), Ag(PVP), and Au@Ag nanorods (NRs). The Ag NPs and Au@Ag NRs were 0.01 mg/ml and 0.1nM, respectively. GSH or each of the three silver nanomaterials was added to DPPH control alone to examine their individual reducing effect on DPPH radical. GSH was premixed with different Ag NPs at 37 ^{o}C for 10 min. ESR spectra were recorded 1 min after mixing DPPH radical with other reagents using the following instrument settings: microwave power 20 mW; field modulation 1.5 G; and scan range 100 G. The signal intensity of DPPH radical in sample solutions was normalized to that in DPPH control solution.

4.2.4 Azo radical scavenging activity

We examined the ability of GSH to scavenge azo radicals, in the absence and presence of Au@Ag NRs. Azo radicals were generated by the thermal decomposition of the

hydrophilic radical generator AAPH. Scavenging of azo radical was determined by ESR using 4-POBN as the spin trap in PBS (10 mM pH 7.4). Twenty μM GSH was pre-mixed with 0.1 nM Ag NRs at 23 or 37 ºC for 10 min to study the temperature dependence for the reaction between GSH and Au@Ag NRs. Each sample was then mixed with 50 mM 4-POBN and 10 mM AAPH. Thereafter, the mixture was incubated in water bath (37 ºC) for 10 min to generate azo radicals. ESR spectra were recorded 1 min after sample removal from water bath. The instrument settings: 20 mW microwave power; 1 G field modulation; and 100 G scan range, were used for present and following ESR experiment.

4.2.5 Hydroxyl radical (·OH) scavenging activity

Hydroxyl radicals were produced by irradiating a zinc oxide nano dispersion with light emitted from a 500 watt Xe arc lamp directed through a WG320 filter. This filtered light source emits radiation having wavelengths greater than 350 nm (*282*). The yield of ·OH was quantified using the spin trap 4-POBN in solution containing ethanol (20%, v/v) (*253, 283*). The final control mixtures contained 0.02 mg/ml ZnO dispersion, 1mM 4-POBN, and 20% ethanol (v/v) in 10 mM pH 7.4 phosphate buffer. Au@Ag nanorods were preincubated with GSH or Cys at 37 ºC for 10 min prior to photoirradiation of the ZnO control mixture. ESR spectra were recorded 4 min after the initiation of exposure to light.

4.2.6 Superoxide radical ($O^{\bullet -}_2$) scavenging activity

Superoxide radical oxidizes CP-H, which is ESR silent, to a stable nitroxide radical CP· that is detectable by ESR spectroscopy (*284*). The xanthine-xanthine oxidase system (XAN-XOD) was used to generate the superoxide radical. The final control mixtures contained 1 mM xanthine, 0.1mM CP-H, 0.1 mM DTPA and 0.2 U/mL XOD in 10 mM pH 7.4 phosphate buffer. Au@Ag nanorods were preincubated with 10 mM GSH or Cys

at 37 °C for 10 min before addition to the control mixture without XOD. Radical generation was initiated by addition of XOD, and the ESR signal was recorded 4 min afterwards.

4.3 Results and Discussion

Silver nanomaterials have been widely used in cosmetics, dietary supplement, food packaging, medical devices and accessories, electronics clothing, textiles, and various household products (*219-222*). The goal of this study was to show the potential effect of Ag nanomaterials on the antioxidant activity of thiol-containing antioxidants. We have investigated antioxidant activity by studying biologically relevant hydroxyl and superoxide radicals, as well as the DPPH and azo radicals.

4.3.1 Characterization of Au@Ag nanorods and Ag nanoparticles

The UV-vis spectra of noble metal nanoparticles can be used to monitor their size and aggregation state. This property derives from the surface plasmon resonance (SPR) attributable to these nanoparticles. UV-vis extinction spectra of the silver nanoparticles are illustrated in Figure 4-1. Both Ag(cit) and Ag(PVP) (50 nm) show an absorption peaked at 420 nm. The nanoparticles were well dispersed due to the protection of coatings that prevent aggregation. When incubated with GSH, the adsorption maximum of both Ag NPs gradually decreased in intensity and a second absorption maximum appeared at progressively higher wavelength. The initial reduction rate of peak at 420 nm of Ag(cit) and Ag(PVP) was 0.26 and 0.17 min^{-1}, respectively. These spectral changes indicate that the silver nanoparticles are aggregating and may be attributable to the formation of a Ag-S bond. However, the maximum adsorption of Ag(cit) diminished faster than that of Ag(PVP). This may because the neutral PVP coating is not as readily displaced from the surface of Ag NPs as the negatively charged citrate coating. The characteristic SPR peak of in-house prepared Au@Ag NRs with CTAB was unaffected during incubation for 5 min

in absent of GSH (data not shown, but consistent with previous report (*280*)), but the intensity slightly decreased in presence of GSH. The inconspicuous alteration of the SPR peaks of the nanorods may be a consequence of excessive CTAB, a good positively charged stabilizer.

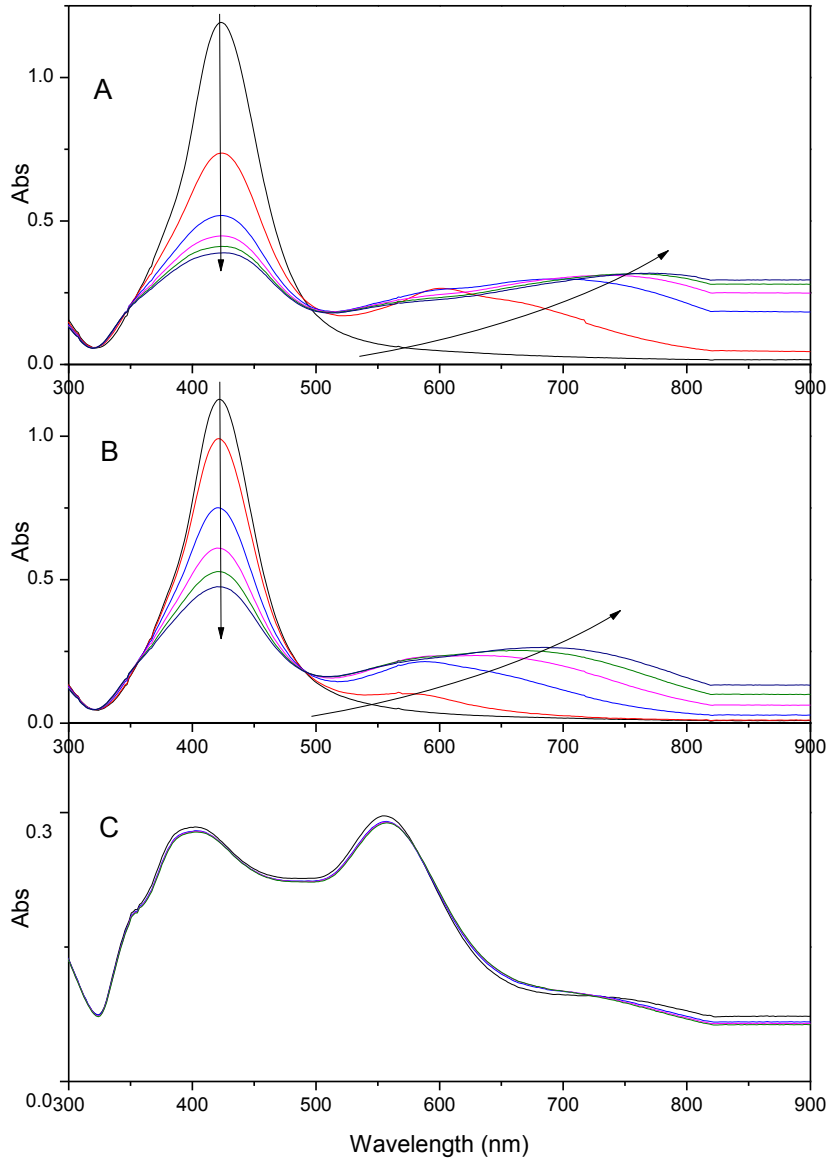

Figure 4-1 Evolution of UV-vis spectra of Ag nanomaterials incubated with GSH at 23 ºC. The spectra were recorded every 1 min for 5 min. Sample solutions included 1 mM GSH and 0.01 mg/ml Ag NPs Citrate 50 nm (A), Ag NPs PVP 50 nm (B), or 0.1 nM Au@Ag NRs CTAB. Arrow indicates increasing time.

The morphology of Ag nanorods and nanoparticles is shown in TEM images (Figure 4-2). The Au@Ag nanorods, which contain a molar ratio of Ag/Au 0.83, have an orange core/shell structure with Au nanorods as a core (~60 in length and ~15 nm in width) and a thick and anisotropic Ag shell (~10 nm in thickness) (Figure 4-2A). The detailed method for their preparation was previously described (*280*). The morphology and size of Au@Ag nanorods remained the same after reacting with GSH (Figure 4-2A and A').The thin film-like compounds in the TEM image may be solvent residue. The size of Ag(cit) before and after treatment with GSH was 70.09 ± 6.19 and 64.42 ± 7.62 nm, respectively (Figure 4-2B and B'). The slight shrinkage of silver nanoparticles indicates dissolution of Ag(cit) NPs. Since silver is vulnerable to oxidation in oxygenated media, silver ions (Ag^+) are possibly accumulated on the surface of silver nanoparticles. It is noticeable that after reacting with GSH, products having a cross-linked structure appeared. These cross-linked structures may be silver sulfide complexes formed from superficial Ag^+ and GSH. In contrast to changes observed with Ag(cit) NPs the size of Ag(PVP) NPs was 65.60 ± 8.85 and 66.9 ± 6.16 nm, before and after mixing with GSH, respectively (Figure 4-2C and C'). The particle morphology remained the same as well. This observation is consistent with previous reports that the dissolution of Ag NPs coated with citrate is faster than that for Ag NPs coated with PVP (*285*).

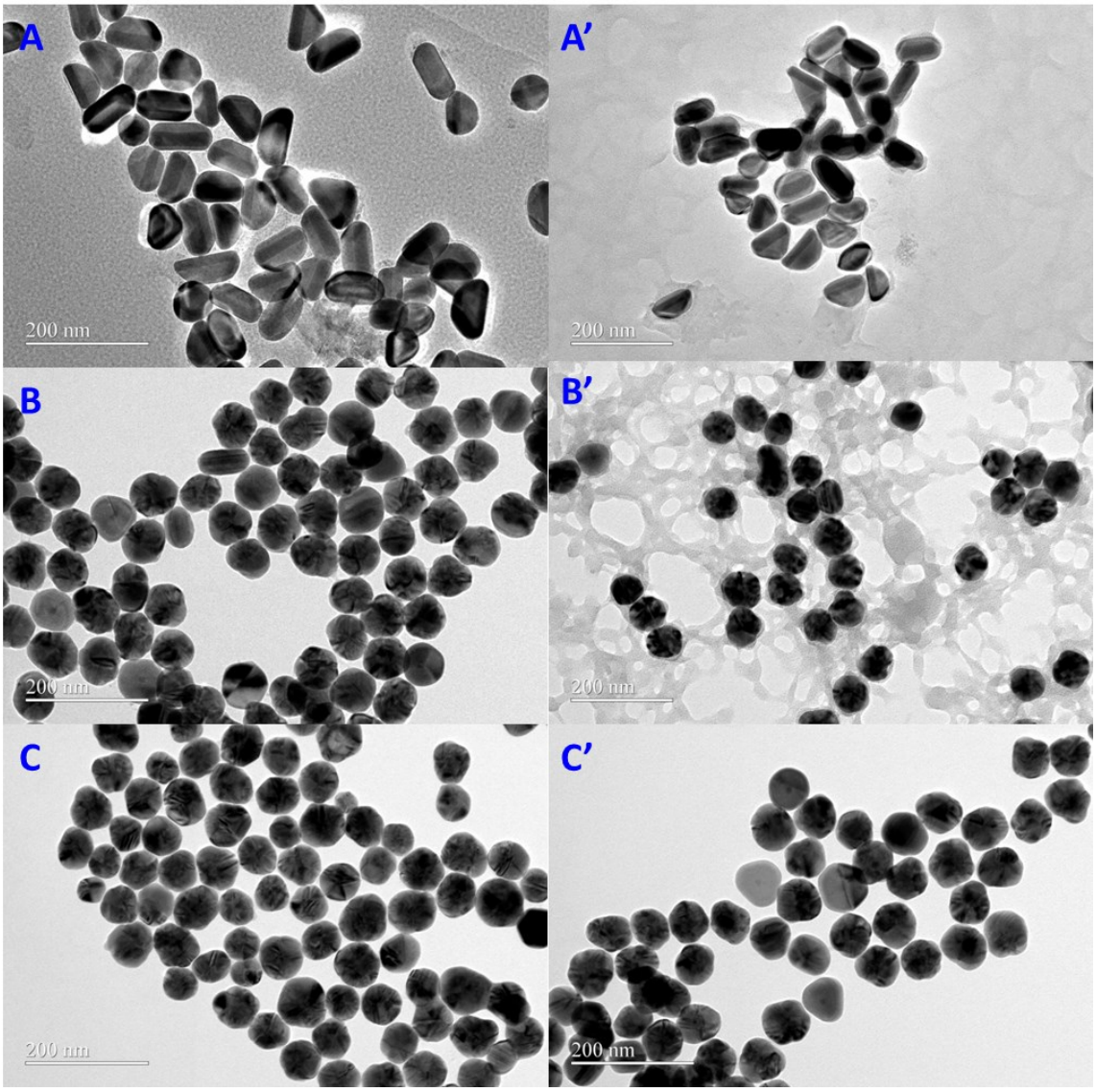

Figure 4-2 TEM image of Au@Ag nanorods (A) and Ag NPs coated with citrate (B) and PVP (C) before (A,B,C) and after (A', B', C') incubation with GSH at 23 ºC for 10 min.

4.3.2 DPPH radical scavenging activity

In many applications, in order to estimate the antioxidant capacity of food or their extracts, the stable nitrogen centered radical DPPH has been used (*286*). The assay has been generally accepted as a simple and sensitive method in antioxidant studies (*287*). DPPH radical is ESR detectable with a one-line spectrum, as shown in the inset to Figure 4-3. When the DPPH radical accepts one H-atom from antioxidants, it becomes ESR silent. In Figure 4-3, the ESR signal intensity from each sample solution was normalized to that from

control solution and expressed as a percentage; thus the antioxidant ability is inversely proportional to the normalized signal intensity. Three thiol-containing antioxidants Cys, GSH, and DHLA all quenched DPPH radical to various extents (Figure 4-3 red). Also, we found that Au@Ag NRs can scavenge DPPH radical (Figure 4-3 blue). When pre-incubated with Ag NRs, the scavenging ability of the three antioxidants was reduced (Figure 4-3 green).

The reduced scavenging ability of the antioxidants may be caused by the replacement of functional –SH with -Ag-S, which is formed through partially electrostatic and partially covalent binding (*288*). It has been previously found that bio-thiols, e.g. homocysteine, cysteine, and glutathione, were absorbed to the surface of Ag NPs *via* conjugated Ag-S bond (*289*). Sulfide complexation of Ag NPs also occurred in formation to Ag_2S or precipitate and the surface of Ag NPs (oxidized to Ag^+) reacted with sulfide anions producing Ag_xS_y (*258*).

In the same range of concentration, the scavenging ability of DHLA was similar to that of GSH. However, after incubating with Au@Ag NRs, the scavenging ability of DHLA was less affected than the scavenging ability of GSH. This indicates a less efficient binding of Ag NRs to DHLA than GSH, which may be attributed to the more bulky structure of DHLA and thus ineffective interfacial contact of DHLA with Ag NRs.

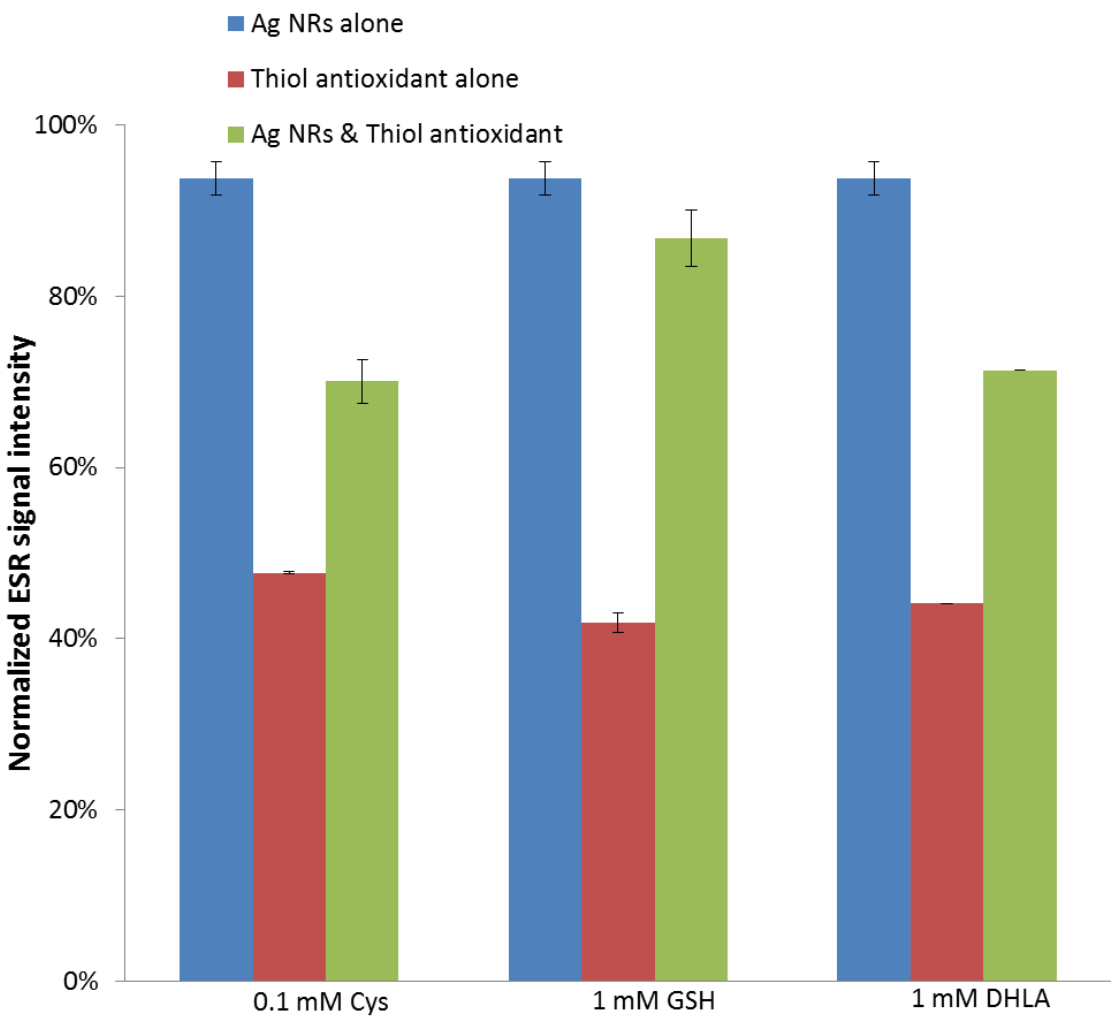

Figure 4-3 DPPH scavenging effect for different thiol-containing hydrophilic and lipophilic antioxidants influenced by 0.1 nM Au@Ag NRs CTAB. The inset shows ESR spectrum of DPPH radical.

Both commercial Ag NPs and the Au@Ag NRs prepared in-house were used to examine their inhibitory effect on the DPPH radical scavenging activity of GSH, an important endogenous antioxidant containing thiol. Direct quenching of the DPPH radical by Ag NPs was observed. Citrate coated Ag NPs quenched the DPPH radical to a greater extent than PVP coated Ag NPs (Figure 4-4 blue). Significant quenching of DPPH was seen in the presence of GSH (Figure 4-4 red). When GSH was pre-incubated with the Ag nanomaterials, the quenching activity of GSH toward DPPH was diminished to varying

degrees (Au@Ag NRs>Ag NPs coated with citrate> Ag NPs coated with PVP). The results suggest a greater affinity of GSH to citrate-coated Ag NPs than PVP-coated Ag NPs. The result is in agreement with the previous finding that GSH induced more rapid aggregation of Ag NPs with citrate (Figure 4-1). Among them, pre-incubation of GSH with the Au@Ag NRs had the most effect on GSH's ability to quench DPPH. This indicates that the Ag layers in an orange slice-like shape partially deactivate GSH due to the formation of Ag-S bond.

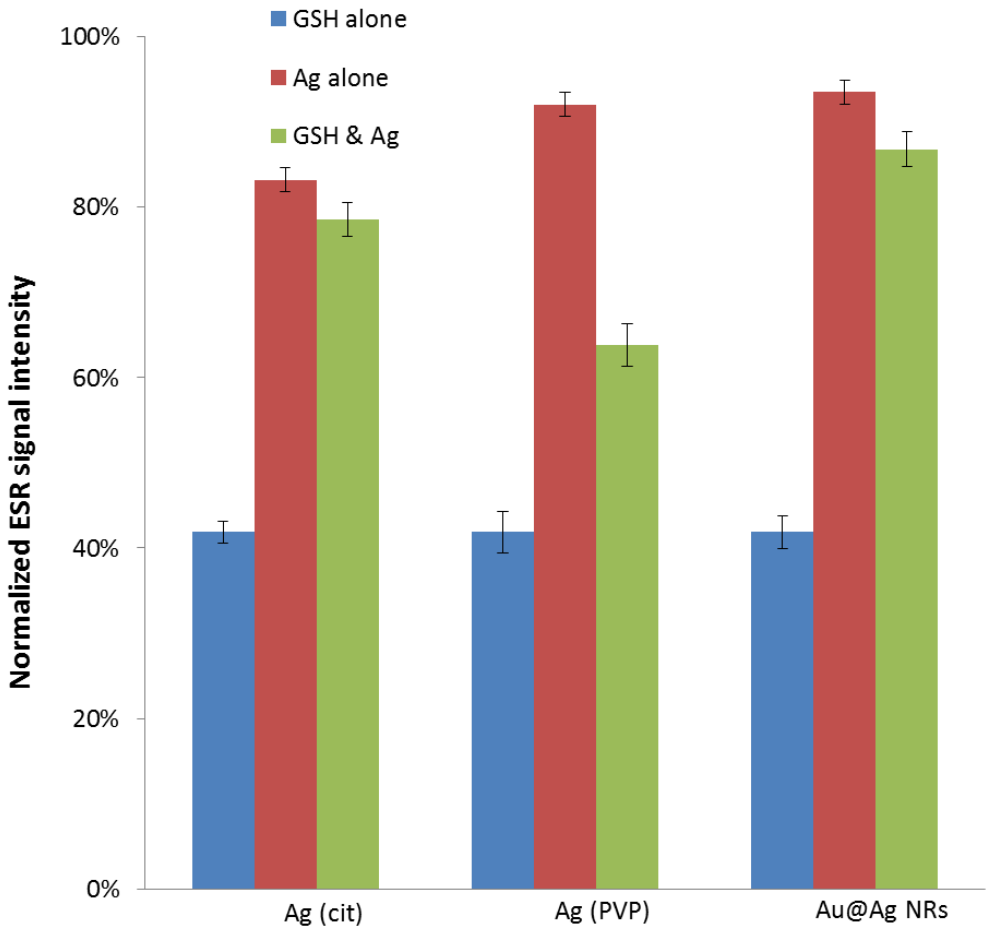

Figure 4-4 Effect of Ag nanomaterials on DPPH radical scavenging by 1 mM GSH. Ag nanomaterials including 0.01 mg/ml Ag NPs in Citrate or PVP and 0.1 nM Au@Ag NRs were pre-incubated with GSH. The control sample included 0.2mM DPPH and 10% ethanol in 10mM pH 7.4 phosphate buffer.

4.3.3 Azo radical scavenging activity

AAPH is a hydrophilic radical generator widely used as an inducer of lipid peroxidation in many in vitro assays to determine antioxidant activity (*290-292*). AAPH undergoes thermal decomposition to generate azo radicals, which can be trapped by 4-POBN to form spin adduct 4-POBN/·A (*293*). In the presence of 10 mM AAPH, AAPH derived radicals were detected in the form of 4-POBN/·A with hyperfine splitting parameters of a_N = 14.92 G, a_H = 2.57 G, shown as 6 lines shape (Figure 4-5), which are similar to previous reports (*293*). With the addition of Au@Ag NRs, the intensity of the characteristic signal was slightly reduced, while 1 mM GSH nearly eliminated the signal for the spin adduct. The interaction between the Au@Ag NRs and GSH, and effects on scavenging azo radicals generated by AAPH was investigated at 23 ^{o}C and at a physiologically relevant temperature, 37 ^{o}C. As seen clearly in spectra 5 and 6 of Figure 4-5, premixing of Au@Ag NRs at both temperatures reduced scavenging of azo radicals by GSH. This reduction in GSH's scavenging activity was more pronounced at the higher temperature. This is indicating that GSH was more vulnerable to adsorb on Ag NRs and thus to form Ag-S bond at elevated temperature. Therefore, less GSH was available in electron donating from its thiol group to azo radical.

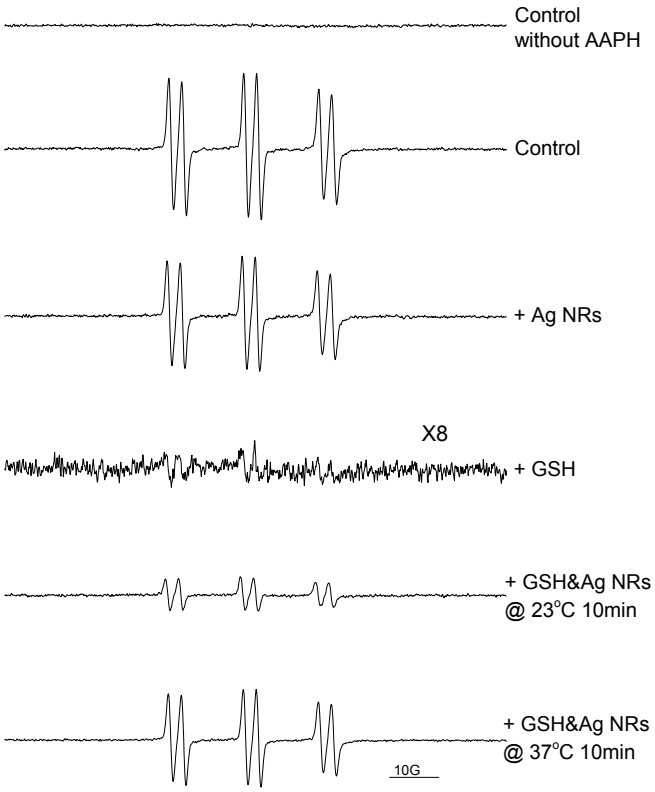

Figure 4-5 AAPH radical scavenging effect of 1 mM GSH impacted by 0.1 nM Au@Ag NRs. Control sample contained 10 mM AAPH and 50 mM 4-POBN in 10 mM pH 7.4 phosphate buffer.

4.3.4 Hydroxyl radical scavenging activity

As the most reactive ROS, hydroxyl radicals (·OH) are an excellent indicator to estimate antioxidant property of a target compound. Because of the reactivity of hydroxyl radicals, we utilized a double spin trapping system, in which the radical product from ·OH and a ·OH scavenger, usually an organic solvent such as ethanol, is trapped by a nitrone-based spin trap (*253*). In the current study, hydroxyl radicals were generated by irradiating an aqueous suspension of ZnO. The hydroxyl radicals then reacted with ethanol followed by the formation of spin adduct 4-POBN/·$CH(OH)CH_3$. This spin adduct has a characteristic a six-line ESR spectrum with splitting parameters of a_N = 15.58 and a_H = 2.60. The introduction of Au@Ag NRs alone slightly changed the shape and amplitude of the ESR

signal expected for 4-POBN/·CH(OH)CH_3 spin adduct (Figure 4-6 spectra 1 and 2). Antioxidants cysteine and GSH had comparable power in reducing the signal of hydroxyl radical (Figure 4-6 spectra 3 and 5). Thiol-containing antioxidants quench the hydroxyl radical by donation of one electron or H-atom from sulfhydryl group to the hydroxyl radical with concomitant formation of a relatively unreactive thiyl radical, which cannot be trapped by 4-POBN. After premixing at a biologically relevant temperature, Au@Ag NRs influenced the ability of both GSH and cysteine to react with hydroxyl radicals to different degrees. The scavenging capability of cysteine was almost completely diminished (Figure 4-6 spectrum 6), while a substantial amount of scavenging remained for GSH (Figure 4-6 spectrum 4). This may be caused by structure of GSH, which may have placed steric limitations on its interaction with Au@Ag NRs compared to cysteine.

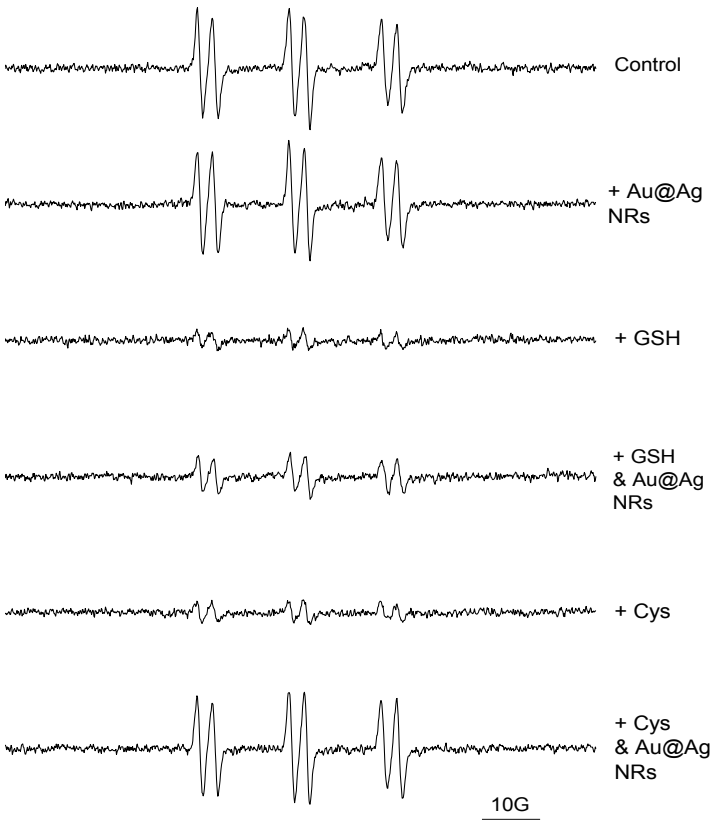

Figure 4-6 Hydroxyl radical scavenging effect of 10 mM Cys and GSH affected by 1 nM Au@Ag NRs. Control sample consisted of 0.02 mg/ml ZnO dispersion, 1mM 4-POBN, and 20% ethanol in 10mM pH 7.4 phosphate buffer.

4.3.5 Superoxide radical scavenging activity

Superoxide radical ($O_2^{\cdot-}$) is another physiologically important ROS which is continuously generated in cells. The endogenous antioxidant enzyme superoxide dismutase (SOD) is a critical part of the cellular defense against superoxide radical. As with other radicals, superoxide radicals can be trapped by ESR-silent spin probe such as DMPO and BMPO to form a stable nitroxide radical DMPO/·OOH and BMPO/·OOH, respectively. In addition, superoxide radicals can oxidize CP-H to CP·, which may be identified and quantified by ESR. However, the reaction rate of superoxide radical with CP-H is significantly higher than other spin traps (*284, 294*). Therefore CP-H may be used at lower concentrations for

trapping the superoxide radicals, avoiding artifacts due to the introduction of spin probes. Xanthine/Xanthine oxidase system was employed to generate superoxide radicals, which in turn abstract an H-atom from CP-H to form CP·. The ESR spectrum of CP· consists of a three-line spectrum with hyperfine splitting constant a_N = 16.2 G (Figure 4-7). Au@Ag NRs had negligible effect on the production of superoxide radicals (Figure 4-7, spectra 2 and 3), but both cysteine and GSH showed strong quenching activity on the radicals (Figure 4-7, spectra 4 and 6). It has been previously described by Dikalov that nitroxyl radicals, CP·, can be reduced to CP-H by antioxidants GSH, cysteine, and ascorbate (*284*). Pre-incubation of cysteine and GSH with Ag NRs resulted in a partially decreased scavenging ability of the two antioxidants against superoxide radical (Figure 4-7, spectra 5 and 7).

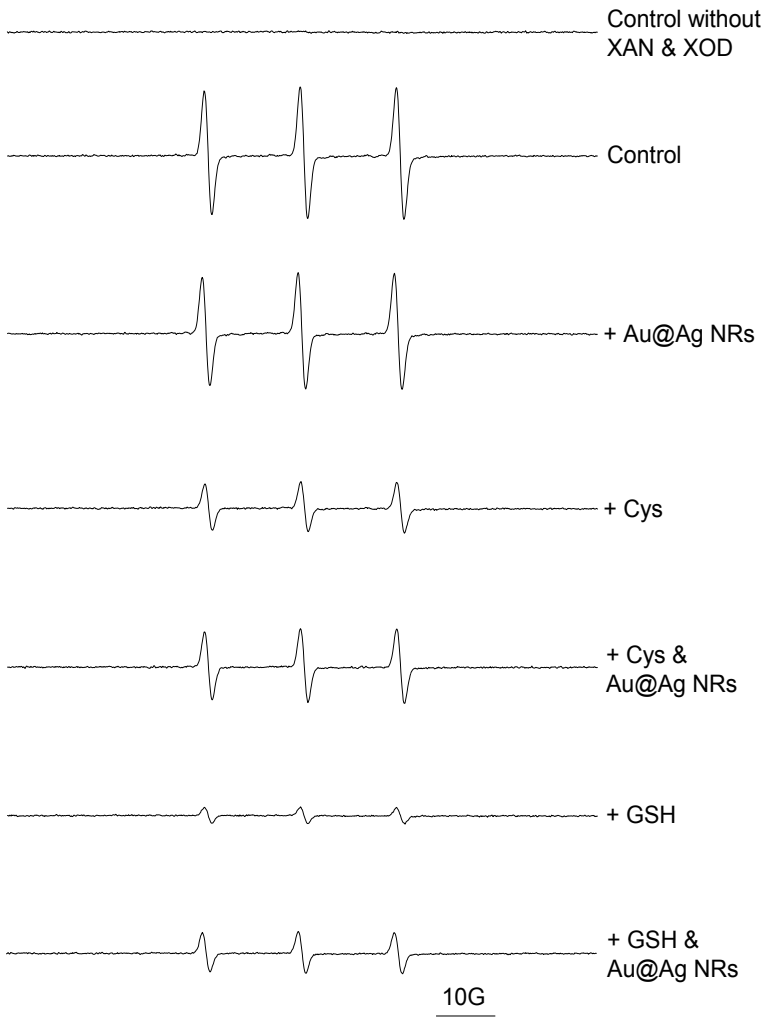

Figure 4-7 Superoxide radical scavenging effect of 10 mM cysteine and GSH influenced by 1 nM Au@Ag NRs. The control solution contained 1mM xanthine, 0.1mM DTPA, 0.1mM CPH, and 0.2 U/ml XOD in 10mM pH 7.4 phosphate buffer.

4.4 Conclusion

Using DPPH radical generation system, all three Ag nanomaterials, Ag(cit), Ag(PVP), Au@Ag nanorods, reduced the quenching of DPPH radical by GSH to varying degrees (Ag(cit), Au@Ag nanorods>Ag(PVP)). We also observed that Au@Ag nanorods reduced the quenching of DPPH by any of the three antioxidants: GSH, cysteine, and dihydrolipoic acid. This may be attributed to the formation of Ag-S, which diminished the reducing ability of sulfhydryl group. In addition, we examined the temperature dependence for effects of Au@Ag nanorods on GSH using azo radical. The effect of Au@Ag nanorods on

scavenging the azo radical was greater at physiological temperature than at room temperature. This would be expected as a result of an accelerated reaction between the sulfhydryl group and Ag NPs at higher temperature. Moreover, Au@Ag nanorods significantly reduced the ability of hydrophilic endogenous antioxidants, GSH and cysteine, to quench hydroxyl and superoxide radicals.

Many previous studies indicate that the toxicity induced by Ag NPs involves oxidative stress or ROS (*199, 273*). Our study directly investigates the effect of Ag nanomaterials on individual free radicals and their potential role in weakening the capability of biologically important and dietary antioxidants. This suggests that Ag nanomaterials may cause oxidative stress by jeopardizing either endogenous or dietary antioxidant defense. The work presented here demonstrates the importance of examining the chemical interactions between nanomaterials used in products and physiologically important antioxidants.

4.5 Acknowledgement

We thank Wayne Wamer at CFSAN/FDA for his valuable discussion and comments. This article is not an official US Food and Drug Administration (FDA) guidance or policy statement. No official support or endorsement by the US FDA is intended or should be inferred. This work was partially supported by a regulatory science grant under the FDA Nanotechnology CORES Program and by the Office of Cosmetics and Colors, CFSAN/FDA (Y.Z., W.H., and J.Y.). We acknowledge the support of the Maryland NanoCenter and its NispLab. The NispLab is supported in part by the NSF as a MRSEC shared experimental facility.

Chapter 5: Enzyme-like activity of Au@Pt nanorods and their combined effect with ascorbic acid

Partially adapted from Zhou, Y. T.; He, W.; Wamer, W. G.; Hu, X.; Wu, X.; Lo, Y. M.; Yin, J. J., Enzyme-mimetic effects of gold@platinum nanorods on the antioxidant activity of ascorbic acid.

5.1 Introduction

Because of their substrate specificity and efficient catalytic ability, enzymes have been commercially used in various areas such as sewage treatment, textile finishing, household products preparation, food and beverage processing (*295*), and energy conversion (*296*). However, since most enzymes are sensitive to environmental conditions and are difficult to prepare in large scale, considerable efforts have been attempted to immobilize enzymes for more convenient preparation, and easier separation of the enzyme from the product, thus facilitating reuse of the enzyme (*297*). In recent years, finding enzyme alternatives has become possible through advances in nanotechnology.

The unique physical and chemical properties of nanoparticles (NPs) have led to their use in a wide range of applications. Amongst these applications, nanoparticles have been found to be candidates as enzyme mimetics with the advantages of low cost, controlled synthesis, tunable catalytic activities, and a high stability even under severe reaction conditions. Currently, peroxidase and oxidase activities have been observed for a number of nanoparticles including ferromagnetic NPs (*298*), FeS (*299*), CuS (*300*), graphene oxide (*301*), Co_3O_4 (*302*), single-walled carbon nanotubes (*303*), gold nanoparticles and clusters (*304-307*), cerium oxide(*308*) and platinum nanoparticles (*182, 309*). These nanoparticles could potentially replace the use of enzymes in biosensors or in biodiagnostic medical devices.

The behavior of nanoparticles as oxidase mimics is of particular interest. In the presence of oxygen, oxidases can oxidatively degrade reducing agents and thus prevent these potent antioxidants from intercepting reactive oxygen species (ROS) (*217*). Examples of biologically important antioxidants are ascorbic acid, uric acid, and polyphenol, which may be oxidatively degraded by ascorbic acid oxidase, uricase, and polyphenol oxidase, respectively. For example, polyphenol oxidase is the main contributor to fruit or vegetable browning and causes degradation of polyphenols. Therefore, along with the application of nanoparticles as enzyme mimetics, the use of NPs could result in deleterious interactions with antioxidants.

The platinum family of NPs has been explored as multi-enzyme mimetics for potential usage in various fields. For example, Pt NPs have been reported to catalyze the peroxidation of 3,3',5,5"-tetramethylbenzidine (*183*) and *o*-phenylenediamine (*182, 260, 310*) in presence of H_2O_2. In conjunction with glucose oxidase and cholesterol oxidase, Pt NPs have been used as replacements for horseradish peroxidase in biosensors for glucose and cholesterol (*182*). Studies have found that bimetallic and biostabilized Pt NPs can scavenge the superoxide radical ($O_2^{-\cdot}$) like superoxide dismutase and reduce H_2O_2 to oxygen like catalase (*188-190*). In addition to their peroxidase-like activity, Pt NPs have been found to resemble uricase in catalyzing oxidation of uric acid (*309*).

Several investigators have examined the biochemical properties of Pt NPs. Rehman et al. have observed reduced inflammatory responses in macrophages treated with Pt NPs (*201*). Kim et al. reported that treatment with Pt NPs extended the lifespan of C. *elegans (311)*. Hamasaki et al. found that Pt NPs lacked cytotoxicity. These investigators also determined that Pt NPs scavenged intracellular ROS such as superoxide radical and hydrogen peroxide,

and protected cells from toxicity elicited by these ROS (*312*). Additionally, Pt NPs have been found to inhibit fatty acid peroxidation and scavenge DPPH radicals, indicating ability to efficiently intercept free radicals (*313*). These studies demonstrated that Pt NPs are excellent antioxidants. While these studies demonstrate that Pt NPs are excellent antioxidants, they did not provide direct evidence that Pt NPs scavenged the most physiologically important radical, hydroxyl radicals. Also, as with many antioxidants, Pt NPs may also exhibit pro-oxidant activity under some conditions. To date, little is known about the interactions between Pt NPs and biologically important antioxidants.

Ascorbic acid (AA), a phytonutrient abundant in fruits and vegetables, is known to protect the human body against chronic diseases due to its antioxidant properties and has been widely used in foods, dietary supplements, and cosmetic products. However, AA is easily degraded through oxidation, especially in the presence of ascorbic acid oxidase (AAO), which exists endogenously in the extracellular matrix of plant cells. AAO mimetics may also reduce the antioxidant activity of AA. Therefore, it is important to identify any AAO-mimetic activity of Pt NPs and understand the interaction between Pt NPs and AA under conditions expected in commercial products.

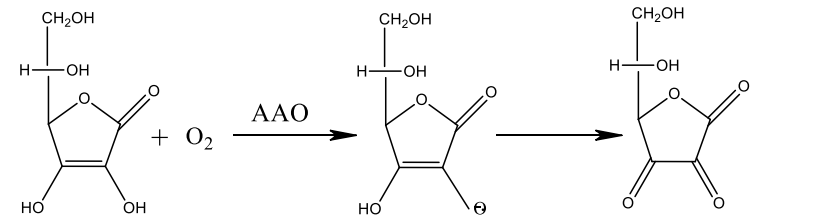

Ascorbic acid Ascorbyl radical Dehydroascorbic acid

Scheme 5-1 Enzymatic oxidation of ascorbic acid in presence of oxygen.

In the current study, Au@Pt nanorods have been found to act as AAO mimetics in catalyzing oxidation of AA to ascorbyl radicals in presence of O_2, which can be detected by Electron Spin Resonance (ESR). ESR spectroscopy with spin trapping is the most reliable and direct method for identification and quantification of short-lived free radicals. Radicals such as ascorbyl radicals can be directly detected via ESR. However, more reactive radicals, such as hydroxyl radicals and superoxide anions, require the use of spin traps for ESR detection (*217, 244, 246*). In addition, ESR was used to compare the thermal and pH stability of Au@Pt nanorods and AAO. The reaction kinetics of AAO and Au@Pt nanoparticles was determined by UV-vis spectroscopy. Using the ESR spin trapping technique, we examined the role of Au@Pt nanorods in scavenging hydroxyl radicals, generated through the Fenton reaction and through excitation of metal oxides with UV radiation. Using three radical generation systems, we compared the antioxidant activity of AA alone and its combined effect with Au@Pt nanorods.

5.2 Experimental

5.2.1 Materials

Sodium borohydride ($NaBH_4$), gold(III) chloride hydrate ($HAuCl_4 \cdot 3H_2O$), cetyltrimethylammonium bromide (CTAB), potassium tetrachloroplatinate (II) (K_2PtCl_4), poly(styrenesulfate) (PSS) were all purchased from Alfa Aesar (Ward Hill, MA) and used as received. The spin traps, 5, 5-dimethyl-1pyrroline N-oxide (DMPO) and 5-(diethoxyphosphoryl)-5-methyl-1-pyrroline-N-oxide (DEPMPO) were purchased from Radical Vision (Marseille, France). The spin trap 5-tert-butoxycarbonyl-5-methyl-1-pyrroline-N-oxide (BMPO) (Alexis® Biochemicals) was obtained from Enzo Life Science, Inc (Farmingdale, NY). Aeroxide® TiO_2 P25 was a gift from EVONIK Industries AG (Frankfurt, Germany). The spin label 3-carbamoyl-2,5-dihydro-2,2,5,5-tetramethyl-1H-

pyrrol-1-yloxyl (CTPO), ascorbate oxidase, 1,1-diphenyl-2-picryl-hydrazyl radical (DPPH•), L- ascorbic acid (AA), ammonium iron(II) sulfate heptahydrate, ZnO, 30% H_2O_2 aqueous solution, standard buffer solutions were all purchased from Sigma Aldrich (St. Louis, MO). Platinum nanoparticles dispersion (3 nm, spherical Pt NPs with no coating) was purchased from US Research Nanomaterials, Inc. (Houston, TX). Each buffer stock solution (pH 1.2 HCl-KCl, pH 4.6 HAc-NaAc, pH 7.4 PBS, pH 9.0 borax and pH 11.0 borax) was 0.1 M. Before use, each buffer was treated with Chelex® 100 molecular biology grade resin from Bio-Rad Laboratories (Hercules, CA) to remove trace metal ions. Milli-Q water (18 MΩ cm) was used for preparation of all solutions.

5.2.2 Synthesis of Au@Pt nanorods coated with PSS

The entire preparation procedure has been described in a previous study (*314*). Firstly, gold nanorods were prepared via seed-mediated growth. CTAB-capped Au seeds were synthesized through chemical reduction of $HAuCl_4$ by $NaBH_4$. After 30 min, growth solution for Au nanorods, consisting of 0.1 M CTAB, 0.024 M $HAuCl_4$, 0.5 M H_2SO_4, 10 mM $AgNO_3$ and 0.1 M AA, was added to Au seeds to initiate the growth of Au nanorods. After 12 h, the Au nanorods were purified by centrifugation (12,000 rpm, 5 min) and the precipitates were collected and resuspended in deionized water for further use. Secondly, the Au nanorods suspension was mixed with a 2 mM K_2PtCl_4 solution. Then, 0.1 M AA was added to the mixture which was shaken vigorously, and then placed in a 30 ^oC water bath. Formation of Au@Pt nanorods was evidenced by a color change from pink-red to dark grey. Additional 0.1 M CTAB was further added to stop the reaction and prevent aggregation of the nanorods. The suspension was centrifuged (10,000 rpm, 5 min) once more and the precipitate was redispersed in deionized water. Lastly, the Au@Pt nanorods solution was mixed with PSS solution, containing 20 mg/ml PSS and 60 mM NaCl, and

placed at 30 °C for at least 3 hr. Subsequently, the reaction mixture was centrifuged (10,000 rpm, 5 min) again to remove excess PSS. The precipitate was redispersed in deionized water for future use. The concentration of Au@Pt nanorods stock solution was 5 nM, which was used to study their enzyme mimetics activity, and the atomic concentration of the Pt nanodots was 1 mM, which was used to study their effect on free radicals. Unless otherwise stated, this nanorod concentration has been used in current study.

5.2.3 Characterization of Au@Pt nanorods

Scanning electron microscopy (SEM) images were taken on a field emission scanning electron microscope (FESEM, Hitachi S-4800). High-resolution transmission electron microscopy (HRTEM) images and selected-area electron diffraction patterns were captured at an accelerating voltage of 200 kV from the same microscope.

5.2.4 Kinetic parameters using UV-Vis spectroscopy

UV-vis absorption spectra were obtained using a Varian Cary 300 spectrophotometer. The oxidation of AA catalyzed by AAO or Au@Pt nanorods in buffers at different pHs was performed at 20 °C as follows: AA was mixed with different pH buffers and made up with H_2O to a final concentration of 5 mM or 10 mM. Then, sufficient AAO or Au@Pt nanorods were added to give a final concentration of 0.09 nM or 0.05 nM, respectively. The reaction kinetics for the catalytic oxidation of AA was studied by recording the absorption spectra at 1 min intervals in the scanning kinetics mode. The disappearance of AA was monitored by measurement of its absorbance at the λ_{max} appropriate for each pH. The kinetic parameters were calculated based on the Michaelis-Menten equation $v = V_{max} \times [S]/(K_m + [S])$, where v is the initial velocity, V_{max} is the maximal reaction velocity, [S] is the concentration of substrate and K_m is the Michaelis constant.

5.2.5 ESR measurements

Samples were put in 50 μL glass capillary tubes and placed in the ESR cavity. All ESR measurements were carried out using a Bruker EMX ESR spectrometer (Billerica, MA) at ambient temperature.

5.2.5.1 Oxidation of AA catalyzed by Au@Pt nanorods

Ascorbyl radical is an intermediate formed during the oxidation of ascorbic acid by oxygen. ESR can directly detect this radical which has a 10 min half-life (*315*). Au@Pt nanorods at different concentrations were added to 5 mM AA in 50 mM PBS buffer (pH 7.4) to start the reaction. The peak to peak value of the first line of the ascorbyl radical ESR spectrum was recorded to indicate the amount of ascorbyl radical formed. Spectra were recorded under the following conditions: 20 mW microwave power; 1 G field modulation; 25 G scan width.

5.2.5.2 Thermal stability of Au@Pt nanorods

In order to compare the catalytic activity of AAO and Au@Pt nanorods with respect to temperature, they were pre-incubated at three temperatures 23, 40, and 70 ^{o}C for 3 and 6 hrs in a water bath. Other steps were the same as described in the previous paragraph.

5.2.5.3 pH dependent enzyme-like activity of Au@Pt nanorods using ESR oximetry

The catalytic activity of AAO and Au@Pt nanorods at different pHs was evaluated through oxygen consumption monitoring. ESR spin label oximetry was employed to measure oxygen change during the reaction. Solutions containing 0.1 mM of the water-soluble spin label CTPO and 1 mM AA in 50 mM buffers with various pHs were studied. AAO or Au@Pt nanorods were added to initiate the catalytic oxidation of ascorbic acid. The capillary tube was then sealed and positioned in the ESR instrument. ESR spectra were then recorded at 0.5, 1.5, 3, 5, 8, and 10 min at the low field line of CTPO (at 23 ^{o}C).

Signals were obtained with a 1 G scanning width, 1mW incident microwave power, and with 100 kHz field modulation.

5.2.5.4 Scavenging effect of Au@Pt nanorods on hydroxyl radical

5.2.5.4.1 Effects of Au@Pt nanorods on hydroxyl radicals generated by the Fenton reaction

Solutions containing $FeSO_4$, H_2O_2, and the spin trap DEPMPO in PBS buffer were used to study scavenging of hydroxyl radicals generated through the classical Fenton reaction. Hydroxyl radicals (•OH) were trapped by DEPMPO as the spin adduct DEPMPO/•OH. To assess whether Au@Pt nanorods scavenged hydroxyl radicals or interacted with the Fenton reagents, the nanorods were first mixed with either iron or hydrogen peroxide for different time periods. Also, ascorbic acid was used to compare the hydroxyl radical scavenging activities of ascorbic acid and Au@Pt nanorods.

In order to investigate the effect of Au@Pt nanorods on the antioxidant property of ascorbic acid, the same Fenton reaction system was employed except that spin trap DMPO was used instead of DEPMPO to detect hydroxyl radicals as the spin adduct DMPO/•OH. Ascorbic acid, Au@Pt nanorods, or their mixture were premixed at room temperature for 48 hrs. Then, they were individually introduced into a freshly prepared Fenton reaction system. Generation of hydroxyl radicals was initiated by adding H_2O_2.

Spectra were recorded under using the following conditions: 20 mW microwave power; 1 G field modulation; 100 G scan width.

5.2.5.4.2 Effects of Au@Pt nanorods on hydroxyl radicals generated by TiO_2 and ZnO/UV

Metal oxides TiO_2 (P25) and ZnO were irradiated at 320 and 340 nm, respectively, to generate hydroxyl radicals, which were trapped by the spin trap DMPO in the form of the

spin adduct DMPO/•OH. Using this method for generation of hydroxyl radicals, we examined quenching of hydroxyl radicals by AA, Au@Pt nanorods, or a combination of AA and Au@Pt nanorods. Spectra were recorded 1 min after the initiation of exposure to UV light under the following conditions: 20 mW microwave power; 1 G field modulation; 100 G scan width.

5.2.5.5 Effect of Au@Pt nanorods on the antioxidant property of ascorbic acid

5.2.5.5.1 Effects of Au@Pt nanorods on the DPPH radical

DPPH radical (DPPH•) is a stable, nitrogen-centered free radical. The attenuation of its ESR signal is one of the methods widely used to demonstrate a chemical's ability to scavenge free radicals. The effect of ascorbic acid, Au@Pt nanorods, and their combination on the ESR spectrum of DPPH• was examined. Ascorbic acid, Au@Pt nanorods, or their mixture were stored at room temperature for 24 hrs. Afterwards, they were individually added to a control sample containing DPPH•, ethanol, and 10 mM PBS buffer. The reaction was initiated by adding DPPH•. Spectra were obtained at 2.5 min using 15mW incident microwave power and 100 kHz field modulation of 2 G.

5.2.5.5.2 Effects of Au@Pt nanorods on the superoxide radical generated by xanthine/xanthine oxidase

Superoxide radicals (•OOH) were produced using the xanthine/XOD system and trapped as the spin adduct BMPO/•OOH. The method of superoxide radical detection using spin trap BMPO was essentially the same as described by Yin et al *(316)*. Ascorbic acid, Au@Pt nanorods, or their mixtures were stored at room temperature for 48 hrs. Then, they were individually introduced into a freshly prepared xanthine/XOD mixture where generation of superoxide radical was initiated by addition of XOD. The ESR spectra were recorded at 1.5 min using 20 mW microwave power, 1 G field modulation, and 100 G scan width.

5.3 Results and Discussion

5.3.1 Synthesis and characterization of Au@Pt nanorods coated with PSS

The TEM image in Figure 5-1 shows the core/shell morphology of the Au@Pt nanorods. The Au nanorods, ~10 nm in diameter and ~60 nm in length, served as a template and Pt nanodots, ~3 nm in diameter, were grown on them. It has been reported that Pt nanoparticles, especially smaller than 5 nm, exhibit great catalytic activity (*314*). In the current study, Pt nanodots were distributed homogeneously on the surface of Au nanorods (Figure 5-1right), as expected because Pt grows in a Stranski-Krastanow mode (*182*). Such nanorods are expected to exhibit greatly enhanced catalytic activity due to the large surface area associated with the small diameter of the nanodots (*314*). Also, the Pt/Au interface can result in superior catalytic activity toward redox reactions. Here, the Au@Pt nanorods were coated with PSS to prevent aggregation.

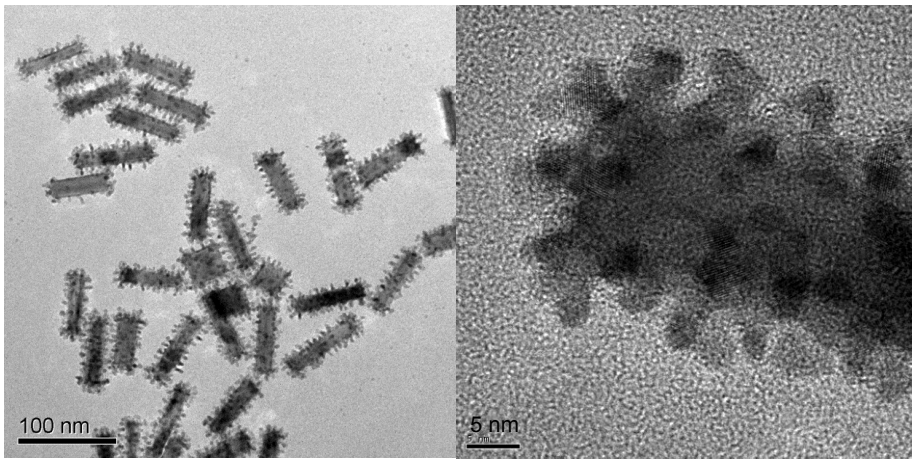

Figure 5-1 Morphology of core/shell structure of Au@Pt nanorods. TEM image (left) and high resolution TEM image (right).

5.3.2 Ability of Au@Pt nanorods to catalyze oxidation of ascorbic acid

Ascorbic acid, an active reducing agent, is oxidized by oxygen slowly. However, oxidation is accelerated by addition of ascorbic acid oxidase (AAO), where the intermediate ascorbyl radical (AA•) is an indicator of the oxidation (Scheme 5-1). The ESR spectrum of AA• is shown in the inset for Figure 5-2. We observed a hyperfine splitting constant $\alpha_{H4} = 0.177$ and g = 2.0052 that are consistent with previous studies (*317, 318*). Oxidation of ascorbic acid to AA• was dependent on the concentration of Au@Pt nanorods as shown in Figure 5-2. At concentrations of Au@Pt nanorods below 0.5 nM, an increase in the concentration of Au@Pt nanorods resulted in an increase in levels of ascorbyl radicals. At higher concentrations of Au@Pt nanorods, no increase in ascorbyl radical levels was observed with increasing nanorods concentration. The saturation of ascorbyl radical formation likely resulted from the depletion of one or both substrates (oxygen and ascorbic acid). The ascorbyl radical was not formed when the reaction solution was deoxygenated with nitrogen in the presence of either AAO or Au@Pt nanorods (data not shown), indicating that Au@Pt nanorods are a catalyst rather than an oxidant. A similar experiment was conducted except that Au@Pt nanorods were replaced with Pt nanoparticles. We observed

that the AA• production was also dependent on the concentration of Pt NPs (Figure 5-3A). Furthermore, we found out that with the regard to AA• production, Au@Pt nanorods were much more efficient than Pt NPs. This may be due to a number of factors including resistance toward aggregation for Au@Pt nanorods and the promotional effect on catalytic activity of Au nanorods (*319*).

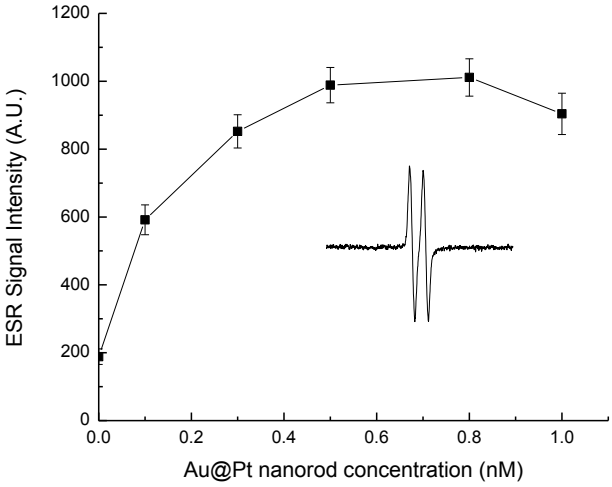

Figure 5-2 Ascorbyl radical production is dependent on the concentration of Au@Pt nanorods. Samples contained 5 mM AA and Au@Pt nanorods at variable concentrations in 50 mM PBS (pH 7.4). The inset shows the ESR spectrum of the ascorbyl radical. The ESR signal intensity was measured as the peak-to-peak value of the first line of the spectrum. ESR spectra were collected at 1min after sample mixing.

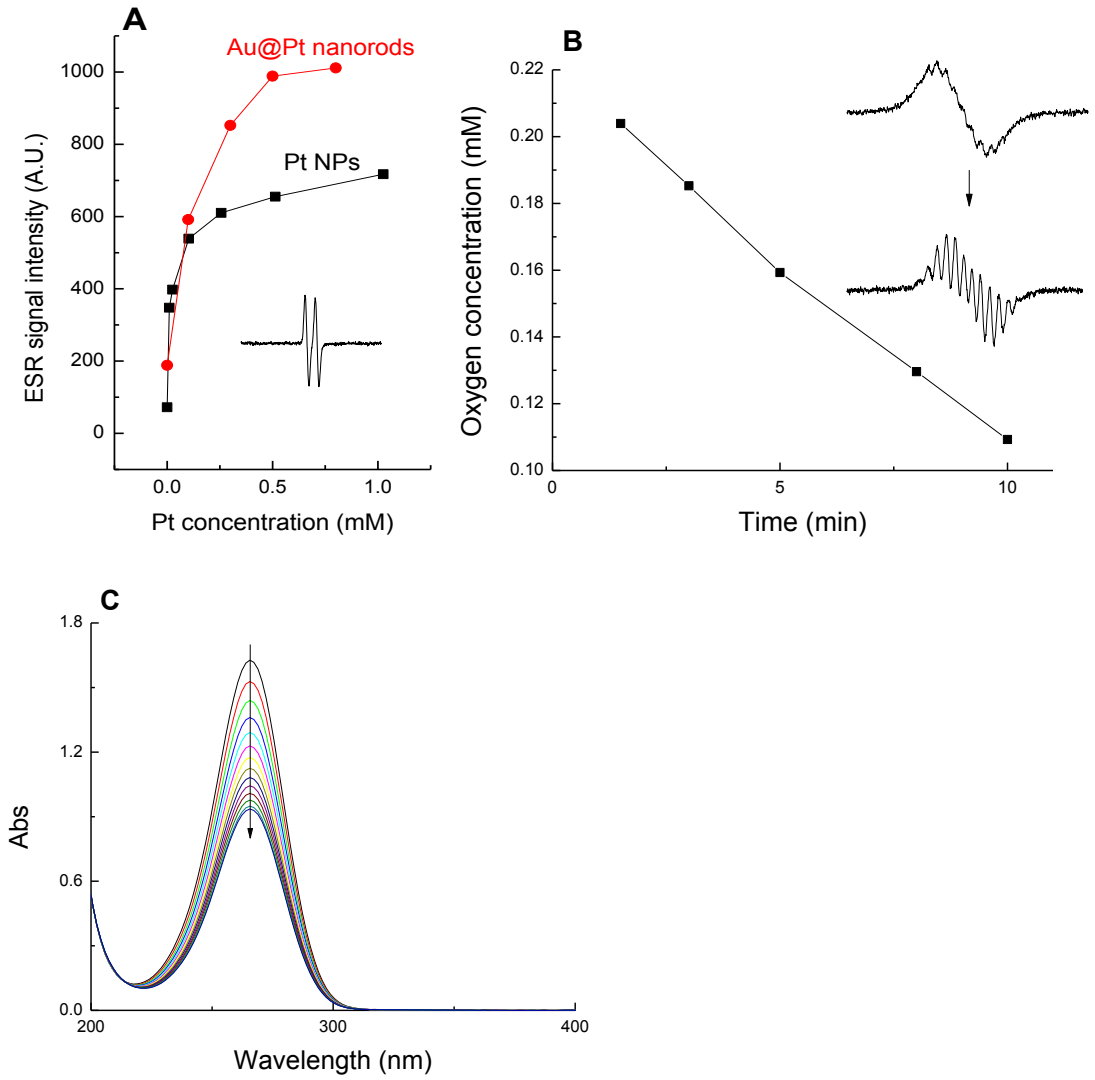

Figure 5-3 (A) Ascorbyl radical production is dependent on the concentration of Au@Pt nanorods and Pt NPs. Samples contained 5 mM AA and Au@Pt nanorods or Pt NPs at variable concentrations in 50 mM PBS (pH 7.4).The inset shows the ESR spectrum of the ascorbyl radical. The ESR signal intensity was measured as the peak-to-peak value of the first line of the spectrum. (B) Oxygen consumption during the oxidation of ascorbic acid catalyzed by Pt NPs. Samples contained 5 mM AA, 0.14mM CTPO, 0.05 mM Pt NPs, and 50 mM PBS buffer (pH 7.4). The Inset shows the ESR spectrum change of CTPO. (C) UV-Vis spectra evolution of 0.1 mM AA in presence of 5 µM Pt NPs in 50 mM PBS buffer (pH 7.4) during 30 min. Arrow shows decrease in absorbance. The concentration of nanoparticles refers to atomic concentration.

5.3.3 Thermal stability of Au@Pt nanorods as AAO mimetics

Enzymes are sensitive to temperature changes and may be denatured upon heating. By contrast, Au@Pt nanorods are expected to be relatively insensitive to changes in temperature. We compared the thermal stability of Au@Pt nanorods and AAO, as shown in Figure 5-4. Here, ascorbyl radical was used as an indicator of oxidation, where the

intensity of the ESR spectrum of ascorbyl radical represented the amount of oxidation product. Both AAO and Au@Pt nanorods were preincubated at 23, 40, and 70 ºC in a water bath for 0, 3, or 6 hours prior to examining effects on oxidation of a freshly made AA solution. A time dependent decrease in the activity of the enzyme, AAO, was observed at all temperatures. Higher temperatures resulted in more rapid decreases in the activity of AAO (Figure 5-4, left). However, Au@Pt nanorods were much more stable than AAO during preincubation for up to 6 hrs. The activity of Au@Pt nanorods in catalyzing the oxidation of AA remained above 95% (Figure 5-4, right), which indicates the superior thermal stability of Au@Pt nanorods.

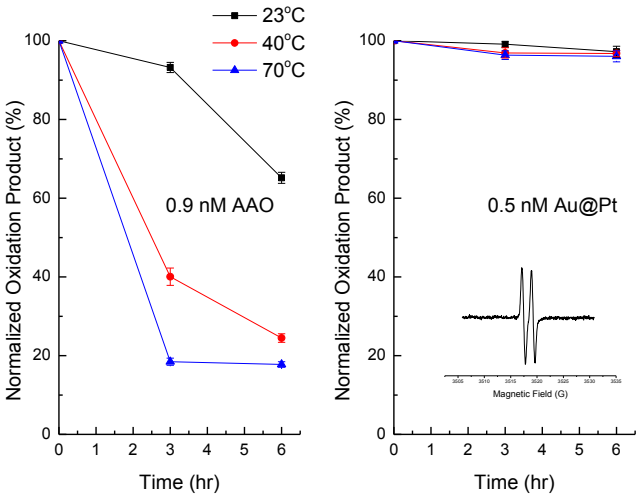

Figure 5-4 Thermal stability of AAO and Au@Pt nanorods. 0.9 nM AAO and 0.5 nM Au@Pt nanorods were preincubated at 23, 40, or 70 ºC for 0, 3, and 6 hrs prior to oxidation reaction of 5 mM AA in 50 mM PBS (pH 7.4). Inset represents ESR spectrum of ascorbyl radical. The signal intensity was measured as the peak-to-peak value of the first line of the spectrum. ESR spectra were collected at 1 min after sample mixing.

5.3.4 pH dependent activity of AAO and Au@Pt nanorods as AAO mimetics

The stability of ascorbyl radicals varies with reaction conditions such as pH. Therefore, oxygen consumption was used to examine the effects of pH on the oxidation of AA catalyzed by AAO or Au@Pt nanorods. Oxygen consumption was measured by ESR

oximetry. The ESR spin label CTPO, in a closed chamber, was used to monitor oxygen concentrations during the oxidation of AA. ESR spectra of the spin label CTPO exhibit three lines because of the hyperfine interaction of the unpaired electron with the nitrogen nucleus. Each line is further split into another group of lines because of proton super hyperfine interaction. The resolution of the super hyperfine structure of the low-field line of the ESR spectrum of CTPO depends on the oxygen concentration of the sample solution. Figure 5-5 shows the evolution of the CTPO spectrum during oxidation of AA catalyzed by Au@Pt nanorods. A time dependent increase in super hyperfine splitting was observed. This indicates the disappearance of oxygen in solution during oxidation of AA catalyzed by Au@Pt nanorods. Quantitative estimates of oxygen consumption were obtained from the calibration chart relating the *K* parameter to oxygen concentration, where *K* was calculated based on the super hyperfine splitting shape of the ESR spectrum (*213*). Herein, the consumption rate of oxygen was used to indicate the apparent activity of both AAO and Au@Pt nanorods. The Pt NPs also catalyzed the oxidization of AA in presence of oxygen (Figure 5-3B). It is well established that oxidative degradation of AA is enhanced at increased pH, however the rate of the uncatalyzed degradation is relatively low. Thus, the reaction rate is mainly dependent on the catalytic activity. The usual pH-dependence for enzyme activity is a bell shape curve. The optimum pH range of AAO is reported to be 4-8, which is consistent with our finding that AAO was less active in extreme acidic or alkaline condition (Figure 5-6). By contrast, the apparent activity of Au@Pt nanorods increased rapidly with increasing pH (Figure 5-6). This may attributed to the coating material, PSS, which is negatively charged and may make the nanorods more

homogenously distributed under alkaline condition. These results demonstrate that Au@Pt nanorods are much more stable catalysts than AAO over a wide range of pHs.

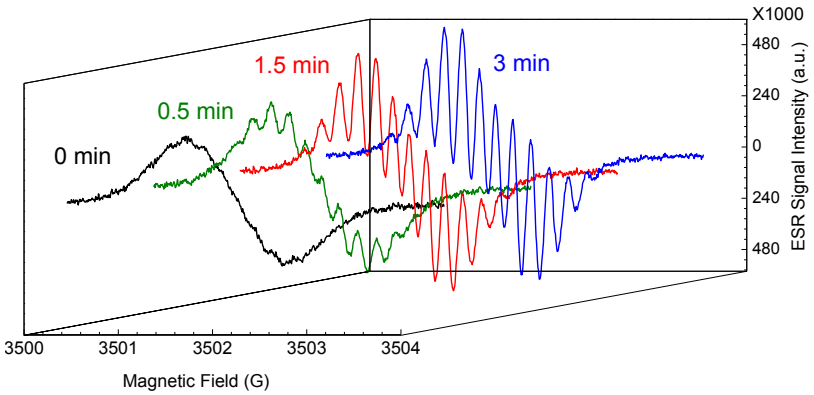

Figure 5-5 Evolution of ESR spectrum of the spin label CTPO during the oxidation of AA catalyzed by Au@Pt nanorods. Sample solutions contained 0.1 mM CTPO, 5 mM AA, 50 mM PBS (pH 7.4), in the absence (control) and in the presence of 0.5 nM Au@Pt nanorods. ESR spectra were obtained at 0.5, 1.5, and 3 min after addition of Au@Pt nanorods.

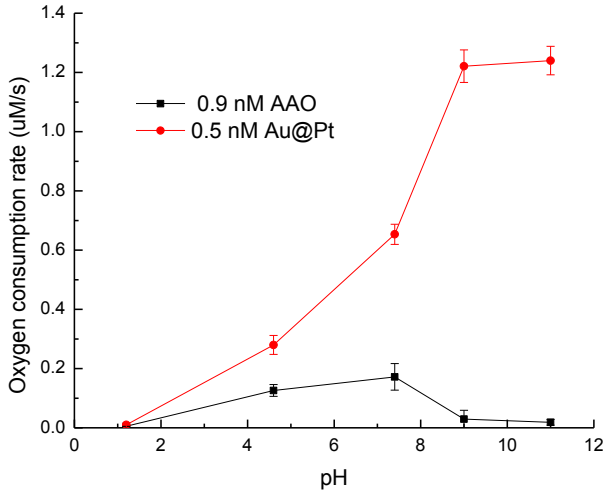

Figure 5-6 Ability of AAO and Au@Pt nanorods in catalyzing AA oxidation determined by initial O_2 consumption over a wide pH range. Sample solutions included 0.1 mM CTPO, 5 mM AA, and 50 mM buffers at different pHs.

The catalytic mechanism for the nanorods may be attributed to the surface-mediated electron transfer between two substrates. The Michaelis constant (K_m) and catalytic constant (K_{cat}) are key characteristics to describe properties of enzymes. A low K_m

represents high affinity between substrate and enzyme, while a high K_{cat} indicates a high catalytic ability of the enzyme. Using AA as the substrate, values for K_m and K_{cat} were determined for both AAO and Au@Pt nanorods over the pH range described in Table 5-1. Under neutral conditions, the K_m of Au@Pt nanorods was much higher than that of AAO, which suggests that binding of AA to AAO is more specific than binding to Au@Pt nanorods. In contrast, the K_{cat} of Au@Pt was many times of that of AAO. This demonstrates that Au@Pt nanorods catalyzed the enzymatic reaction more rapidly than AAO, although they had less affinity for the substrate. Our results are consistent with previous findings that Pt nanoparticles behaved similarly as peroxidase (*182, 183, 246, 260*), catalase (*189*), and uric acid oxidase (*309*); Au@Pt nanorods are therefore potentially broad enzyme mimetics.

Table 5-1 Kinetic parameter for 0.09 nM AAO and 0.05 nM Au@Pt nanorods as AAO mimetics. K_m is the Michaelis constant, V_{max} is the maximum reaction rate and K_{cat} is the catalytic constant. Reaction conditions: 50 mM buffers at 23 °C. The reaction is monitored through recording spectrum peak (220-270 nm) of ascorbic acid in UV-VIS spectrophotometer.

pH	K_m, nM		V_{max}, nM s^{-1}		K_{cat}, s^{-1}	
	AAO	Au@Pt	AAO	Au@Pt	AAO	Au@Pt
1.2	219	18.4	0.003	0.764	0.028	15.3
4.6	16.5	16.5	0.17	6.57	1.89	131
7.4	3.1	24.5	0.409	2.09	4.54	41.7
9	4.0	29.1	0.484	2.27	5.38	45.5
11	11.9	27.9	0.465	7.12	5.16	142

5.3.5 Inhibitive effect of Au@Pt nanorods on generation of hydroxyl radicals

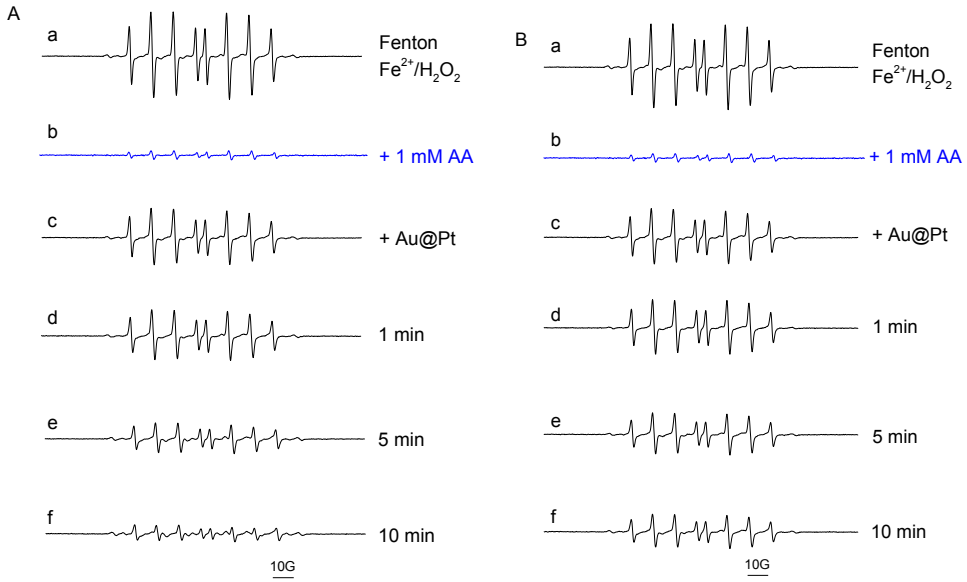

Figure 5-7 Effect of Au@Pt nanorods on hydroxyl radicals generated through the Fenton reaction. Reaction mixtures contained 10 mM PBS buffer (pH 7.4), 10mM DEPMPO, 1 mM H_2O_2, 0.2 mM Au@Pt nanorods or 1 mM AA, and 0.5 mM Fe^{2+} (this order was followed in preparing the control (a), AA added to the control sample (b), and Au@Pt added to the control sample (c-f)). For time premixing, the Au@Pt nanorods were first mixed with A (d-f) H_2O_2 or B (d-f) Fe^{2+} for 1, 5, and 10 min and then Fe^{2+} (panel A) or H_2O_2 (panel B) was added before adding the spin trap. ESR conditions: power 20 mW, field modulation 1G, scan width 100 G. Pt nanodots concentration was used for Au@Pt nanorods.

The hydroxyl radical possesses the highest one-electron reduction potential of all the physiologically relevant ROS and is extremely reactive with almost every type of biomolecule (*10, 320*). The Fenton reaction, a widely accepted method for generating hydroxyl radicals, was used to examine the interaction between Au@Pt nanorods and

hydroxyl radicals (Figure 5-7). ESR spin trapping using the spin trap DEPMPO was employed to detect the short-lived hydroxyl radical in the form of spin adduct DEPMPO/•OH, which has eight lines with intensity ratios of 1:2:2:1:1:2:2:1 and hyperfine splitting parameters of a_P = 47.3 G, a_H = 13.2 G, a_N = 14.0 G (*283*). A significant reduction of the ESR signal for DEPMPO/•OH was observed following addition of AA, a well-known scavenger for ROS. Addition of Au@Pt nanorods also reduced the signal intensity suggesting that Au@Pt nanorods behave as antioxidants by quenching hydroxyl radicals. However, an alternative mechanism is inhibition of hydroxyl radical formation through interactions of Au@Pt with H_2O_2 or Fe^{2+}. To distinguish these mechanisms, Au@Pt was mixed with either H_2O_2 or Fe^{2+} for selected times prior to initiating the Fenton reaction. As shown in Figure 5-7 A and B d-f, lower levels of hydroxyl radicals were produced following longer premixing times, indicating that the Au@Pt nanorods reduced hydrogen peroxide and interacted with Fe^{2+}. These results indicate that Au@Pt nanorods act as catalase mimetics, consistent with previous studies (*188, 189*), and may facilitate the oxidation or other reactions of Fe^{2+} rather than directly scavenging hydroxyl radicals.

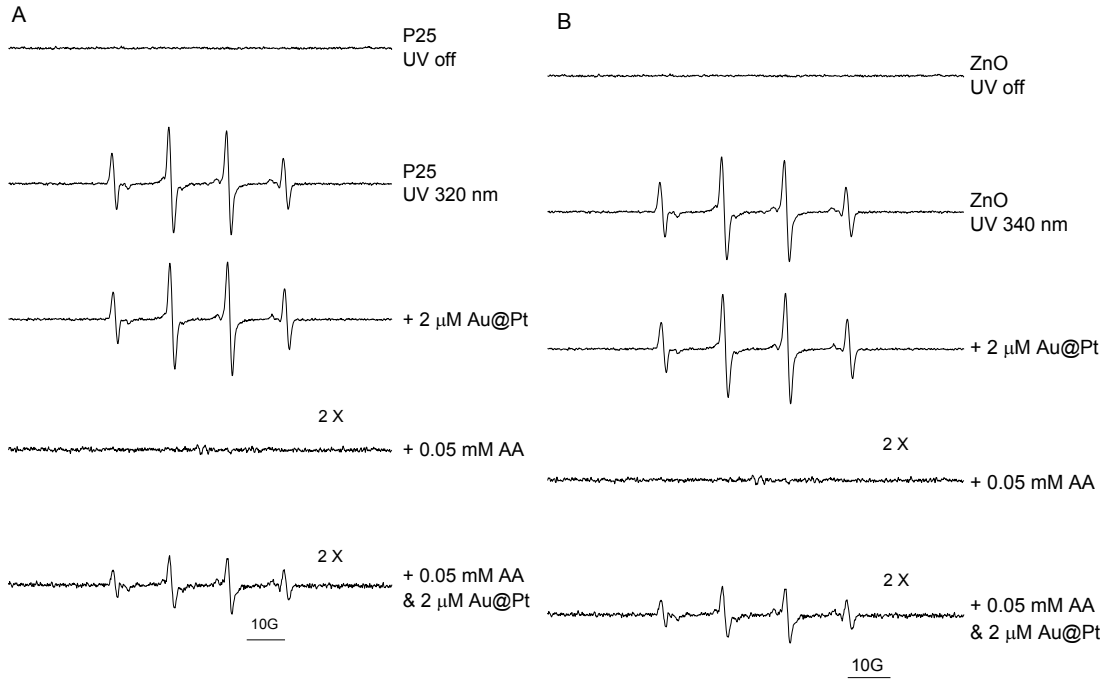

Figure 5-8 The effect of Au@Pt nanorods on hydroxyl radical levels and their combined effect with ascorbic acid to scavenge hydroxyl radicals generated during irradiation of metal oxides. (A) Sample solutions containing 0.1 mg/ml P25 (TiO_2) and 50 mM DMPO were exposed to UV radiation (340nm). Samples in A and B contained Au@Pt nanorods, AA, or their combination. ESR spectra were collected at 1 min after UV light was turned on. Pt nanodots concentration was used for Au@Pt nanorods.

Both TiO_2 (P25) and ZnO generate hydroxyl radicals when exposed to UV radiation at 320 and 340 nm, respectively. In irradiated samples containing DMPO and one of the metal oxides, we observed a four-line spectrum with relative intensities of 1:2:2:1, and hyperfine splitting parameters of $a_N = a_H = 14.9$ G. This ESR spectrum is characteristic for the spin adduct between DMPO and hydroxyl radical (DMPO/•OH) (*251*). In Figure 5-8, a substantial level of hydroxyl radicals was produced following irradiation of ZnO or TiO_2. The addition of AA significantly reduced the ESR signal observed for the DMPO/•OH adduct. A previous study stated that Pt nanoparticles were able to scavenge •OH generated during UV irradiation of H_2O_2 (*312*). However, we observed no significant reduction in the ESR signal characteristic of the DMPO/•OH adduct when Au@Pt nanorods were added

and observed for hydroxyl radicals (Figure 5-8). These results indicate that Au@Pt nanorods do not directly scavenge •OH. Therefore, reexamination of the aforementioned scavenging effect of Pt NPs towards hydroxyl radicals is warranted to determine the role of their catalase-like ability to degrade H_2O_2 (*189*), which is also demonstrated in Figure 5-7. It is noteworthy that, when added together with AA, Au@Pt nanorods inhibited the ability of AA to scavenge hydroxyl radicals (Figure 5-8). These phenomena were observed in both TiO_2 and ZnO/UV systems. This finding suggests that while Au@Pt nanorods themselves cannot scavenge hydroxyl radicals, they might reduce the antioxidative properties of other antioxidants.

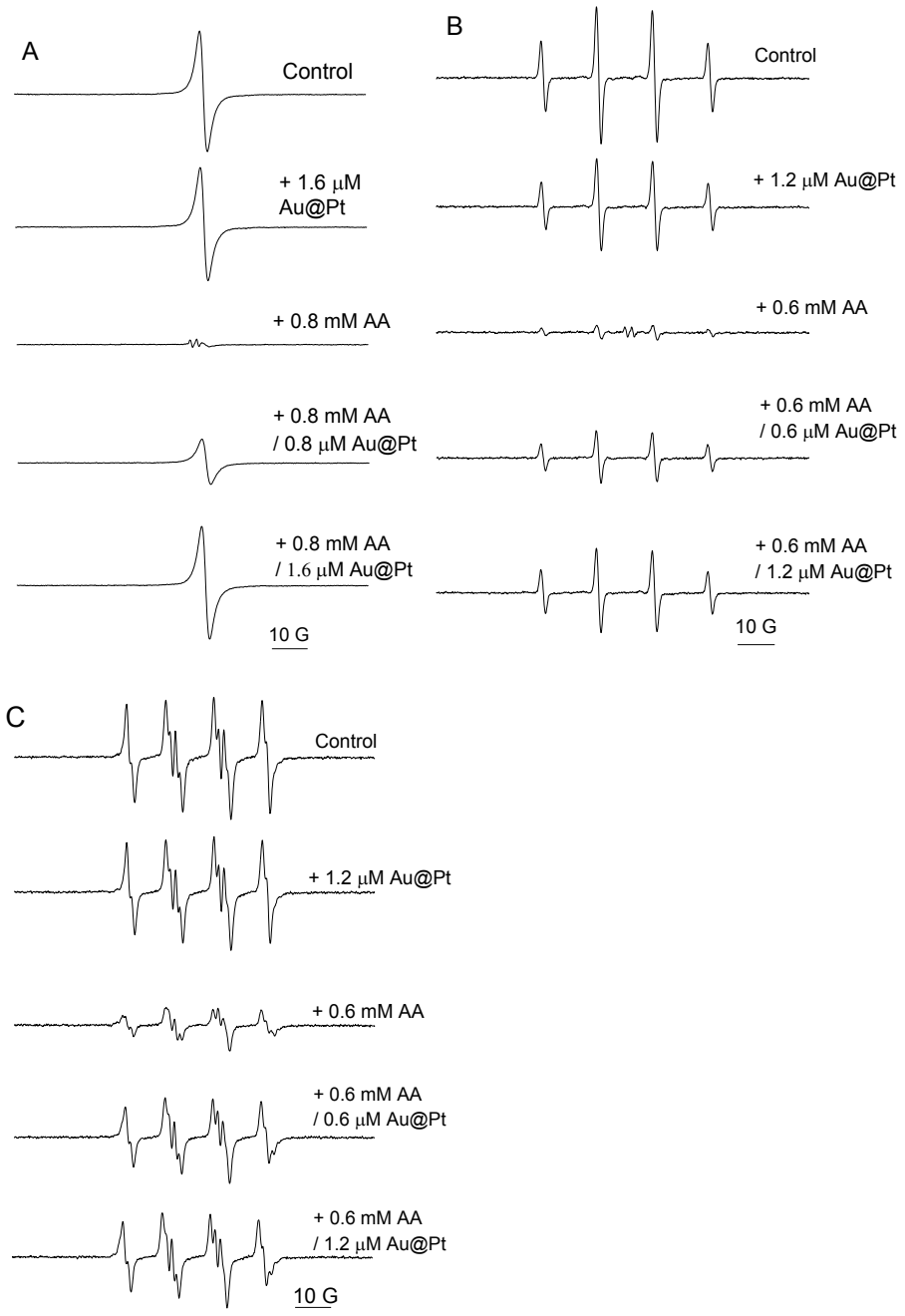

Figure 5-9 Effects of Au@Pt nanorods on the antioxidant ability of ascorbic acid. Control sample in (A) contained 0.1 mM DPPH•, 10% (v/v) ethanol, and 10 mM PBS buffer (pH 7.4); samples containing AA, Au@Pt nanorods, or a mixture of these were kept at room temperature for 24 hr. Control sample in (B) was a Fenton reaction system consisting of 50 mM DMPO, 10 mM PBS buffer (pH 7.4), 0.1 mM Fe^{2+}, and 1 mM H_2O_2; AA, Au@Pt nanorods, or a mixture of these were kept at room temperature for 48 hr. Control sample in (C) included 25 mM BMPO, 10 mM PBS buffer (pH 7.4), 1 mM xanthine, and 0.2 U/ml XOD; AA, Au@Pt nanorods, or a mixture of these were kept at room temperature for 48 hr. Pt nanodots concentration was used for Au@Pt nanorods.

To further investigate the effect of Au@Pt nanorods on the antioxidant activity of ascorbic acid, three systems for generating radicals were employed (Figure 5-9).

DPPH radical (DPPH•) is a stable radical that has been commonly used to evaluate the antioxidant properties of ingredients in foods. Although DPPH• is a stable nitrogen-centered radical that has no involvement in physiological processes, attenuation of the ESR signal for DPPH• is one of the criteria widely used to demonstrate the ability to scavenge ROS (*321*). In Figure 5-9A, a characteristic one line spectrum was obtained for the control solution of 0.1 mM DPPH• and 10% ethanol in PBS buffer. We observed that the ESR signal for the DPPH radical nearly disappeared when the well-recognized antioxidant, ascorbic acid, was added (Figure 5-9A spectrum 1 compared with spectrum 3). In contrast, Au@Pt nanorods at a concentration of 1.6 μM (Pt nanodots) had little effect in reducing the ESR signal for the DPPH radical. However, after 24 hr, the mixture of nanorods (at the same concentration) and AA resulted in a significant increase in the ESR signal compared with the ESR signal observed when only AA was present (Figure 5-9A, spectrum 3 compared with spectrum 5). Even when the concentration of Au@Pt nanorods was reduced to an extremely low level, 0.8 μM (Pt nanodots), premixing of AA with nanorods still resulted in a significant reduction in AA's antioxidant activity in this system (Figure 5-9A, spectrum 4 compared to spectrum 3).

The Fenton reaction is a key contributor to hydroxyl radical generation in biological systems. By means of DMPO, hydroxyl radicals were trapped in the spin adduct DMPO/•OH (*251*). In biological systems, ascorbic acid is one of main antioxidants that scavenge reactive hydroxyl radicals and thereby prevent oxidative damage in cells. In our model system, a convincing scavenging effect for AA is shown in Figure 5-9B spectrum

3. Au@Pt nanorods also had a perceivable inhibitive effect on the hydroxyl radical generation through the Fenton reaction. This may result from its catalytic effect on decomposition of H_2O_2 or oxidation of Fe^{2+} as discussed previously. However, premixing of AA and Au@Pt nanorods for 48 hrs resulted in a larger ESR signal for the DMPO/•OH adduct compared to the ESR signal observed in the presence of AA alone (Figure 5-9 spectra 3 and 4). Similar results were obtained when the concentration of Au@Pt nanorods was reduced by one half.

In the xanthine/XOD system used for generating superoxide radical, BMPO was chosen as a spin trap to form spin adduct BMPO/•OOH. The ESR spectrum characteristic for this spin adduct has four lines with relative intensities of 1:1:1:1 and hyperfine splitting parameters of a_N = 13.4, a^{β}_H = 12.1(*251*). Pt nanoparticles have been reported to be effective superoxide radical scavengers, behaving like SOD (*188*). We observed no significant change in the ESR signal for BMPO/•OOH when the nanorods were added to the system for generating superoxide radicals (Figure 5-9C). It should be noted that we used a much lower concentration of Au@Pt nanorods compared with concentrations of Pt nanoparticles used by investigators reporting quenching of superoxide radicals. As expected, ascorbic acid effectively quenched superoxide radicals resulting in a dramatic reduction in the ESR signal for BMPO/•OOH (Figure 5-9C, spectrum 3). Premixing AA with Au@Pt nanorods for 48 hrs resulted in a loss in the ability of AA to quench superoxide radicals as seen by the increase in the ESR signal for BMPO/•OOH (Figure 5-9C, spectra 3, 4, and 5).

In contrast to previous studies where platinum NPs, at higher concentrations, were capable of quenching DPPH radicals (*313*) and super oxide radicals (*188*), we did not observe the

scavenging effect of Au@Pt nanorods under our experiment conditions (Figure 5-9). In addition, we find that Au@Pt nanorods do not scavenge hydroxyl radical, the most reactive biologically relevant free radical (Figure 5-8). Our results generally suggest that the mechanisms for previously reported radical scavenging by Pt NPs should be reexamined and that indirect mechanisms for radical scavenging should be considered.

Since the human body is not able to synthesize AA, AA must be provided by dietary sources, predominantly fruits and vegetables. AAO is endogenously present in various plants and it is a main factor resulting in enzymatic degradation of AA (*322*). The mechanical processing of plants in food production can expose AA to AAO causing degradation of AA, thus reducing antioxidant protection by AA. Platinum nanoparticles have been considered as antioxidants because, under some experimental conditions, they scavenge biologically relevant ROS. Therefore, it is possible that in current or future applications, Pt NPs may be incorporated in complex commercial formulations with multiple components.

In this work, we have found that Au@Pt nanorods and Pt NPs catalyze oxidation of ascorbic acid, acting similar to AAO. As a strong antioxidant, AA scavenges hydroxyl radicals (Figure 5-8), DPPH radicals, and superoxide radicals (Figure 5-9). Added alone, Au@Pt nanorods, at the concentrations in our study, did not change levels of the above radicals. However, when combined with AA, Au@Pt nanorods significantly reduced the antioxidant property of AA. Our findings suggest that Au@Pt nanorods at the stated levels do not exert antioxidant function in scavenging radicals, but instead can reduce the protective effects of antioxidants such as AA.

5.4 Conclusion

In the current study, we have systematically investigated the properties of Au@Pt nanorods as ascorbic acid oxidase mimetics. Commercially available Pt NPs were also found to be AAO mimetics despite their low efficiency. The Au@Pt nanorods were found to be more thermally stable than AAO. In addition, Au@Pt nanorods maintained catalytic activity over a wider pH range than AAO. Results obtained from studying reaction kinetics demonstrated that Au@Pt nanorods were able to rapidly catalyze the oxidation of AA, although AA had a lower affinity to Au@Pt nanorods than to AAO. Similar to the reported peroxidase, catalase, and uricase activities of other Pt nanoparticles, Au@Pt nanorods may be viewed as multi-enzyme mimetics with broad substrate specificities.

In our study, we examined the radical scavenging ability of Au@Pt nanorods using systems which generated DPPH, hydroxyl or superoxide radicals. No evidence for direct scavenging of these radicals by Au@Pt nanorods was seen under our experimental conditions. Previously reported studies have found that Pt nanoparticles scavenged DPPH and superoxide radicals, but their experimental conditions were different from ours. Most notably, we have investigated lower concentrations of nanoparticles and have used direct methods for assessing free radical quenching. Au@Pt nanorods may exert different effects toward free radicals. Our results indicate that Au@Pt nanorods cannot be simply considered as direct antioxidants, but are enzyme mimetics instead. Consistent with their catalytic activity, trace amount of Au@Pt nanorods were found to significantly reduce the antioxidant ability of ascorbic acid to scavenge hydroxyl, superoxide, and DPPH radicals. This suggests that as oxidase mimetics, Au@Pt nanorods may have antagonistic effects on antioxidants such as AA (Scheme 5-2). Factors such as experimental conditions, product formulation or product use may dramatically alter the overall effects of Au@Pt nanorods.

Therefore, the performance of nanoparticles, such as Au@Pt nanorods, in complex formulations should be evaluated under real use conditions.

5.5 Acknowledgement

We thank Dr. John Callahan for his valuable discussion and comments. This article is not an official US Food and Drug Administration (FDA) guidance or policy statement. No official support or endorsement by the US FDA is intended or should be inferred. This work was supported by a regulatory science grant under the FY11 FDA Nanotechnology CORES Program.

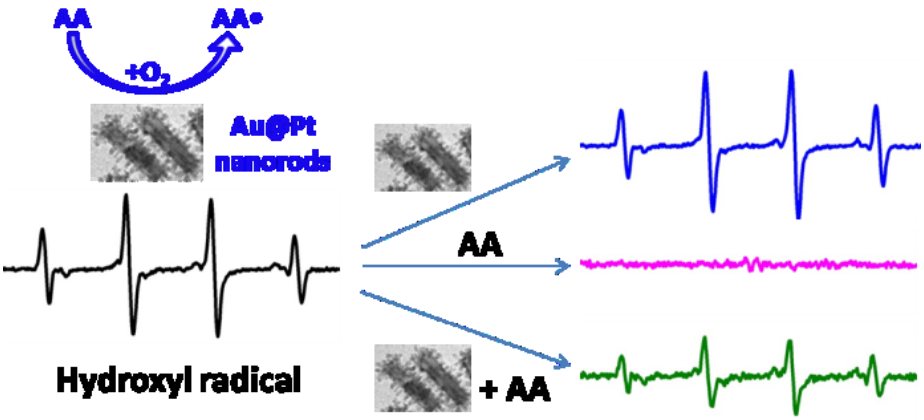

Scheme 5-2 Au@Pt nanorods are ascorbic acid oxidase mimetics rather than antioxidants and thus reduce the antioxidant activity of ascorbic acid.

Chapter 6: Enzyme-like activity of Au@Pt nanorods and their combined effect with phenolics

6.1 Introduction

Tyrosinase (monophenol, dihydroxyphenylalanine: oxygen oxidoreductase EC 1.14.18.1) catalyzes the hydroxylation of monophenolic compounds to *o*-diphenols (cresolase reaction) and the oxidation of the latter to *o*-quinones (catecholase reaction) in the presence of oxygen (*323*) (Figure 6-1). Tyrosinase is an important enzyme for the synthesis of melanin since *o*-quinones continuously undergo several reactions to eventually form melanin. The accumulation of melanin could cause enzymatic browning of fruits and vegetables, which can be resolved in the food industry by blanching to deactivate the enzyme. On the other side, the pigment melanin in human skin is a major defense mechanism against ultraviolet light, but the increased accumulation and redistribution of epidermal melanin could cause serious aesthetic problems, such as dermal darkening for oriental people. Therefore, researchers are encouraged to find out potent tyrosinase inhibitors in cosmetics. Some well recognized natural antioxidants, namely green tea components (*324*), caffeic acid or its esters mainly sourced from coffee (*325*), and resveratrol that is rich in grapes (*326*), are original substrates for tyrosinase and have been recognized as promising whitening ingredients in cosmetics to prevent overproduction of melanin.

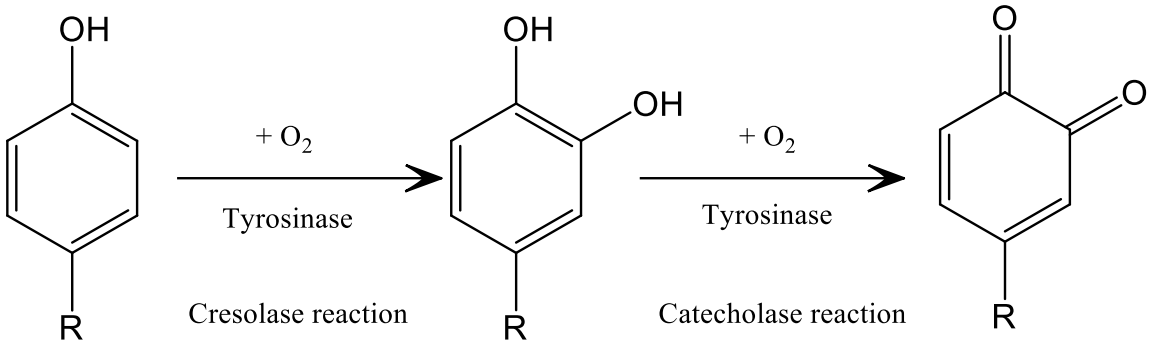

Figure 6-1 Enzymatic oxidation of phenolics in presence of oxygen catalyzed by tyrosinase.

Phenolics exert protective effect *in vivo* by acting as reducing agents, hydrogen donating antioxidants, singlet oxygen quenchers, as well as metal chelating agents in some cases (*327*). The antioxidant property of phenolics is predicted by the phenolic hydrogen that donates hydrogen to scavenge radicals, which can be seen in the structure of the selected phenolics (Figure 6-2). Therefore, the antioxidative activity of phenolics may be decreased as the oxidation of phenolics is catalyzed by tyrosinase. For example, it has been found that there were higher caffeic acid derivatives in blanched artichokes than in raw ones, which may attributed to the oxidation of phenolic compounds in polyphenol oxidase-catalyzed reactions. Artichokes are a rich source of polyphenol oxidase activity and blanching involves PPO inactivation with the subsequent preservation of phenolics (*328*).

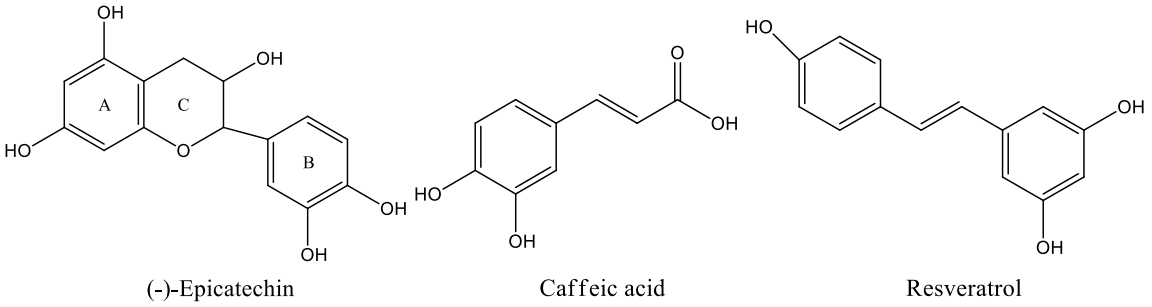

Figure 6-2 Chemical structure of (-)-Epicatechin, caffeic acid, and resveratrol.

The intrinsic enzyme-like activity of nanoparticles (NPs) has become a growing area of interest. Compared with natural enzymes, these enzyme-like NPs are stable against denaturation, low in cost, highly resistant to high concentrations of substrate, and easy to be functionalized for different purposes. These advantages make them promising for various applications especially as bio-devices. Recently developed NPs of enzyme mimetics include magnetic NPs, cerium-oxide NPs, and noble-metal NPs (*308, 329, 330*). We have previously reported the enzyme mimetic property of Au@Pt nanorods in oxidizing ascorbic acid and in turn jeopardized its antioxidant activity in Chapter 0. In the current study, we extended the possible substrates of Au@Pt nanorods as an oxidizing enzyme to another group of antioxidant phenolics. Gold@platinum nanorods were employed to catalyze the oxidation of flavonoids (-)-Epicatechin and resveratrol plus *o*-diphenols caffeic acid, which was monitored by UV-vis spectroscopy and Electron Spin Resonance (ESR) oximetry. The free radical scavenging effect of the selected phenolics was evaluated by ESR. Also, the effect of Au@Pt nanorods on the phenolics to quench free radicals was investigated.

6.2 Materials and methods

6.2.1 Materials

Spin trap a-(4-pyridyl-1-oxide)-N-tert-butylnitrone (4-POBN), 3-carbamoyl-2,5-dihydro-2,2,5,5-tetramethyl-1H-pyrrol-1-yloxyl (CTPO), 1,1-diphenyl-2-picryl-hydrazyl radical (DPPH•), ethanol, xanthine, (-)-Epicatechin (EC), caffeic acid (CFA), resveratrol (RES), and tyrosinase (Tyr) were all purchased from Sigma-Aldrich (Saint Louis, MO). Xanthine oxidase (XOD) was obtained from Roche Diagnostics GmbH (Mannheim, Germany). Zinc oxide nanoparticles aqueous dispersion (20 wt%, 30-40 nm) was purchased from US Research Nanomaterials, Inc (Houston, TX). Spin trap 5-tertbutoxycarbonyl 5-methyl-1-

pyrroline N-oxide (BMPO) was from Bioanalytical Labs (Sarasota, FL). Gold@Platinum (Au@Pt) nanorods were synthesized using previous method (*281*). For TEM sampling, copper grids coated with carbon film were purchase from SPI supplies (West Chester, PA)

6.2.2 Characterization

6.2.3 Transmission electron microscopy (TEM)

TEM images were captured on a JEM 2100 FEG (JEOL) transmission electron microscope at an accelerating voltage of 200 kV located at the NanoCenter, University of Maryland, College Park, MD. To observe the morphological evolution of the nanoparticles after catalysis reaction, 0.1 nM Au@Pt nanorods and 1 mM (-)-Epicatechin were mixed in 0.5 mL 10mM pH 6.0 phosphate buffer solution for 30 min and twice centrifuged (12,000 rpm, 5 min). After the supernatants were decanted, twenty milliliter of water was added to redisperse the precipitates. The samples for TEM analysis were prepared by adding drops of the redispersed colloidal solutions onto standard carbon-coated copper grids, which were then air dried at room temperature.

6.2.4 UV-vis spectroscopy

UV-vis absorption spectra were obtained using a Varian Cary 300 spectrophotometer. To monitor the evolution of each phenolic during oxidation catalyzed by tyrosinase or Au@Pt nanorods, phenolics were mixed with tyrosinase or Au@Pt nanorods in buffers at different pHs at 23 ^{o}C. The spectra were recorded at a predetermined interval for 30 min.

In order to study the enzymatic kinetics of tyrosinase and Au@Pt nanorods as enzyme mimetics, the oxidation reaction of selected phenolics was monitored through recording spectrum peak of (-)-Epicatechin, caffeic acid, and resveratrol using UV-VIS spectrophotometer. Then, sufficient tyrosinase or Au@Pt nanorods were added to give a

final concentration of 0.022 nM or 0.1 nM, respectively. The reaction kinetics for the catalytic oxidation of phenolics was studied by recording the absorption spectra at 1 min intervals in the scanning kinetics mode. The disappearance of phenolics was monitored by measurement of absorbance change at the λ_{max} appropriate for (-)-Epicatechin, caffeic acid, and resveratrol at 389, 285, and 305 nm, respectively. The extinction coefficient is 1,370; 29,000; and 19,510 $M^{-1}cm^{-1}$, respectively. The kinetic parameters were calculated based on the Michaelis-Menten equation $v = V_{max} \times [S]/(K_m + [S])$, where v is the initial velocity, V_{max} the maximal reaction velocity, [S] the concentration of substrate, and K_m the Michaelis constant.

6.2.5 Electron Spin Resonance (ESR) Measurement

All ESR measurements were carried out using a Bruker EMX ESR spectrometer (Billerica, MA) at ambient temperature. All samples were put in 50 μL glass capillary tubes and placed in the ESR cavity.

6.2.5.1 Oxidation of phenolics catalyzed by enzyme or platinum nanomaterials using ESR oximetry

The catalytic activity of tyrosinase and Au@Pt nanorods on different phenolics was assessed through observation of oxygen consumption. ESR spin label oximetry was employed to measure oxygen change during the reaction (*213*). Solutions containing 0.1 mM of the water-soluble spin label CTPO and 1 mM (-)-Epicatechin, caffeic acid, or resveratrol in 50 mM buffers at pH 6.0, 6.0, and 6.8 respectively. Among the phenolics, caffeic acid and resveratrol were dissolved in ethanol. The capillary tube was then sealed and positioned in the ESR instrument. ESR spectra were then recorded at 1, 3, 5, 7, and 10 min at the low field line of CTPO (at 23 ºC). Signals were obtained with a 1 G scanning

width, 1mW incident microwave power, and with 100 kHz field modulation. The detailed calculation method was described in our previous review article (*213*).

6.2.5.2 DPPH radical scavenging

DPPH radical is a stable synthesized nitrogen-centered radical. Since DPPH radical is UV-vis spectroscopy detectable, it has been commonly used as a target for antioxidant activity evaluation. In ESR spectroscopy, the peak to peak height of signal represents the amount of DPPH radical, thus the reduction of the signal is an indicator of scavenging ability. Control samples contained 0.2 mM DPPH radical and 10% ethanol in 10 mM buffer (pH 7.4). Different phenolics (-) - Epicatechin (1 mM), resveratrol (1 mM), or caffeic acid (0.05 mM) was added into sample solution to initiate reaction. To investigate the effect of Au@Pt nanorods on the phenolic in scavenging DPPH radical, the nanomaterials were premixed with the three phenolics for 30 min. The quenching effect of Au@Pt nanorods was also examined. The DPPH radical scavenging ability was represented as the signal reduction of sample against control solution in percentage. Spectra were recorded at 1 min under using the following conditions: 20 mW microwave power; 1 G field modulation; 100 G scan width.

6.2.6 Superoxide radical scavenging ability

Superoxide radicals (•OOH) were produced using the xanthine/xanthine oxidase (XOD) system and trapped as the spin adduct BMPO/•OOH. The method of superoxide radical detection using spin trap BMPO was essentially the same as described by Yin et al *(316)*. Phenolics, Au@Pt nanorods, or their mixtures were stored at room temperature for 30 min. Then, they were individually introduced into a freshly prepared xanthine/XOD mixture where generation of superoxide radical was initiated by addition of 0.2 U/ml XOD. Control solution included 25 mM BMPO, 1 mM xanthine, 0.1 mM DTPA, and 0.2 U/ml XOD in

10 mM pH 7.4 buffer. The scavenging ability on superoxide radicals was shown as the intensity reduction of BMPO/•OOH. The ESR spectra were recorded at 1.5 min using 20 mW microwave power, 1 G field modulation, and 100 G scan width.

6.2.6.1 Hydroxyl radical scavenging ability

Zinc oxide (ZnO) is a photosensitive compound that generates hydroxyl radicals when exposed to UV light. Samples were photoirradiated at 340 nm in the microwave cavity using light emitted from a 500 watt Xe arc lamp directed through a McPherson monochromator, model DM200 (Chelmsford, MA). In presence of ethanol, hydroxyl radicals are trapped by spin trap 4-POBN to form spin adduct 4-POBN/·OH. The control solution contained 25 mM 4-POBN, 0.04 mg/ml ZnO, and 20 % (v/v) ethanol in 10 mM buffer (pH 7.4). Spectra were recorded 1 min after the initiation of exposure to UV light under the following conditions: 20 mW microwave power; 1 G field modulation; 100 G scan width. The intensity reduction of 4-POBN/•OH signal was shown as scavenging ability on hydroxyl radical.

6.3 Results and discussion

6.3.1 Characterization of Au@Pt nanorods

The Au@Pt nanorods were prepared *via* seed-growth, described in a previous study (Chapter 0). The Au@Pt nanorods were in a core/shell structure consisting of Au nanorods as template and Pt nanodots growing on their surface. The morphology of Au@Pt nanorods before and after catalytic oxidation of (-)-Epicatechin was examined using TEM (Figure 6-3). It is obvious that the morphology of the nanorods remained the same after participation in oxidation of EC, except that a thin transparent layer surrounded the nanorods afterwards (Figure 6-3b). This might be the residue leftover from the oxidation reaction caused by insufficient centrifugal separation. In addition, the oxidation of EC catalyzed by Au@Pt

nanorods was observed when the original EC and Au@Pt nanorods turned into the bright, yellowish oxidation product (Figure 6-4).

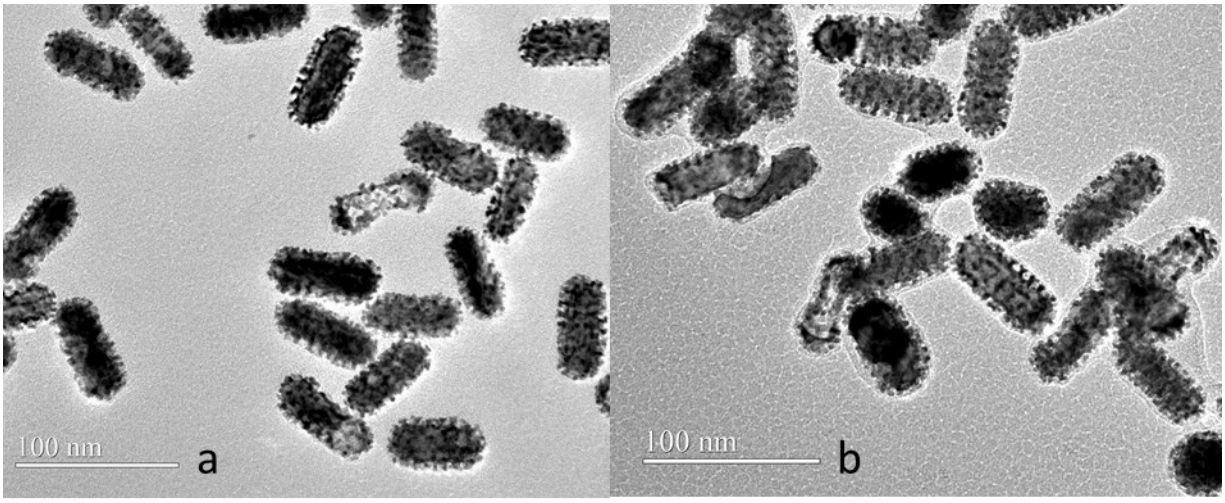

Figure 6-3 TEM image of Au@Pt nanorods before (a) and after (b) reaction with (-)-Epicatechin.

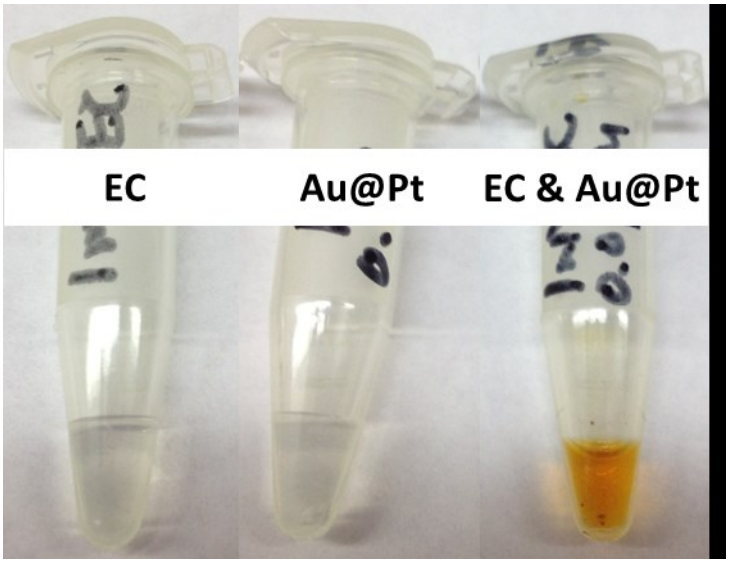

Figure 6-4 Visional change of (-)-Epicatechin before and after oxidation catalyzed by Au@Pt nanorods.

6.3.2 Spectrophotometric studies of phenolics

UV-vis spectroscopy experiments were conducted to investigate the catalytic effect of both tyrosinase and Au@Pt nanorods on selected phenolics. The oxidation process of phenolics was monitored by the disappearance of substrates or appearance of products. Each phenolic

presented distinct UV-vis absorption but all of the spectra for (-)-Epicatechin (Figure 6-5a), caffeic acid (Figure 6-6a), and resveratrol (Figure 6-7a) remained unchanged in absence of tyrosinase or Au@Pt nanorods for 30 min.

When added with Tyr, an absorption peak at ~389 nm appeared and became noticeable as a function of time, which means formation of a new compound (Figure 6-5b). The addition of Au@Pt nanorods also produced an absorbance at 389 nm and the higher amount of the nanorods resulted in a larger extent of amplitude (Figure 6-5c and d). This is indicative of the development of the same enzymatic oxidation product as Tyr catalyzed, and the more evolved the "enzyme" Au@Pt nanorods, the more efficient the oxidation. It is also apparent that the oxidation product formation rate slowed down over time, suggesting a saturation of enzyme Tyr at a level of 5 U/ml. However, the Au@Pt nanorods provided more steady generation of oxidized EC.

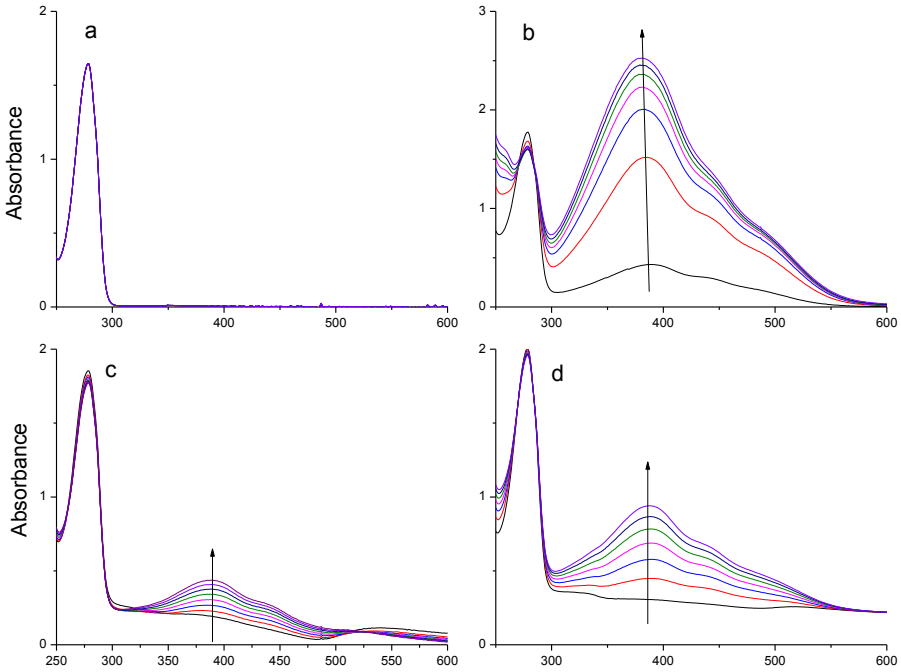

Figure 6-5 UV spectrum of 0.5mM (-)-Epicatechin in the absence (a), presence of 5 U/ml tyrosinase (b), 0.05 nM(c), and 0.1 nM (d) Au@Pt NRs in 10 mM phosphate buffer (pH 6.0). The spectra were recorded at 5-min intervals for a total of 30 min. Arrows show increase in absorbance.

In Figure 6-6, CFA exhibited two absorption maximums at 288 and 311 nm, which coincides with the findings by Haghbeen and Tan (*331*). In the presence of Tyr, both peaks diminished over time (Figure 6-6b), indicating the occurrence of a catecholase reaction. By monitoring the spectrum change, the enzymatic oxidation of CFA by Tyr was completed after 15 min with a rapid initiation rate. Beyond this time, no further change was observed. In the presence of Au@Pt nanorods, the characteristic peaks of CFA were progressively reduced as well (Figure 6-6c and d). The oxidation of CFA catalyzed by 0.1 nM Au@Pt NRs was completed in 30 min.

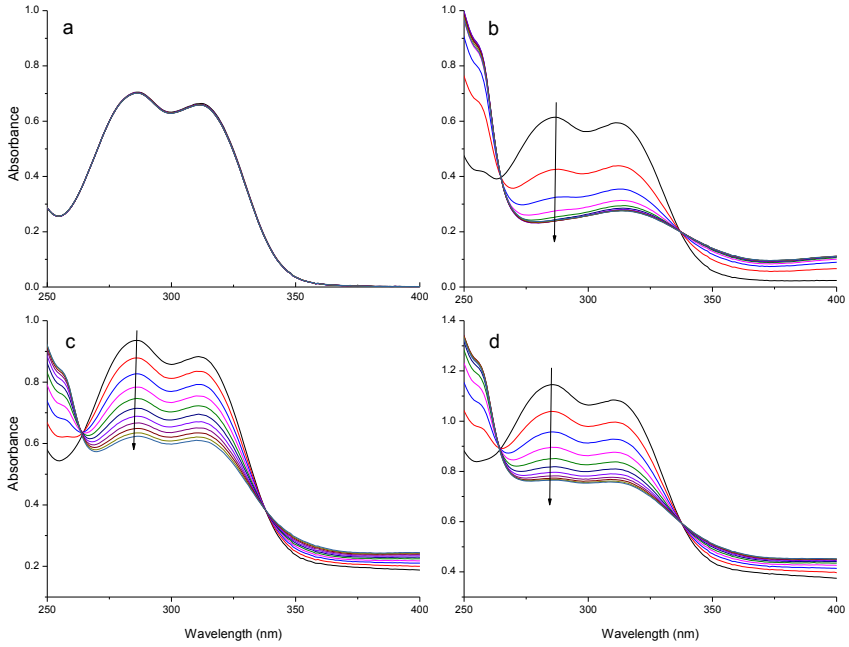

Figure 6-6 UV spectrum of 0.05 mM caffeic acid in the absence (a), presence of 5 U/ml tyrosinase (b), 0.05 nM(c), and 0.1 nM (d) Au@Pt NRs in 1% ethanol and 10 mM phosphate buffer (pH 6.0). The spectra were recorded at 3-min intervals for a total of 30 min. Arrows show decrease in absorbance.

Figure 6-7 shows a maximum range for RES at 305 to 345 nm. The addition of Tyr resulted in a disappearance of the adsorption peak over time. The peak at 305 nm decreased rapidly, while there was a shift in the adsorption maximum to 275 nm and the peak at 345 slightly to 348 nm (Figure 6-7b). It is equally noteworthy that the reduction of the maximum peak experienced an initial increase and a decrease afterwards, suggesting a second order reaction. This may because REV underwent both cresolase and catecholase reaction catalyzed by Tyr. REV only has two hydroxyl groups on *meta* position attached to the benzene ring instead of two adjacent hydroxyl groups (Figure 6-2). This is different from EC and CFA, both of which have two hydroxyl groups in *ortho* position of benzene ring. With the addition of Au@Pt nanorods, the adsorption peaks both declined and the degree of reduction was proportional to the amount of nanorods, although both changes were less evident than that caused by Tyr (Figure 6-7c and d). However, the shifting at 305 nm was

not noticeable and the reduction rate of the adsorption maximum appeared constant, which indicates a dominance of one order reaction catalyzed by Au@Pt nanorods.

According to the evolution of the selected phenolics in presence of either Tyr or Au@Pt nanorods via UV-vis spectroscopy, the main enzyme mimetic activity of Au@Pt nanorods was exhibited in the oxidation of *o*-diphenols to *o*-quinones.

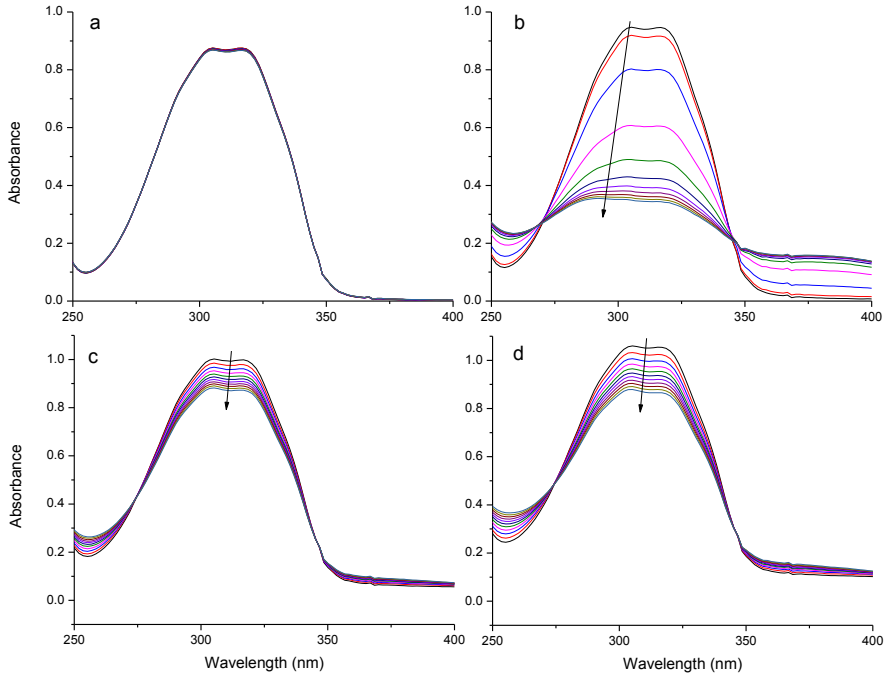

Figure 6-7 UV spectrum of 0.1 mM resveratrol in the absence (a), presence of 5 U/ml tyrosinase (b), 0.05 nM(c), and 0.1 nM (d) Au@Pt NRs in 2% ethanol and 10 mM phosphate buffer (pH 6.0). The spectra were recorded at 3-min intervals for a total of 30 min. Arrows show decrease in absorbance.

6.3.3 ESR oximetry

Besides monitoring the change of selected phenolics, another critical participant, oxygen, was examined during enzymatic oxidation using ESR oximetry. Parameter K was obtained from the ESR spectrum of CTPO (*213*) and calibration curve was calculated based on $[O_2] = aK+b$. In Figure 6-8, oxygen content in all sample solutions decreased rapidly upon the addition of Tyr and Au@Pt nanorods at different levels during 10 min. This set of data indicates the catalytic role of Au@Pt nanorods in the oxidation of selected phenolics rather

than the reactants. Among the three phenolics, Tyr showed strongest catalytic activity towards EC while Au@Pt nanorods, at a level of 0.5 nM, resulted in more oxygen consumption during oxidation of CFA and REV. This may be attributed to the inefficiency of Tyr caused by organic solvent that was used to dissolve CFA and REV. This also brings up one advantage of nanoparticles over natural enzymes is that the former is more resistant to environment condition.

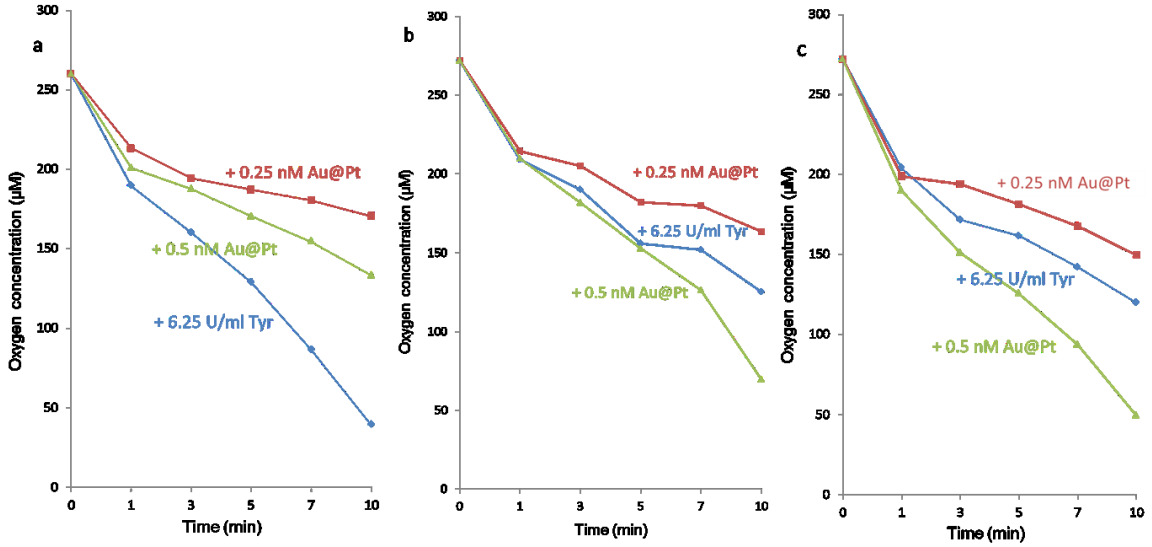

Figure 6-8 Oxygen consumption during oxidation of (-)-Epicatechin (a), caffeic acid (b), and resveratrol (c) in presence of Au@Pt nanorods and tyrosinase (Tyr).

6.3.4 Kinetic parameters using UV-Vis spectroscopy

The property of enzymes towards particular substrates could be characterized by catalytic constant (K_{cat}) and Michaelis constant (K_m). A larger catalytic constant K_{cat} represents a higher enzyme activity, i.e., catalysis efficiency whereas a higher Michaelis constant value indicates less affinity of the enzyme to substrate. The kinetic parameters of Tyr and enzyme mimetic parameters of Au@Pt nanorods towards EC, CFA, and REV, in individual optimum conditions could be identified in Table 6-1. The extinction coefficient for each phenolics is: 1370 $M^{-1}cm^{-1}$ @389 nm for EC (*332*), 19,510 $M^{-1}cm^{-1}$@285 nm for CFA,

and 29,000 $M^{-1}cm^{-1}$ @305 nm for REV (*333*), respectively. In summary, tyrosinase is more efficient in catalyzing oxidation of EC, CFA, and REV than Au@Pt nanorods. Both tyrosinase and Au@Pt nanorods showed increased enzymatic activity on the oxidation of phenolics in an order of EC >> CFA > REV. This may because caffeic acid and resveratrol were both dissolved in ethanol, which may partially deactivate the enzyme and limited the water soluble nanorods in the contact with the substrate. However, the K_m values of Tyr, when CFA and REV were employed as substrates, were much lower than the one of Tyr with EC, which suggests that Tyr was preferable to CFA and REV than EC. In the oxidation of all the three phenolics, Au@Pt nanorods exhibited lower catalytic activity yet higher affinity to the substrates. The active sites for Au@Pt nanorods are Pt nanodots, 3-5 nm in diameter. Therefore, the large surface area of Pt nanodots may be promoting electron transfer during the oxidation reaction. The catalysis advantage of Tyr over Au@Pt nanorods towards CFA and REV was less than that to EC, indicating that the enzymatic property of the nanorods is more solvent resistant than the enzyme.

Table 6-1 Kinetic parameters for 0.022 nM Tyr and 0.1 nM Au@Pt nanorods as Tyr mimetics. K_m is the Michaelis constant, V_{max} is the maximum reaction rate and K_{cat} is the catalytic constant. Reaction conditions: 50 mM buffers at 23 °C.

Substrate	pH	K_m, mM		V_{max}, nM s^{-1}		K_{cat}, s^{-1}	
		Tyr	Au@Pt	Tyr	Au@Pt	Tyr	Au@Pt
(-)-Epicatechin	6.0	0.9	2.0×10^{-2}	1.0×10^{4}	2.0×10^{2}	4.5×10^{5}	4.1×10^{3}
Caffeic acid	6.0	0.04	2.6×10^{-3}	99.0	32.9	4.5×10^{3}	6.6×10^{2}
Resveratrol	6.8	0.03	5.2×10^{-4}	57.5	10.4	2.6×10^{3}	1×10^{2}

6.3.5 ESR study

Three free radicals were selected in the current study to evaluate the scavenging ability of the phenolics and their oxidation product catalyzed by either Tyr or Au@Pt nanorods. DPPH radical is a stable radical dissolved in ethanol with a one line spectrum in ESR

spectroscopy (Figure 6-9 spectrum 1). In the xanthine/XOD system used for generating superoxide radical, BMPO was chosen as a spin trap to form spin adduct BMPO/•OOH. The spin adduct has four lines with relative intensities of 1:1:1:1 and was fitted with a_N = 13.5 G, a^{β}_H = 11.2 G (Figure 6-9 spectrum 2). Another ROS hydroxyl radical was produced by photoirradiating ZnO nanodispersion at 340 nm. In order to detect the generation of the most reactive ROS hydroxyl radical, we used 4-POBN/ethanol system. In this system, ·OH reacts with ethanol to yield α-hydroxyethyl radical, which then was rapidly trapped by 4-POBN to form 4-POBN/·OH spin adduct. The control sample yielded an ESR spectrum of 4-POBN/·OH with hyperfine splitting constants a_N = 15.58 G and a_H = 2.62 G (Figure 6-9 spectrum 3), which was consistent with reported data (*334*). The scavenging ability of phenolics or their oxidized product is expressed as the resulted attenuation of the spectrum for each radical or spin adduct.

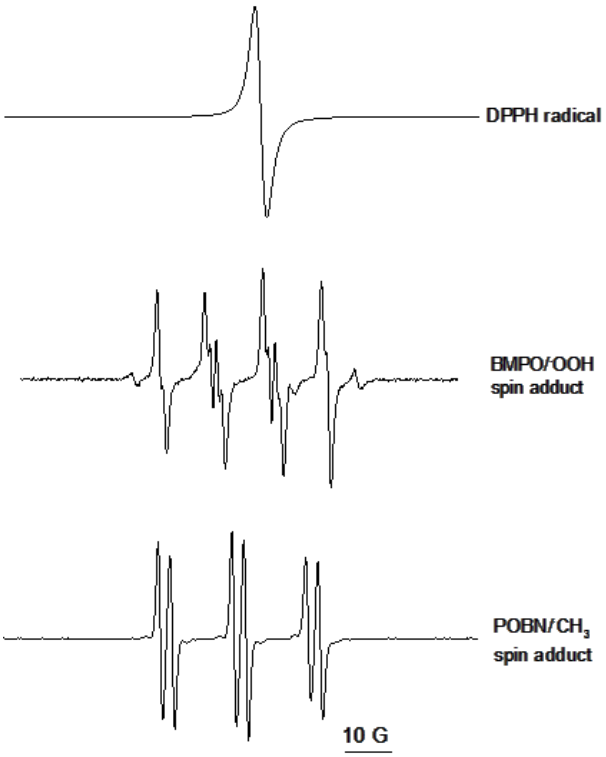

Figure 6-9 ESR spectra of radicals or their spin adducts.

6.3.5.1 DPPH radical scavenging

The DPPH radical scavenging ability of the selected phenolics was listed in Table 6-2. When DPPH radical abstracts one hydrogen atom, it becomes a reduced form that is ESR silent. All the phenolics showed quenching capability against DPPH radical and CFA was the strongest one amongst them. Consistent with previous reports that platinumnanoparticles could scavenge DPPH radical, our Au@Pt nanorods also showed a concentration dependent scavenging activity. Nevertheless, it is interesting to realize that the scavenging effect of all the phenolics were reduced after premixing with Au@Pt nanorods, which may due to the formation of *o*-quinone that is not able to provide H atom. Yet, they were still quite efficient in reducing DPPH radical possibly because 1) the scavenging ability of the nanorods themselves and 2) other H atom donation group of the phenolics rather than *o*-diphenols.

Table 6-2 DPPH radical scavenging ability of phenolics influenced by Au@Pt nanorods (n = 3).

Phenolics	DPPH scavenging ability, %		
	Au@Pt NRs, nM		
	None	0.05	0.1
(-) - Epicatechin, 1 mM	94.9 ± 2.0	N/A	84.6 ± 1.26
Resveratrol, 1 mM	71.2 ± 1.33	N/A	55.0 ± 2.74
Caffeic acid, 0.05 mM	47.1 ± 0.12	29.7 ± 1.04	N/A
None	N/A	22.7 ± 1.51	47.8 ± 0.75

6.3.5.2 Superoxide radical scavenging

The superoxide radical scavenging effect of the three phenolics was also investigated shown in Table 6-3. All three phenolics effectively reduced superoxide radical but their ability stayed the same even after mixing with Au@Pt nanorods. Considering the scavenging effect from nanorods themselves, it is possible that the reduced scavenging ability of phenolics owing to their partial catalytic oxidation was compensated by Au@Pt nanorods. When the superoxide radical was produced from xanthine/XOD system, spin trap BMPO was employed to form a spin adduct BMPO/·OOH, which is ESR detectable as shown in Figure 6-9 spectrum 1. The shape of spin adduct BMPO/·OOH dominated in ESR spectrum as phenolics and their pre-mixture with Au@Pt nanorods were added at levels mentioned in Table 6-3.

.

Table 6-3 Superoxide radical scavenging ability of phenolics influenced by Au@Pt nanorods (n = 3).

Phenolics	Superoxide radical scavenging ability, %	
	Au@Pt NRs, nM	
	None	0.05
(-) - Epicatechin, 1mM	88.9 ± 1.87	90.3 ± 2.01
Resveratrol, 1mM	71.5 ± 0.44	71.5 ± 1.27
Caffeic acid, 1 mM	93.6 ± 1.52	93.3 ± 0.46
None	N/A	27.8 ± 0.27

6.3.5.3 Hydroxyl radical scavenging ability

Hydroxyl radical is the most reactive ROS and it has been associated with damages of cells and DNA. Compared to previously mentioned radicals, the hydroxyl radical is more resistant to antioxidants. In comparison with DPPH and superoxide radical, higher concentrations of selected phenolics were required to scavenge hydroxyl radicals (Table 6-4). Moreover, EC was the most effective antioxidant in scavenging hydroxyl radicals. This maybe because EC has most hydroxyl groups attached to benzene rings that could readily donate electrons to hydroxyl radicals. We have already reported that Au@Pt nanorods were not able to scavenge hydroxyl radicals in section 5.2.5.4. Therefore, although they are able to reduce superoxide radical and decompose hydrogen peroxide, strictly speaking they are not a universal antioxidant. However, the hydroxyl radical scavenging ability of EC, REV, and CFA was influenced slightly by the inclusion of Au@Pt nanorods. Instead of phenolics, hydroxyl radicals can react with quinone to form OH-adduct and possibly underwent a very rapid water-assisted keto-enol tautomerization to yield dihydroxylphenoxyl radical (*335*). As a result, the hydroxyl radical reduction capability of

the three phenolics was still strong although they have been catalytically oxidized by Au@Pt nanorods.

Table 6-4 Hydroxyl radical scavenging ability of phenolics influenced by Au@Pt nanorods (n = 3).

Phenolics	Hydroxyl radical scavenging ability, %	
	Au@Pt NRs, nM	
	None	0.5
(-) - Epicatechin, 6 mM	96.1 ± 2.1	86.8 ± 0.20
Resveratrol, 25 mM	63.1 ± 1.3	51.2 ± 0.81
Caffeic acid, 25 mM	94.9 ± 1.01	92.4 ± 2.22
None	N/A	0.1 ± 0.01

6.4 Conclusions

In current study, we found that Au@Pt nanorods behaved similarly to tyrosinase in catalyzing oxidation of phenolic to *o*-quinone in the presence of oxygen. However, the nanorods are preferable in assisting the oxidation of *o*-diphenols to the corresponding *o*-quinones instead of hydroxylation of monophenols to *o*-diphenols. The selected phenolics (-)-Epicatechin, caffeic acid, and resveratrol showed dissimilar ability to scavenge DPPH, superoxide, and hydroxyl radicals. The ability of Au@Pt nanorods to reduce the scavenging capability of phenolics was in an order DPPH radicals > hydroxyl radical > superoxide radical. The result indicates that antioxidant property of phenolics was compromised by Au@Pt nanorods because the antioxidants underwent oxidation catalyzed by Au@Pt nanorods. Since tyrosinase plays important roles in the production of melanin or other pigments, which results in fruit and vegetable browning or dermal darkening, our

results could provide insights to the potential usage of platinum nanoparticles in cosmetics, food packaging, or dietary supplements.

Chapter 7: Conclusions and future work

Silver nanomaterials have slightly or negligible effects against free radicals including ROS and organic radicals. Thiol-based antioxidants are important biological antioxidants known to scavenge free radicals via their thiol group. Nevertheless, the premixing of Ag nanomaterials with antioxidants containing thiol groups renders partial activity loss of the latter against free radicals. In presence of a significant biological relevant ROS, hydrogen peroxide, silver nanoparticles induce generation of hydroxyl radicals and oxygen in acidic and alkaline conditions, respectively. Interestingly, in strong alkaline environment, Ag NPs in smaller size (10 or 20 nm) more preferred to participate in a cyclic reaction that silver ions were formed initially and silver elements were reformed afterwards. Our results indicate that alteration of the balance between hydroxyl radicals, oxygen, and hydrogen peroxide should be considered when assessing the effects of Ag NPs.

Platinum nanoparticles have been considered as a good antioxidant against ROS. However, in the current study, Au@Pt nanorods had no effect in scavenging hydroxyl radicals, which are the most reactive ROS in biological systems. Instead, they have shown enzymatic activity similar to ascorbic acid oxidase, an enzyme facilitating oxidation of important dietary antioxidant ascorbic in presence of oxygen. As a result, the platinum nanorods jeopardize the antioxidant activity of ascorbic acid due to their catalytic activity in oxidation of the natural antioxidant. The Au@Pt nanorods also serve as a catalyst similar to polyphenol oxidase to assist in oxidation of selected phenolics. Our results are suggesting potential interaction that may arise between endogenous or dietary antioxidant and platinum nanoparticles when they are applied in consumer related products. However, the relationship between their catalytic ability and the substrates phenolics structure

remains unclear. Also, the underlying mechanism of the enzyme mimetic property of the platinum nanorods is still unknown, which brings up a question for future research: can the nanoparticles be modified to be specific to substrates?

Current study was conducted in vivo mimicking biological microenvironments, which provide unsophisticated ROS system to investigate the mechanism for potential risk that noble metal nanoparticles bring into biological systems. However, the complexity of biological systems and the unpredictability of nanoparticles make the task complicated. Many other factors should be considered. For example, the localization preference of nanoparticles in different cells may alter their behavior and the NPs could impact other biological enzymes, proteins, and DNA. We hope our preliminary study provides insights into the risk assessment of noble metal nanoparticles in biological systems from the aspect of ROS and antioxidants.

Chapter 8: References

1. NNI, Nanotechnology Benefits andApplications. http://www.nano.gov/you/nanotechnology-benefits

2. NNI, Nanotechnology Environmental, Health, and Safety Issues. http://www.nano.gov/you/environmental-health-safety

3. Harman, D., The biologic clock: the mitochondria? *Journal of the American Geriatrics Society* **1972,** *20*, 145-147.

4. Chance, B.; Sies, H.; Boveris, A., HYDROPEROXIDE METABOLISM IN MAMMALIAN ORGANS. *Physiological Reviews* **1979,** *59*, 527-605.

5. Droge, W., Free radicals in the physiological control of cell function. *Physiological Reviews* **2002,** *82*, 47-95.

6. Deby, C.; Goutier, R., New perspectives on the biochemistry of superoxide anion and the efficiency of superoxide dismutases. *Biochemical Pharmacology* **1990,** *39*, 399-405.

7. Steinbeck, M. J.; Khan, A. U.; Karnovsky, M. J., Extracellular production of singlet oxygen by stimulated macrophages quantified using 9,10-diphenylanthracene and perylene in a polystyrene film. *Journal of Biological Chemistry* **1993,** *268*, 15649-15654.

8. Lu, S. C., Regulation of glutathione synthesis. *Molecular Aspects of Medicine* **2009,** *30*, 42-59.

9. Halliwell, B.; Gutteridge, J. M. C., The chemistry of oxygen radicals and other oxygen derived species. In *Free radicals in biology and medicine*, 3rd ed.; Halliwell, B.; Gutteridge, J. M. C., Eds. Oxford University Press: New York, **1989**; pp 22-81.

10. Buettner, G. R.; Jurkiewicz, B. A., Catalytic metals, ascorbate and free radicals: Combinations to avoid. *Radiation Research* **1996,** *145*, 532-541.

11. Evans, M. D.; Dizdaroglu, M.; Cooke, M. S., Oxidative DNA damage and disease: induction, repair and significance. *Mutation Research-Reviews in Mutation Research* **2004,** *567*, 1-61.

12. Lubec, G., The hydroxyl radical: From chemistry to human disease. *Journal of Investigative Medicine* **1996,** *44*, 324-346.

13. Sun, Y.; Oberley, L. W., Redox regulation of transcriptional activators. *Free Radical Biology and Medicine* **1996,** *21*, 335-348.

14. Valko, M.; Leibfritz, D.; Moncol, J.; Cronin, M. T. D.; Mazur, M.; Telser, J., Free radicals and antioxidants in normal physiological functions and human disease. *International Journal of Biochemistry & Cell Biology* **2007,** *39*, 44-84.

15. Suzuki, Y. J.; Forman, H. J.; Sevanian, A., Oxidants as stimulators of signal transduction. *Free Radical Biology and Medicine* **1997,** *22*, 269-285.

16. Gerschman, R.; Gilbert, D. L.; Nye, S. W.; Dwyer, P.; Fenn, W. O., Oxygen poisoning and X-irradiation - a mechanism in common. *Science* **1954,** *119*, 623-626.

17. Harman, D., Aging: a theory based on free radical and radiation chemistry. *Journal of Gerontology* **1956,** *11*, 298-300.

18. Beckman, K. B.; Ames, B. N., The free radical theory of aging matures. *Physiological Reviews* **1998,** *78*, 547-581.

19. Kehrer, J. P., Free-radicals as mediators of tissue-injury and disease. *Critical Reviews in Toxicology* **1993,** *23*, 21-48.

20. Stadtman, E. R.; Berlett, B. S., Reactive oxygen-mediated protein oxidation in aging and disease. *Drug Metabolism Reviews* **1998,** *30*, 225-243.

21. Sohal, R. S.; Mockett, R. J.; Orr, W. C., Mechanisms of aging: An appraisal of the oxidative stress hypothesis. *Free Radical Biology and Medicine* **2002,** *33*, 575-586.

22. Valko, M.; Rhodes, C. J.; Moncol, J.; Izakovic, M.; Mazur, M., Free radicals, metals and antioxidants in oxidative stress-induced cancer. *Chemico-Biological Interactions* **2006,** *160*, 1-40.

23. Sachidanandam, K.; Fagan, S. C.; Ergul, A., Oxidative stress and cardiovascular disease: Antioxidants and unresolved issues. *Cardiovascular Drug Reviews* **2005,** *23*, 115-132.

24. Bodamyali, T.; Stevens, C. R.; Blake, D. R.; Winyard, P. G., Reactive oxygen/nitrogen species and acute inflammation: a physiological process. In *Free Radicals in Inflammation*, 1st ed.; Winyard, P. G.; Blake, D. R.; Evans, C. H., Eds. Birkhauser: Basel, Switzerland, **2000**; pp 11-19.

25. Butterfield, D. A., Alzheimer's a-amyloid peptide and free radical oxidative stress. In *Reactive Oxygen Species in Biological Systems: An Interdisciplinary Approach*, 1st ed.; Colton, C.; Gilbert, D., Eds. Kluwer Academic Publishers: New York, **1999**; pp 609-638.

26. Cohen, G., Oxidative stress and Parkinson's disease. In *Reactive Oxygen Species in Biological Systems: An Interdisciplinary Approach*, 1st ed.; Gilbert, D. L.; Colton, C. A., Eds. Kluwer Academic Publishers: New York, **1999**; pp 593-608.

27. Niedowicz, D. M.; Daleke, D. L., The role of oxidative stress in diabetic complications. *Cell Biochemistry and Biophysics* **2005,** *43*, 289-330.

28. Kawanishi, S.; Hiraku, Y.; Murata, M.; Oikawa, S., The role of metals in site-specific DNA damage with reference to carcinogenesis. *Free Radical Biology and Medicine* **2002,** *32*, 822-832.

29. Butterfield, D. A.; Kanski, J., Brain protein oxidation in age-related neurodegenerative disorders that are associated with aggregated proteins. *Mechanisms of Ageing and Development* **2001,** *122*, 945-962.

30. Poli, G.; Leonarduzzi, G.; Biasi, F.; Chiarpotto, E., Oxidative stress and cell signalling. *Current Medicinal Chemistry* **2004,** *11*, 1163-1182.

31. Crawford, D. R., Regulation of mammalian gene expression by reactive oxygen species. In *Reactive Oxygen Species in Biological Systems: An Interdisciplinary Approach*, 1st ed.; Gilbert, D. L.; Colton, C. A., Eds. Kluwer Academic Publishers: New York, **1999**; pp 155-171.

32. Marnett, L. J., Lipid peroxidation - DNA damage by malondialdehyde. *Mutation Research-Fundamental and Molecular Mechanisms of Mutagenesis* **1999,** *424*, 83-95.

33. Fink, S. P.; Reddy, G. R.; Marnett, L. J., Mutagenicity in Escherichia coli of the major DNA adduct derived from the endogenous mutagen malondialdehyde. *Proceedings of the National Academy of Sciences of the United States of America* **1997,** *94*, 8652-8657.

34. Fedtke, N.; Boucheron, J. A.; Walker, V. E.; Swenberg, J. A., Vinyl chloride-induced DNA adducts. 2. Formation and persistence of 7-(2'-oxoethyl)guanine and n2,3-ethenoguanine in rat-tissue DNA. *Carcinogenesis* **1990,** *11*, 1287-1292.

35. Davies, K. J. A., Oxidative stress, antioxidant defenses, and damage removal, repair, and replacement systems. *Iubmb Life* **2000,** *50*, 279-289.

36. Spear, N.; Aust, S. D., Effects of glutathione on Fenton reagent-dependent radical production and DNA oxidation. *Archives of Biochemistry and Biophysics* **1995,** *324*, 111-116.

37. Butterfield, D. A.; Castegna, A.; Drake, J.; Scapagnini, G.; Calabrese, V., Vitamin E and neurodegenerative disorders associated with oxidative stress. *Nutritional Neuroscience* **2002,** *5*, 229-239.

38. Butterfield, D. A.; Castegna, A.; Pocernich, C. B.; Drake, J.; Scapagnini, G.; Calabrese, V., Nutritional approaches to combat oxidative stress in Alzheimer's disease. *Journal of Nutritional Biochemistry* **2002,** *13*, 444-461.

39. Poon, H. F.; Calabrese, V.; Scapagnini, G.; Butterfield, D. A., Free radicals and brain aging. *Clinics in Geriatric Medicine* **2004,** *20*, 329-359.

40. Pocernich, C. B.; La Fontaine, M.; Butterfield, D. A., In-vivo glutathione elevation protects against hydroxyl free radical-induced protein oxidation in rat brain. *Neurochemistry International* **2000,** *36*, 185-191.

41. Pocernich, C. B.; Cardin, A. L.; Racine, C. L.; Lauderback, C. M.; Butterfield, D. A., Glutathione elevation and its protective role in acrolein-induced protein damage in synaptosomal membranes: relevance to brain lipid peroxidation in neurodegenerative disease. *Neurochemistry International* **2001,** *39*, 141-149.

42. Hammond, C. L.; Lee, T. K.; Ballatori, N., Novel roles for glutathione in gene expression, cell death, and membrane transport of organic solutes. *Journal of Hepatology* **2001,** *34*, 946-954.

43. Shahidi, F.; Naczk, M., *Phenolics in Food and Nutraceuticals*. CRC Press: Boca Raton, Florida, **2004**.

44. Hossain, M. A.; Asada, K., Monodehydroascorbate reductase from cucumber is a flavin adenine-dinucleotide enzyme. *Journal of Biological Chemistry* **1985,** *260*, 2920-2926.

45. Chen, L.; Hu, J. Y.; Wang, S. Q., The role of antioxidants in photoprotection: A critical review. *Journal of the American Academy of Dermatology* **2012,** *67*, 1013-1024.

46. Huang, H.; Manton, K. G., The role of oxidative damage in mitochondria during aging: A review. *Frontiers in Bioscience* **2004,** *9*, 1100-1117.

47. Peterkofsky, B., Ascorbate requirement for hydroxylation and secretion of procollagen - relationship to inhibition of collagen-synthesis in scurvy.*American Journal of Clinical Nutrition* **1991,** *54*, S1135-S1140.

48. Houglum, K. P.; Brenner, D. A.; Chojkier, M., Ascorbic-acid stimulation of collagen biosynthesis independent of hydroxylation. *American Journal of Clinical Nutrition* **1991,** *54*, S1141-S1143.

49. Ha, T. Y.; Otsuka, M.; Arakawa, N., The regulatory effect of ascorbate on the carnitine synthesis in primary cultured guinea-pig hepatocytes. *Journal of Nutritional Science and Vitaminology* **1991,** *37*, 371-378.

50. Rebouche, C. J., Ascorbic-acid and carnitine biosynthesis. *American Journal of Clinical Nutrition* **1991,** *54*, S1147-S1152.

51. Siegenberg, D.; Baynes, R. D.; Bothwell, T. H.; Macfarlane, B. J.; Lamparelli, R. D.; Car, N. G.; Macphail, P.; Schmidt, U.; Tal, A.; Mayet, F., Ascorbic-acid prevents the

dose-dependent inhibitory effects of polyphenols and phytates on nonheme-iron absorption. *American Journal of Clinical Nutrition* **1991,** *53*, 537-541.

52. Kyrtopoulos, S. A.; Pignatelli, B.; Karkanias, G.; Golematis, B.; Esteve, J., Studies in gastric carcinogenesis .5. The effects of ascorbic-acid on n-nitroso compound formation in human gastric-juice invivo and invitro. *Carcinogenesis* **1991,** *12*, 1371-1376.

53. Licht, W. R.; Tannenbaum, S. R.; Deen, W. M., Use of ascorbic-acid to inhibit nitrosation - kinetic and mass-transfer considerations for an invitro system. *Carcinogenesis* **1988,** *9*, 365-372.

54. Krinsky, N. I., Micronutrients and their influence on mutagenicity and malignant transformation. *Annals of the New York Academy of Sciences* **1993,** *686*, 229-242.

55. Chandra, R. K., Effect of vitamin and trace-element supplementation on immune-responses and infection in elderly subjects. *Lancet* **1992,** *340*, 1124-1127.

56. Jacob, R. A.; Kelley, D. S.; Pianalto, F. S.; Swendseid, M. E.; Henning, S. M.; Zhang, J. Z.; Ames, B. N.; Fraga, C. G.; Peters, J. H., Immunocompetence and oxidant defense during ascorbate depletion of healthy-men. *American Journal of Clinical Nutrition* **1991,** *54*, S1302-S1309.

57. Carr, A. C.; Zhu, B. Z.; Frei, B., Potential antiatherogenic mechanisms of ascorbate (vitamin C) and alpha-tocopherol (vitamin E). *Circulation Research* **2000,** *87*, 349-354.

58. Kaugars, G. E.; Silverman, S.; Lovas, J. G. L.; Brandt, R. B.; Thompson, J. S.; Singh, V. N., A review of the use of antioxidant supplements in the treatment of human oral leukoplakia. *Journal of Cellular Biochemistry* **1993**, 292-298.

59. Huber, M. H.; Lee, J. S.; Hong, W. K., Chemoprevention of lung-cancer. *Seminars in Oncology* **1993,** *20*, 128-141.

60. Garland, D. L., Ascorbic-acid and the eye. *American Journal of Clinical Nutrition* **1991,** *54*, S1198-S1202.

61. Meydani, S. N., Vitamin mineral supplementation, the aging immune-response, and risk of infection. *Nutrition Reviews* **1993,** *51*, 106-115.

62. Gerster, H., Potential role of beta-carotene in the prevention of cardiovascular-disease. *International Journal for Vitamin and Nutrition Research* **1991,** *61*, 277-291.

63. Simon, J. A., Vitamin-c and cardiovascular-disease - A review. *Journal of the American College of Nutrition* **1992,** *11*, 107-125.

64. Jacques, P. F.; Sulsky, S. I.; Perrone, G. A.; Schaefer, E. J., ASCORBIC-ACID AND PLASMA-LIPIDS. *Epidemiology* **1994,** *5*, 19-26.

65. Fujita, K.; Shinpo, K.; Yamada, K.; Sato, T.; Niimi, H.; Shamoto, M.; Nagatsu, T.; Takeuchi, T.; Umezawa, H., Reduction of adriamycin toxicity by ascorbate in mice and guinea-pigs. *Cancer Research* **1982,** *42*, 309-316.

66. Shimpo, K.; Nagatsu, T.; Yamada, K.; Sato, T.; Niimi, H.; Shamoto, M.; Takeuchi, T.; Umezawa, H.; Fujita, K., Ascorbic-acid and adriamycin toxicity. *American Journal of Clinical Nutrition* **1991,** *54*, S1298-S1301.

67. Rose, R. C.; Bode, A. M., Biology of free-radical scavengers - an evaluation of ascorbate. *Faseb Journal* **1993,** *7*, 1135-1142.

68. Buettner, G. R.; Jurkiewicz, B. A., Ascorbate free-radical as a marker of oxidative stress - an epr study. *Free Radical Biology and Medicine* **1993,** *14*, 49-55.

69. Yen, G. C.; Duh, P. D.; Tsai, H. L., Antioxidant and pro-oxidant properties of ascorbic acid and gallic acid. *Food Chemistry* **2002,** *79*, 307-313.

70. Niki, E., Interaction of ascorbate and alpha-tocopherol. *Annals of the New York Academy of Sciences* **1987,** *498*, 186-199.

71. Perly, B.; Smith, I. C. P.; Hughes, L.; Burton, G. W.; Ingold, K. U., Estimation of the location of natural alpha-tocopherol in lipid bilayers by c-13-nmr spectroscopy. *Biochimica Et Biophysica Acta* **1985,** *819*, 131-135.

72. Patel, V.; Fisher, M.; Voelker, M.; Gessner, U., Gastrointestinal effects of the addition of ascorbic acid to aspirin. *Pain Practice* **2012,** *12*, 476-484.

73. Shahidi, F.; Naczk, M., Biosynthesis, classification, and nomenclature of phenolics in food and nutraceuticals. In *Phenolics in Food and Nutraceuticals*, Shahidi, F.; Naczk, M., Eds. CRC Press: Boca Raton, FL, **2004**.

74. Myer, R. O.; Gorbet, D. W., Waxy and normal grain sorghums with varying tannin contents in diets for young-pigs. *Animal Feed Science and Technology* **1985,** *12*, 179-186.

75. Guyot, S.; Pellerin, P.; Brillouet, J. M.; Cheynier, V., Inhibition of beta-glucosidase (Amygdalae dulces) by (+)-catechin oxidation products and procyanidin dimers. *Bioscience Biotechnology and Biochemistry* **1996,** *60*, 1131-1135.

76. Sell, D. R.; Rogler, J. C.; Featherston, W. R., The effects of sorghum tannin and protein level on the performance of laying hens maintained in 2 temperature environments. *Poultry Science* **1983,** *62*, 2420-2428.

77. Shahidi, F.; Naczk, M., Antioxidant properties of food phenolics. In *Phenolics in Food and Nutraceuticals*, Shahidi, F.; Naczk, M., Eds. CRC Press: Boca Raton, FL, **2004**.

78. Sherwin, E. R., Oxidation and antioxidants in fat and oil processing. *Journal of the American Oil Chemists Society* **1978,** *55*, 809-814.

79. Nawar, W. W., Lipids. In *Food Chemistry*, 3rd ed.; Fennema, O. R., Ed. Marcel Dekker Inc.: New York, **1996**; pp 225-319.

80. Shahidi, F.; Naczk, M., Contribution of phenolic compounds to flavor and color characteristics of foods. In *Phenolics in Food and Nutraceuticals*, Shahidi, F.; Naczk, M., Eds. CRC Press: Boca Raton, FL, **2004**.

81. Lee, C. Y., Enzymatic oxidation of phenolic-compounds in fruits. *Acs Symposium Series* **1992,** *506*, 305-317.

82. Dziedzic, S. Z.; Hudson, B. J. F., Polyhydroxy chalcones and flavanones as anti-oxidant for edible oils. *Food Chemistry* **1983,** *12*, 205-212.

83. Zaveri, N. T., Green tea and its polyphenolic catechins: Medicinal uses in cancer and noncancer applications. *Life Sciences* **2006,** *78*, 2073-2080.

84. Khalil, M. I.; Sulaiman, S. A., The potential role of honey and its polyphenols in preventing heart diseases: a review. *African Journal of Traditional Complementary and Alternative Medicines* **2010,** *7*, 315-321.

85. Watanabe, M. A. E.; Amarante, M. K.; Conti, B. J.; Sforcin, J. M., Cytotoxic constituents of propolis inducing anticancer effects: a review. *Journal of Pharmacy and Pharmacology* **2011,** *63*, 1378-1386.

86. Akyol, S.; Ginis, Z.; Armutcu, F.; Ozturk, G.; Yigitoglu, M. R.; Akyol, O., The potential usage of caffeic acid phenethyl ester (CAPE) against chemotherapy-induced and radiotherapy-induced toxicity. *Cell Biochemistry and Function* **2012,** *30*, 438-443.

87. Shahidi, F.; Naczk, M., Phenolic Compounds in Fruits and Vegetables. In *Phenolics in Food and Nutraceuticals*, Shahidi, F.; Naczk, M., Eds. CRC Press: Boca Raton, FL, **2004**.

88. Stivala, L. A.; Savio, M.; Carafoli, F.; Perucca, P.; Bianchi, L.; Maga, G.; Forti, L.; Pagnoni, U. M.; Albini, A.; Prosperi, E.; Vannini, V., Specific structural determinants are responsible for the antioxidant activity and the cell cycle effects of resveratrol. *Journal of Biological Chemistry* **2001,** *276*, 22586-22594.

89. Belguendouz, L.; Fremont, L.; Linard, A., Resveratrol inhibits metal ion-dependent and independent peroxidation of porcine low-density lipoproteins. *Biochemical Pharmacology* **1997,** *53*, 1347-1355.

90. Teissedre, P. L.; Frankel, E. N.; Waterhouse, A. L.; Peleg, H.; German, J. B., Inhibition of in vitro human LDL oxidation by phenolic antioxidants from grapes and wines. *Journal of the Science of Food and Agriculture* **1996,** *70*, 55-61.

91. Hsieh, T. C.; Wu, J. M., Differential effects on growth, cell cycle arrest, and induction of apoptosis by resveratrol in human prostate cancer cell lines. *Experimental Cell Research* **1999,** *249*, 109-115.

92. Carbo, N.; Costelli, P.; Baccino, F. M.; Lopez-Soriano, F. J.; Argiles, J. M., Resveratrol, a natural product present in wine, decreases tumour growth in a rat tumour model. *Biochemical and Biophysical Research Communications* **1999,** *254*, 739-743.

93. Shahidi, F.; Naczk, M., Methods of Analysis and Quantification of Phenolic Compounds. In *Phenolics in Food and Nutraceuticals*, Shahidi, F.; Naczk, M., Eds. CRC Press: Boca Raton, FL, **2004**.

94. Macheix, J.-J.; Fleuriet, A.; Billot, J., *Fruit Phenolics*. CRC Press Inc.: Boca Raton, FL, **1990**.

95. Packer, L.; Kraemer, K.; Rimbach, G., Molecular aspects of lipoic acid in the prevention of diabetes complications. *Nutrition* **2001,** *17*, 888-895.

96. Packer, L.; Witt, E. H.; Tritschler, H. J., ALPHA-LIPOIC ACID AS A BIOLOGICAL ANTIOXIDANT. *Free Radical Biology and Medicine* **1995,** *19*, 227-250.

97. Carreau, J. P., Biosynthesis of lipoic acid via unsaturated fatty acids *Methods Enzymology* **1979,** *62*, 152-158.

98. Saggu, H.; Cooksey, J.; Dexter, D.; Wells, F. R.; Lees, A.; Jenner, P.; Marsden, C. D., A selective increase in particulate superoxide-dismutase activity in parkinsonian substantia nigra. *Journal of Neurochemistry* **1989,** *53*, 692-697.

99. Dexter, D. T.; Carayon, A.; Javoy-Agid, F.; Agid, Y.; Wells, F. R.; Daniel, S. E.; Lees, A. J.; Jenner, P.; Marsden, C. D., Alterations in the levels of iron, ferritin and other trace metals in Parkinson's disease and other neurodegenerative diseases affecting the basal ganglia. *Brain* **1991,** *114 (Pt 4)*, 1953-1975.

100. Shoffner, J. M.; Watts, R. L.; Juncos, J. L.; Torroni, A.; Wallace, D. C., Mitochondrial oxidative-phosphorylation defects in parkinsons-disease. *Annals of Neurology* **1991,** *30*, 332-339.

101. Scheer, B.; Zimmer, G., Dihydrolipoic acid prevents hypoxic reoxygenation and peroxidative damage in rat-heart mitochondria. *Archives of Biochemistry and Biophysics* **1993,** *302*, 385-390.

102. Serbinova, E.; Reznick, S.; Packer, L., Thioctic acid protects against ischemia-reperfusion injury in the isolated perfused langendorff heart. *Free Radical Research Communications* **1992,** *17*, 49-58.

103. Haramaki, N.; Packer, L.; Assadnazari, H.; Zimmer, G., Cardiac recovery during postischemic reperfusion is improved by combination of vitamin-e with dihydrolipoic acid. *Biochemical and Biophysical Research Communications* **1993,** *196*, 1101-1107.

104. Ramakrishnan, N.; Wolfe, W. W.; Catravas, G. N., Radioprotection of hematopoietic tissues in mice by lipoic acid. *Radiation Research* **1992,** *130*, 360-365.

105. Handelman, G. J.; Han, D.; Tritschler, H.; Packer, L., Alpha-lipoic acid reduction by mammalian-cells to the dithiol form, and release into the culture-medium. *Biochemical Pharmacology* **1994,** *47*, 1725-1730.

106. Podda, M.; Han, D.; Koh, B.; Fuchs, J.; Packer, L., Conversion of lipoic acid to dihydrolipoic acid in human keratinocytes. *Clinical Research* **1994,** *42*, A41-A41.

107. Suzuki, Y. J.; Tsuchiya, M.; Packer, L., Thioctic acid and dihydrolipoic acid are novel antioxidants which interact with reactive oxygen species. *Free Radical Research Communications* **1991,** *15*, 255-263.

108. Scott, B. C.; Aruoma, O. I.; Evans, P. J.; Oneill, C.; Vandervliet, A.; Cross, C. E.; Tritschler, H.; Halliwell, B., Lipoic and dihydrolipoic acids as antioxidants - a critical-evaluation. *Free Radical Research* **1994,** *20*, 119-133.

109. Haenen, G.; Bast, A., Scavenging of hypochlorous acid by lipoic acid. *Biochemical Pharmacology* **1991,** *42*, 2244-2246.

110. Stevens, B.; Perez, S. R.; Small, R. D., Photoperoxidation of unsaturated organic-molecules .9. lipoic acid inhibition of rubrene autoperoxidation. *Photochemistry and Photobiology* **1974,** *19*, 315-316.

111. Stary, F. E.; Jindal, S. L.; Murray, R. W., Oxidation of alpha-lipoic acid. *Journal of Organic Chemistry* **1975,** *40*, 58-62.

112. Sigel, H.; Prijs, B.; McCormick, D. B.; Shih, J. C. H., Stability and structure of binary and ternary complexes of alpha-lipoate and lipoate derivatives with Mn^{2+}, Cu^{2+}, and Zn^{2+} in solution. *Archives of Biochemistry and Biophysics* **1978,** *187*, 208-214.

113. Busse, E.; Zimmer, G.; Schopohl, B.; Kornhuber, B., Influence of alpha-lipoic acid on intracellular glutathione invitro and in vivo. *Arzneimittel-Forschung/Drug Research* **1992,** *42-1*, 829-831.

114. Kagan, V. E.; Shvedova, A.; Serbinova, E.; Khan, S.; Swanson, C.; Powell, R.; Packer, L., Dihydrolipoic acid - a universal antioxidant both in the membrane and in the aqueous phase - reduction of peroxyl, ascorbyl and chromanoxyl radicals. *Biochemical Pharmacology* **1992,** *44*, 1637-1649.

115. Sies, H., Strategies of antioxidant defense. *European Journal of Biochemistry* **1993,** *215*, 213-219.

116. Packer, L., New horizons in antioxidant research: Action of the thioctic acid/dihydrolipoic acid couple in biological systems. In *Thioctseure:2. International thioctic acid workshop*, Schmidt, K.; Ulrich, H., Eds. Universimed Verlag GmbH: Frankfurt, **1992**; pp 35-44.

117. Bonomi, F.; Werth, M. T.; Kurtz, D. M., Assembly of $Fe_2S_2(Sr)_4^{2-}$, $Fe_4S_4(Sr)_4^{2-}$ in aqueous-media from iron salts, thiols, and sulfur, sulfide, or thiosulfate plus rhodanese. *Inorganic Chemistry* **1985,** *24*, 4331-4335.

118. Bonomi, F.; Pagani, S.; Cariati, F.; Pozzi, A.; Crisponi, G.; Cristiani, F.; Nurchi, V.; Russo, U.; Zanoni, R., Synthesis and characterization of iron derivatives of dihydrolipoic acid and dihydrolipoamide. *Inorganica Chimica Acta* **1992,** *195*, 109-115.

119. Walter, P.; Welcomme, E.; Hallegot, P.; Zaluzec, N. J.; Deeb, C.; Castaing, J.; Veyssiere, P.; Breniaux, R.; Leveque, J. L.; Tsoucaris, G., Early use of PbS nanotechnology for an ancient hair dyeing formula. *Nano Letters* **2006,** *6*, 2215-2219.

120. Feynman, R. There's Plenty of Room at the Bottom. http://www.zyvex.com/nanotech/feynman.html

121. Piner, R. D.; Zhu, J.; Xu, F.; Hong, S. H.; Mirkin, C. A., "Dip-pen" nanolithography. *Science* **1999,** *283*, 661-663.

122. Roduner, E., Size matters: why nanomaterials are different. *Chemical Society Reviews* **2006,** *35*, 583-592.

123. EPA, Nanomaterials EPA is Assessing. http://www.epa.gov/nanoscience/quickfinder/nanomaterials.htm

124. Choudhary, V.; Gupta, A., Polymer/Carbon Nanotube Nanocomposites. In *Carbon Nanotubes - Polymer Nanocomposites*, Yellampalli, S., Ed. InTech: **2011**; pp 65-90.

125. Kane, C. L.; Mele, E. J., Size, shape, and low energy electronic structure of carbon nanotubes. *Physical Review Letters* **1997,** *78*, 1932-1935.

126. Tans, S. J.; Devoret, M. H.; Dai, H. J.; Thess, A.; Smalley, R. E.; Geerligs, L. J.; Dekker, C., Individual single-wall carbon nanotubes as quantum wires. *Nature* **1997,** *386*, 474-477.

127. Jacobs, C. B.; Peairs, M. J.; Venton, B. J., Review: Carbon nanotube based electrochemical sensors for biomolecules. *Analytica Chimica Acta* **2010,** *662*, 105-127.

128. Claussen, J. C.; Franklin, A. D.; ul Haque, A.; Porterfield, D. M.; Fisher, T. S., Electrochemical biosensor of nanocube-augmented carbon nanotube networks. *ACS Nano* **2009,** *3*, 37-44.

129. Popov, A. P.; Zvyagin, A. V.; Lademann, J.; Roberts, M. S.; Sanchez, W.; Priezzhev, A. V.; Myllyla, R., Designing inorganic light-protective skin nanotechnology products. *Journal of Biomedical Nanotechnology* **2010,** *6*, 432-451.

130. Nohynek, G. J.; Dufour, E. K., Nano-sized cosmetic formulations or solid nanoparticles in sunscreens: A risk to human health? *Archives of Toxicology* **2012,** *86*, 1063-1075.

131. Burnett, M. E.; Wang, S. Q., Current sunscreen controversies: a critical review. *Photodermatology Photoimmunology & Photomedicine* **2011,** *27*, 58-67.

132. Baraton, M. I., Nano-TiO_2 for dye-sensitized solar cells. *Recent Patents on Nanotechnology* **2012,** *6*, 10-15.

133. Fan, S. Q.; Li, C. J.; Yang, G. J.; Zhang, L. Z.; Gao, J. C.; Xi, Y. X., Fabrication of nano-TiO_2 coating for dye-sensitized solar cell by vacuum cold spraying at room temperature. *Journal of Thermal Spray Technology* **2007,** *16*, 893-897.

134. Allahverdiyev, A. M.; Abamor, E. S.; Bagirova, M.; Rafailovich, M., Antimicrobial effects of TiO_2 and Ag_2O nanoparticles against drug-resistant bacteria and leishmania parasites. *Future Microbiology* **2011,** *6*, 933-940.

135. Emamifar, A.; Kadivar, M.; Shahedi, M.; Solimanian-Zad, S., EFFECT OF NANOCOMPOSITE PACKAGING CONTAINING AG AND ZNO ON REDUCING PASTEURIZATION TEMPERATURE OF ORANGE JUICE. *Journal of Food Processing and Preservation* **2012,** *36*, 104-112.

136. EPA, EPA Researchers Examine Nanoparticles' Impact on Fuel Emissions and Air Pollution. http://www.epa.gov/AMD/Research/RIA/nano.html

137. Karakoti, A. S.; Monteiro-Riviere, N. A.; Aggarwal, R.; Davis, J. P.; Narayan, R. J.; Self, W. T.; McGinnis, J.; Seal, S., Nanoceria as antioxidant: Synthesis and biomedical applications. *Jom* **2008,** *60*, 33-37.

138. Park, E. J.; Choi, J.; Park, Y. K.; Park, K., Oxidative stress induced by cerium oxide nanoparticles in cultured BEAS-2B cells. *Toxicology* **2008,** *245*, 90-100.

139. Xue, Y.; Zhai, Y. W.; Zhou, K. B.; Wang, L.; Tan, H. N.; Luan, Q. F.; Yao, X., The vital role of buffer anions in the antioxidant activity of CeO_2 nanoparticles. *Chemistry-a European Journal* **2012,** *18*, 11115-11122.

140. Ushakov, N. M.; Ul'zutuev, A. N.; Kosobudskii, I. D., Thermodielectric properties of polymer composites based on CuO-covered Cu particles in high-pressure polyethylene. *Technical Physics* **2008,** *53*, 1597-1601.

141. Chattopadhyay, D. P.; Patel, B. H., Effect of Nanosized Colloidal Copper on Cotton Fabric. *Journal of Engineered Fibers and Fabrics* **2010,** *5*, 1-6.

142. Mary, G.; Bajpai, S. K.; Chand, N., Copper (II) Ions and Copper Nanoparticles-Loaded Chemically Modified Cotton Cellulose Fibers with Fair Antibacterial Properties. *Journal of Applied Polymer Science* **2009,** *113*, 757-766.

143. Ren, G. G.; Hu, D. W.; Cheng, E. W. C.; Vargas-Reus, M. A.; Reip, P.; Allaker, R. P., Characterisation of copper oxide nanoparticles for antimicrobial applications. *International Journal of Antimicrobial Agents* **2009,** *33*, 587-590.

144. Pan, Y.; Du, X. W.; Zhao, F.; Xu, B., Magnetic nanoparticles for the manipulation of proteins and cells. *Chemical Society Reviews* **2012,** *41*, 2912-2942.

145. Liberti, P. A.; Rao, C. G.; Terstappen, L., Optimization of ferrofluids and protocols for the enrichment of breast tumor cells in blood. *Journal of Magnetism and Magnetic Materials* **2001,** *225*, 301-307.

146. Weissleder, R.; Elizondo, G.; Wittenberg, J.; Rabito, C. A.; Bengele, H. H.; Josephson, L., Ultrasmall superparamagnetic iron-oxide - characterization of a new class of contrast agents for mr imaging. *Radiology* **1990,** *175*, 489-493.

147. Ruehm, S. G.; Corot, C.; Vogt, P.; Kolb, S.; Debatin, J. F., Magnetic resonance imaging of atherosclerotic plaque with ultrasmall superparamagnetic particles of iron oxide in hyperlipidemic rabbits. *Circulation* **2001,** *103*, 415-422.

148. Dousset, V.; Gomez, C.; Petry, K. G.; Delalande, C.; Caille, J. M., Dose and scanning delay using USPIO for central nervous system macrophage imaging. *Magnetic Resonance Materials in Physics Biology and Medicine* **1999,** *8*, 185-189.

149. Gilchrist, R. K.; Medal, R.; Shorey, W. D.; Hanselman, R. C.; Parrott, J. C.; Taylor, C. B., Selective inductive heating of lymph nodes. *Annals of Surgery* **1957,** *146*, 596-606.

150. Pankhurst, Q. A.; Connolly, J.; Jones, S. K.; Dobson, J., Applications of magnetic nanoparticles in biomedicine. *Journal of Physics D-Applied Physics* **2003,** *36*, R167-R181.

151. Daniel, M. C.; Astruc, D., Gold nanoparticles: Assembly, supramolecular chemistry, quantum-size-related properties, and applications toward biology, catalysis, and nanotechnology. *Chemical Reviews* **2004,** *104*, 293-346.

152. Jain, P. K.; Huang, X. H.; El-Sayed, I. H.; El-Sayed, M. A., Noble metals on the nanoscale: optical and photothermal properties and some applications in imaging, sensing, biology, and medicine. *Accounts of Chemical Research* **2008,** *41*, 1578-1586.

153. Sokolov, K.; Follen, M.; Aaron, J.; Pavlova, I.; Malpica, A.; Lotan, R.; Richards-Kortum, R., Real-time vital optical imaging of precancer using anti-epidermal growth

factor receptor antibodies conjugated to gold nanoparticles. *Cancer Research* **2003,** *63*, 1999-2004.

154. El-Sayed, I. H.; Huang, X. H.; El-Sayed, M. A., Surface plasmon resonance scattering and absorption of anti-EGFR antibody conjugated gold nanoparticles in cancer diagnostics: Applications in oral cancer. *Nano Letters* **2005,** *5*, 829-834.

155. Underwood, S.; Mulvaney, P., Effect of the solution refractive-index on the color of gold colloids. *Langmuir* **1994,** *10*, 3427-3430.

156. Lee, K. S.; El-Sayed, M. A., Gold and silver nanoparticles in sensing and imaging: Sensitivity of plasmon response to size, shape, and metal composition. *Journal of Physical Chemistry B* **2006,** *110*, 19220-19225.

157. Grunwaldt, J. D.; Maciejewski, M.; Becker, O. S.; Fabrizioli, P.; Baiker, A., Comparative study of Au/TiO(2) and Au/ZrO(2) catalysts for low-temperature CO oxidation. *Journal of Catalysis* **1999,** *186*, 458-469.

158. Valden, M.; Lai, X.; Goodman, D. W., Onset of catalytic activity of gold clusters on titania with the appearance of nonmetallic properties. *Science* **1998,** *281*, 1647-1650.

159. Valden, M.; Pak, S.; Lai, X.; Goodman, D. W., Structure sensitivity of CO oxidation over model Au/TiO2 catalysts. *Catalysis Letters* **1998,** *56*, 7-10.

160. Alexander, J. W., History of the Medical Use of Silver. *Surgical Infections* **2009,** *10*, 289-292.

161. You, C. G.; Han, C. M.; Wang, X. G.; Zheng, Y. R.; Li, Q. Y.; Hu, X. L.; Sun, H. F., The progress of silver nanoparticles in the antibacterial mechanism, clinical application and cytotoxicity. *Molecular Biology Reports* **2012,** *39*, 9193-9201.

162. da Silva Paula, M. M.; Franco, C. V.; Baldin, M. C.; Rodrigues, L.; Barichello, T.; Savi, G. D.; Bellato, L. F.; Fiori, M. A.; da Silva, L., Synthesis, characterization and antibacterial activity studies of poly-{styrene-acrylic acid} with silver nanoparticles. *Materials Science & Engineering C-Biomimetic and Supramolecular Systems* **2009,** *29*, 647-650.

163. Cho, K. H.; Park, J. E.; Osaka, T.; Park, S. G., The study of antimicrobial activity and preservative effects of nanosilver ingredient. *Electrochimica Acta* **2005,** *51*, 956-960.

164. Lee, B. U.; Yun, S. H.; Ji, J.-H.; Bae, G.-N., Inactivation of S-epidermidis, B-subtilis, and E-coli bacteria bioaerosols deposited on a filter utilizing airborne silver nanoparticles. *Journal of Microbiology and Biotechnology* **2008,** *18*, 176-182.

165. Zodrow, K.; Brunet, L.; Mahendra, S.; Li, D.; Zhang, A.; Li, Q.; Alvarez, P. J. J., Polysulfone ultrafiltration membranes impregnated with silver nanoparticles show improved biofouling resistance and virus removal. *Water Research* **2009,** *43*, 715-723.

166. Panacek, A.; Kolar, M.; Vecerova, R.; Prucek, R.; Soukupova, J.; Krystof, V.; Hamal, P.; Zboril, R.; Kvitek, L., Antifungal activity of silver nanoparticles against Candida spp. *Biomaterials* **2009,** *30*, 6333-6340.

167. Lara, H. H.; Ayala-Nunez, N. V.; Ixtepan-Turrent, L.; Rodriguez-Padilla, C., Mode of antiviral action of silver nanoparticles against HIV-1. *Journal of Nanobiotechnology* **2010,** *8*, 1-Article No.: 1.

168. Olson, M. E.; Wright, J. B.; Lam, K.; Burrell, R. E., Healing of porcine donor sites covered with silver-coated dressings. *European Journal of Surgery* **2000,** *166*, 486-489.

169. Wright, J. B.; Lam, K.; Buret, A. G.; Olson, M. E.; Burrell, R. E., Early healing events in a porcine model of contaminated wounds: effects of nanocrystalline silver on matrix metalloproteinases, cell apoptosis, and healing. *Wound Repair and Regeneration* **2002,** *10*, 141-151.

170. Ip, M.; Lui, S. L.; Poon, V. K. M.; Lung, I.; Burd, A., Antimicrobial activities of silver dressings: an in vitro comparison. *Journal of Medical Microbiology* **2006,** *55*, 59-63.

171. Gurunathan, S.; Lee, K.-J.; Kalishwaralal, K.; Sheikpranbabu, S.; Vaidyanathan, R.; Eom, S. H., Antiangiogenic properties of silver nanoparticles. *Biomaterials* **2009,** *30*, 6341-6350.

172. Sheikpranbabu, S.; Kalishwaralal, K.; Venkataraman, D.; Eom, S. H.; Park, J.; Gurunathan, S., Silver nanoparticles inhibit VEGF-and IL-1-induced vascular permeability via Src dependent pathway in porcine retinal endothelial cells. *Journal of Nanobiotechnology* **2009,** *7*, 8-Article No.: 8.

173. Wang, H.-J.; Yang, L.; Yang, H.-Y.; Wang, K.; Yao, W.-G.; Jiang, K.; Huang, X.-L.; Zheng, Z., Antineoplastic activities of protein-conjugated silver sulfide nano-crystals with different shapes. *Journal of Inorganic Biochemistry* **2010,** *104*, 87-91.

174. Sur, I.; Cam, D.; Kahraman, M.; Baysal, A.; Culha, M., Interaction of multi-functional silver nanoparticles with living cells. *Nanotechnology* **2010,** *21*.

175. Braydich-Stolle, L. K.; Lucas, B.; Schrand, A.; Murdock, R. C.; Lee, T.; Schlager, J. J.; Hussain, S. M.; Hofmann, M.-C., Silver nanoparticles disrupt GDNF/Fyn kinase signaling in spermatogonial stem cells. *Toxicological Sciences* **2010,** *116*, 577-589.

176. Li, P.-W.; Kuo, T.-H.; Chang, J.-H.; Yeh, J.-M.; Chan, W.-H., Induction of cytotoxicity and apoptosis in mouse blastocysts by silver nanoparticles. *Toxicology Letters* **2010,** *197*, 82-87.

177. Rhim, J.-W.; Hong, S.-I.; Park, H.-M.; Ng, P. K. W., Preparation and characterization of chitosan-based nanocomposite films with antimicrobial activity. *Journal of Agricultural and Food Chemistry* **2006,** *54*, 5814-5822.

178. Tankhiwale, R.; Bajpai, S. K., Graft copolymerization onto cellulose-based filter paper and its further development as silver nanoparticles loaded antibacterial food-packaging material. *Colloids and Surfaces B-Biointerfaces* **2009,** *69*, 164-168.

179. Tian, N.; Zhou, Z. Y.; Sun, S. G.; Ding, Y.; Wang, Z. L., Synthesis of tetrahexahedral platinum nanocrystals with high-index facets and high electro-oxidation activity. *Science* **2007,** *316*, 732-735.

180. Lee, H.; Habas, S. E.; Kweskin, S.; Butcher, D.; Somorjai, G. A.; Yang, P. D., Morphological control of catalytically active platinum nanocrystals. *Angewandte Chemie-International Edition* **2006,** *45*, 7824-7828.

181. Narayanan, R.; El-Sayed, M. A., Changing catalytic activity during colloidal platinum nanocatalysis due to shape changes: Electron-transfer reaction. *Journal of the American Chemical Society* **2004,** *126*, 7194-7195.

182. Liu, J. B.; Hu, X. N.; Hou, S.; Wen, T.; Liu, W. Q.; Zhu, X.; Yin, J. J.; Wu, X. C., Au@Pt core/shell nanorods with peroxidase- and ascorbate oxidase-like activities for improved detection of glucose. *Sensors and Actuators B-Chemical* **2012,** *166*, 708-714.

183. Ma, M.; Zhang, Y.; Cu, N., Peroxidase-like catalytic activity of cubic Pt nanocrystals. *Colloids and Surfaces a-Physicochemical and Engineering Aspects* **2011,** *373*, 6-10.

184. Kloke, A.; von Stetten, F.; Zengerle, R.; Kerzenmacher, S., Strategies for the Fabrication of Porous Platinum Electrodes. *Advanced Materials* **2011,** *23*, 4976-5008.

185. Zhang, J.; Sasaki, K.; Sutter, E.; Adzic, R. R., Stabilization of platinum oxygen-reduction electrocatalysts using gold clusters. *Science* **2007,** *315*, 220-222.

186. Antolini, E.; Lopes, T.; Gonzalez, E. R., An overview of platinum-based catalysts as methanol-resistant oxygen reduction materials for direct methanol fuel cells. *Journal of Alloys and Compounds* **2008,** *461*, 253-262.

187. Joo, J. B.; Kim, Y. J.; Kim, W.; Kim, N. D.; Kim, P.; Kim, Y.; Yi, J., Methanol-tolerant PdPt/C alloy catalyst for oxygen electro-reduction reaction. *Korean Journal of Chemical Engineering* **2008,** *25*, 770-774.

188. Kajita, M.; Hikosaka, K.; Iitsuka, M.; Kanayama, A.; Toshima, N.; Miyamoto, Y., Platinum nanoparticle is a useful scavenger of superoxide anion and hydrogen peroxide. *Free Radical Research* **2007,** *41*, 615-626.

189. Fan, J.; Yin, J. J.; Ning, B.; Wu, X. C.; Hu, Y.; Ferrari, M.; Anderson, G. J.; Wei, J. Y.; Zhao, Y. L.; Nie, G. J., Direct evidence for catalase and peroxidase activities of ferritin-platinum nanoparticles. *Biomaterials* **2011,** *32*, 1611-1618.

190. Zhang, L. B.; Laug, L.; Munchgesang, W.; Pippel, E.; Gosele, U.; Brandsch, M.; Knez, M., Reducing Stress on Cells with Apoferritin-Encapsulated Platinum Nanoparticles. *Nano Letters* **2010,** *10*, 219-223.

191. Farrell, N. P., Platinum Formulations as Anticancer Drugs Clinical and Pre-Clinical Studies. *Current Topics in Medicinal Chemistry* **2011,** *11*, 2623-2631.

192. Su, H. L.; Chou, C. C.; Hung, D. J.; Lin, S. H.; Pao, I. C.; Lin, J. H.; Huang, F. L.; Dong, R. X.; Lin, J. J., The disruption of bacterial membrane integrity through ROS generation induced by nanohybrids of silver and clay. *Biomaterials* **2009,** *30*, 5979-5987.

193. Dibrov, P.; Dzioba, J.; Gosink, K. K.; Hase, C. C., Chemiosmotic mechanism of antimicrobial activity of Ag^{+} in Vibrio cholerae. *Antimicrobial Agents and Chemotherapy* **2002,** *46*, 2668-2670.

194. Foldbjerg, R.; Dang, D. A.; Autrup, H., Cytotoxicity and genotoxicity of silver nanoparticles in the human lung cancer cell line, A549. *Archives of Toxicology* **2011,** *85*, 743-750.

195. Liu, W.; Wu, Y. A.; Wang, C.; Li, H. C.; Wang, T.; Liao, C. Y.; Cui, L.; Zhou, Q. F.; Yan, B.; Jiang, G. B., Impact of silver nanoparticles on human cells: Effect of particle size. *Nanotoxicology* **2010,** *4*, 319-330.

196. Rosarin, F. S.; Arulmozhi, V.; Nagarajan, S.; Mirunalini, S., Antiproliferative effect of silver nanoparticles synthesized using amla on Hep2 cell line. *Asian Pacific Journal of Tropical Medicine* **2013,** *6*, 1-10.

197. Kim, T. H.; Kim, M.; Park, H. S.; Shin, U. S.; Gong, M. S.; Kim, H. W., Size-dependent cellular toxicity of silver nanoparticles. *Journal of Biomedical Materials Research Part A* **2012,** *100A*, 1033-1043.

198. Kaur, J.; Tikoo, K., Evaluating cell specific cytotoxicity of differentially charged silver nanoparticles. *Food and Chemical Toxicology* **2013,** *51*, 1-14.

199. Piao, M. J.; Kang, K. A.; Lee, I. K.; Kim, H. S.; Kim, S.; Choi, J. Y.; Choi, J.; Hyun, J. W., Silver nanoparticles induce oxidative cell damage in human liver cells through inhibition of reduced glutathione and induction of mitochondria-involved apoptosis. *Toxicology Letters* **2011,** *201*, 92-100.

200. Lim, D.; Roh, J. Y.; Eom, H. J.; Choi, J. Y.; Hyun, J.; Choi, J., Oxidative stress-related PMK-1 P38 MAPK activation as a mechanism for toxicity of silver nanoparticles to reproduction in the nematode Caenorhabditis elegans. *Environmental Toxicology and Chemistry* **2012,** *31*, 585-592.

201. Rehman, M. U.; Yoshihisa, Y.; Miyamoto, Y.; Shimizu, T., The anti-inflammatory effects of platinum nanoparticles on the lipopolysaccharide-induced inflammatory response in RAW 264.7 macrophages. *Inflammation Research* **2012,** *61*, 1177-1185.

202. Nomura, M.; Yoshimura, Y.; Kikuiri, T.; Hasegawa, T.; Taniguchi, Y.; Deyama, Y.; Koshiro, K.; Sano, H.; Suzuki, K.; Inoue, N., Platinum nanoparticles suppress osteoclastogenesis through scavenging of reactive oxygen species produced in RAW264.7 Cells. *Journal of Pharmacological Sciences* **2011,** *117*, 243-252.

203. Takamiya, M.; Miyamoto, Y.; Yamashita, T.; Deguchi, K.; Ohta, Y.; Abe, K., Strong neuroprotection with a novel platinum nanoparticle against ischemic stroke- and tissue plasminogen activator-related brain damages in mice. *Neuroscience* **2012,** *221*, 47-55.

204. Clark, A.; Zhu, A. P.; Sun, K.; Petty, H. R., Cerium oxide and platinum nanoparticles protect cells from oxidant-mediated apoptosis. *Journal of Nanoparticle Research* **2011,** *13*, 5547-5555.

205. Yoshihisa, Y.; Honda, A.; Zhao, Q. L.; Makino, T.; Abe, R.; Matsui, K.; Shimizu, H.; Miyamoto, Y.; Kondo, T.; Shimizu, T., Protective effects of platinum nanoparticles against UV-light-induced epidermal inflammation. *Experimental Dermatology* **2010,** *19*, 1000-1006.

206. Oo, M. K. K.; Yang, Y. M.; Hu, Y.; Gomez, M.; Du, H.; Wang, H. J., Gold nanoparticle-enhanced and size-dependent generation of reactive oxygen species from protoporphyrin IX. *ACS Nano* **2012,** *6*, 1939-1947.

207. Raji, V.; Kumar, J.; Rejiya, C. S.; Vibin, M.; Shenoi, V. N.; Abraham, A., Selective photothermal efficiency of citrate capped gold nanoparticles for destruction of cancer cells. *Experimental Cell Research* **2011,** *317*, 2052-2058.

208. Misawa, M.; Takahashi, J., Generation of reactive oxygen species induced by gold nanoparticles under X-ray and UV Irradiations. *Nanomedicine-Nanotechnology Biology and Medicine* **2011,** *7*, 604-614.

209. Du, L. B.; Suo, S.; Wang, G. Q.; Jia, H. Y.; Liu, K. J.; Zhao, B. L.; Liu, Y., Mechanism and cellular kinetic studies of the enhancement of antioxidant activity by using surface-functionalized gold nanoparticles. *Chemistry-a European Journal* **2013,** *19*, 1281-1287.

210. Menchon, C.; Martin, R.; Apostolova, N.; Victor, V. M.; Alvaro, M.; Herance, J. R.; Garcia, H., Gold nanoparticles supported on nanoparticulate ceria as a powerful agent against intracellular oxidative stress. *Small* **2012,** *8*, 1895-1903.

211. Spasojevic, I., Free radicals and antioxidants at a glance using EPR spectroscopy. *Critical Reviews in Clinical Laboratory Sciences* **2011,** *48*, 114-142.

212. Ahola, T.; Fellman, V.; Kjellmer, I.; Raivio, K. O.; Lapatto, R., Plasma 8-isoprostane is increased in preterm infants who develop bronchopulmonary dysplasia or periventricular leukomalacia. *Pediatric Research* **2004,** *56*, 88-93.

213. Zhou, Y. T.; Yin, J. J.; Lo, Y. M., Application of ESR spin label oximetry in food science. *Magnetic Resonance in Chemistry* **2011,** *49*, S105-S112.

214. Miller, E. R.; Pastor-Barriuso, R.; Dalal, D.; Riemersma, R. A.; Appel, L. J.; Guallar, E., Meta-analysis: High-dosage vitamin E supplementation may increase all-cause mortality. *Annals of Internal Medicine* **2005,** *142*, 37-46.

215. Vivekananthan, D. P.; Penn, M. S.; Sapp, S. K.; Hsu, A.; Topol, E. J., Use of antioxidant vitamins for the prevention of cardiovascular disease: meta-analysis of randomised trials. *Lancet* **2003,** *361*, 2017-2023.

216. Bjelakovic, G.; Nikolova, D.; Simonetti, R. G.; Gluud, C., Antioxidant supplements for prevention of gastrointestinal cancers: a systematic review and meta-analysis. *Lancet* **2004,** *364*, 1219-1228.

217. Yin, J. J.; Fu, P. P.; Lutterodt, H.; Zhou, Y. T.; Antholine, W. E.; Wamer, W., Dual role of selected antioxidants found in dietary supplements: crossover between anti- and pro-oxidant activities in the presence of copper. *Journal of Agricultural and Food Chemistry* **2012,** *60*, 2554-2561.

218. Serafini, M., Back to the origin of the 'antioxidant' hypothesis': the lost role of the antioxidant network in disease prevention. *Journal of the Science of Food and Agriculture* **2006,** *86*, 1989-1991.

219. Geranio, L.; Heuberger, M.; Nowack, B., The behavior of silver nanotextiles during washing. *Environmental Science and Technology* **2009,** *43*, 8113-8118.

220. Wilkinson, L. J.; White, R. J.; Chipman, J. K., Silver and nanoparticles of silver in wound dressings: a review of efficacy and safety. *Journal of Wound Care* **2011,** *20*, 543-9.

221. Nobile, M. A. d.; Cannarsi, M.; Altieri, C.; Sinigaglia, M.; Favia, P.; Iacoviello, G.; D'Agostino, R., Effect of Ag-containing nano-composite active packaging system on survival of alicyclobacillus acidoterrestris. *Journal of Food Science* **2004,** *69*, E379-E383.

222. Benn, T. M.; Westerhoff, P., Nanoparticle silver released into water from commercially available sock fabrics. *Environmental Science and Technology* **2008,** *42*, 4133-9.

223. Navarro, E.; Piccapietra, F.; Wagner, B.; Marconi, F.; Kaegi, R.; Odzak, N.; Sigg, L.; Behra, R., Toxicity of silver nanoparticles to Chlamydomonas reinhardtii. *Environmental Science and Technology* **2008,** *42*, 8959-64.

224. Miao, A. J.; Luo, Z.; Chen, C. S.; Chin, W. C.; Santschi, P. H.; Quigg, A., Intracellular uptake: a possible mechanism for silver engineered nanoparticle toxicity to a freshwater alga Ochromonas danica. *PLoS One* **2010,** *5*, e15196.

225. Panyala, N. R.; Maria Pena-Mendez, E.; Havel, J., Silver or silver nanoparticles: a hazardous threat to the environment and human health? *Journal of Applied Biomedicine* **2008,** *6*, 117-129.

226. AshaRani, P. V.; Low Kah Mun, G.; Hande, M. P.; Valiyaveettil, S., Cytotoxicity and genotoxicity of silver nanoparticles in human cells. *ACS Nano* **2009,** *3*, 279-90.

227. Kittler, S.; Greulich, C.; Diendorf, J.; Koller, M.; Epple, M., Toxicity of silver nanoparticles increases during storage because of slow dissolution under release of silver ions. *Chemistry of Materials* **2010,** *22*, 4548-4554.

228. Feng, Q. L.; Wu, J.; Chen, G. Q.; Cui, F. Z.; Kim, T. N.; Kim, J. O., A mechanistic study of the antibacterial effect of silver ions on Escherichia coli and Staphylococcus aureus. *Journal of Biomedical Materials Research* **2000,** *52*, 662-668.

229. Choi, O.; Hu, Z. Q., Size dependent and reactive oxygen species related nanosilver toxicity to nitrifying bacteria. *Environmental Science and Technology* **2008,** *42*, 4583-4588.

230. Carlson, C.; Hussain, S. M.; Schrand, A. M.; Braydich-Stolle, L. K.; Hess, K. L.; Jones, R. L.; Schlager, J. J., Unique cellular interaction of silver nanoparticles: size-dependent generation of reactive oxygen species. *Journal of Physical Chemistry B* **2008,** *112*, 13608-13619.

231. Suresh, A. K.; Pelletier, D. A.; Wang, W.; Morrell-Falvey, J. L.; Gu, B. H.; Doktycz, M. J., Cytotoxicity induced by engineered silver nanocrystallites is dependent on surface coatings and cell types. *Langmuir* **2012,** *28*, 2727-2735.

232. Neal, A. L., What can be inferred from bacterium-nanoparticle interactions about the potential consequences of environmental exposure to nanoparticles? *Ecotoxicology* **2008,** *17*, 362-371.

233. Jones, A. M.; Garg, S.; He, D.; Pham, A. N.; Waite, T. D., Superoxide-Mediated formation and charging of silver nanoparticles. *Environmental Science and Technology* **2011,** *45*, 1428-1434.

234. He, D.; Jones, A. M.; Garg, S.; Pham, A. N.; Waite, T. D., Silver nanoparticle-reactive oxygen species interactions: application of a charging-discharging model. *Journal of Physical Chemistry C* **2011,** *115*, 5461-5468.

235. Shi, M.; Kwon, H. S.; Peng, Z. M.; Elder, A.; Yang, H., Effects of surface chemistry on the generation of reactive oxygen species by copper nanoparticles. *ACS Nano* **2012,** *6*, 2157-2164.

236. Yang, X. Y.; Gondikas, A. P.; Marinakos, S. M.; Auffan, M.; Liu, J.; Hsu-Kim, H.; Meyer, J. N., Mechanism of silver nanoparticle toxicity is dependent on dissolved silver and surface coating in Caenorhabditis elegans. *Environmental Science and Technology* **2012,** *46*, 1119-1127.

237. Liu, J. Y.; Hurt, R. H., Ion release kinetics and particle persistence in aqueous nano-silver colloids. *Environmental Science and Technology* **2010,** *44*, 2169-2175.

238. Ho, C. M.; Yau, S. K. W.; Lok, C. N.; So, M. H.; Che, C. M., Oxidative dissolution of silver nanoparticles by biologically relevant oxidants: a kinetic and mechanistic study. *Chemistry-an Asian Journal* **2010,** *5*, 285-293.

239. Ho, C. M.; Wong, C. K.; Yau, S. K. W.; Lok, C. N.; Che, C. M., Oxidative Dissolution of Silver Nanoparticles by Dioxygen: A Kinetic and Mechanistic Study. *Chemistry-an Asian Journal* **2011,** *6*, 2506-2511.

240. Ma, R.; Levard, C.; Marinakos, S. M.; Cheng, Y. W.; Liu, J.; Michel, F. M.; Brown, G. E.; Lowry, G. V., Size-Controlled Dissolution of Organic-Coated Silver Nanoparticles. *Environmental Science and Technology* **2012,** *46*, 752-759.

241. Liu, J. Y.; Sonshine, D. A.; Shervani, S.; Hurt, R. H., Controlled Release of Biologically Active Silver from Nanosilver Surfaces. *ACS Nano* **2010,** *4*, 6903-6913.

242. Xiu, Z. M.; Ma, J.; Alvarez, P. J. J., Differential Effect of Common Ligands and Molecular Oxygen on Antimicrobial Activity of Silver Nanoparticles versus Silver Ions. *Environmental Science and Technology* **2011,** *45*, 9003-9008.

243. Zhang, W.; Yao, Y.; Sullivan, N.; Chen, Y. S., Modeling the Primary Size Effects of Citrate-Coated Silver Nanoparticles on Their Ion Release Kinetics. *Environmental Science and Technology* **2011,** *45*, 4422-4428.

244. Yamazaki, I.; Piette, L. H., EPR spin-trapping study on the oxidizing species formed in the reaction of the ferrous ion with hydrogen-peroxide. *Journal of the American Chemical Society* **1991,** *113*, 7588-7593.

245. Halliwell, B.; Clement, M. V.; Ramalingam, J.; Long, L. H., Hydrogen peroxide. Ubiquitous in cell culture and in vivo? *Iubmb Life* **2000,** *50*, 251-257.

246. Roubaud, V.; Sankarapandi, S.; Kuppusamy, P.; Tordo, P.; Zweier, J. L., Quantitative measurement of superoxide generation and oxygen consumption from leukocytes using electron paramagnetic resonance spectroscopy. *Analytical Biochemistry* **1998,** *257*, 210-217.

247. Veal, E.; Day, A., Hydrogen Peroxide as a Signaling Molecule. *Antioxidants and Redox Signaling* **2011,** *15*, 147-151.

248. Rabai, G.; Kustin, K.; Epstein, I. R., Systematic design of chemical oscillators. 52. A systematically designed pH oscillator - the hydrogen peroxide-sulfite-ferrocyanide reaction in a continuous-flow stirred tank reactor. *Journal of the American Chemical Society* **1989,** *111*, 3870-3874.

249. McCord, J. M., Oxygen-derived free-radicals in postischemic tissue-injury. *New England Journal of Medicine* **1985,** *312*, 159-163.

250. Kraeling, M. E. K.; Bronaugh, R. L., In vitro percutaneous absorption of acrylamide and styrene from cosmetic vehicles through fuzzy rat and human skin. *Cutaneous and Ocular Toxicology* **2005,** *24*, 65-79.

251. Zhao, H. T.; Joseph, J.; Zhang, H.; Karoui, H.; Kalyanaraman, B., Synthesis and biochemical applications of a solid cyclic nitrone spin trap: A relatively superior trap for detecting superoxide anions and glutathiyl radicals. *Free Radical Biology and Medicine* **2001,** *31*, 599-606.

252. Singh, R. J.; Karoui, H.; Gunther, M. R.; Beckman, J. S.; Mason, R. P.; Kalyanaraman, B., Reexamination of the mechanism of hydroxyl radical adducts formed from the reaction between familial amyotrophic lateral sclerosis-associated Cu,Zn superoxide dismutase mutants and H_2O_2. *Proceedings of the National Academy of Sciences of the United States of America* **1998,** *95*, 6675-6680.

253. Gunther, M. R.; Hanna, P. M.; Mason, R. P.; Cohen, M. S., Hydroxyl radical formation from cuprous ion and hydrogen-peroxide - a spin-trapping study. *Archives of Biochemistry and Biophysics* **1995,** *316*, 515-522.

254. Zang, L. Y.; Stone, K.; Pryor, W. A., Detection of free-radicals in aqueous extracts of cigarette tar by electron-spin-resonance. *Free Radical Biology and Medicine* **1995,** *19*, 161-167.

255. Ono, Y.; Matsumura, T.; Kitajima, N.; Fukuzumi, S., Formation of superoxide ion during the decomposition of hydrogen peroxide on supported metals. *The Journal of Physical Chemistry* **1977,** *81*, 1307-1311.

256. Suresh, A. K.; Pelletier, D. A.; Wang, W.; Moon, J.-W.; Gu, B.; Mortensen, N. P.; Allison, D. P.; Joy, D. C.; Phelps, T. J.; Doktycz, M. J., Silver nanocrystallites: biofabrication using Shewanella oneidensis, and an evaluation of their comparative toxicity on gram-negative and gram-positive bacteria. *Environmental Science and Technology* **2010,** *44*, 5210-5215.

257. Lipinski, B., Hydroxyl radical and its scavengers in health and disease. *Oxidative Medicine and Cellular Longevity* **2011**, *2011*, Article ID 809696

258. Choi, O.; Cleuenger, T. E.; Deng, B.; Surampalli, R. Y.; Ross, L., Jr.; Hu, Z., Role of sulfide and ligand strength in controlling nanosilver toxicity. *Water Research* **2009,** *43*, 1879-1886.

259. Panda, B. R.; Chattopadhyay, A., Synthesis of Au nanoparticles at "all" pH by H_2O_2 reduction of $HAuCl_4$. *Journal of Nanoscience and Nanotechnology* **2007,** *7*, 1911-1915.

260. He, W.; Wu, X.; Liu, J.; Zhang, K.; Chu, W.; Feng, L.; Hu, X.; Zhou, W.; Xie, S., Formation of AgPt Alloy Nanoislands via Chemical Etching with Tunable Optical and Catalytic Properties. *Langmuir* **2010,** *26*, 4443-4448.

261. Turner, G. L. E., CRC handbook of chemistry and physics - a ready-reference book of chemical and physical data, 70th edition - Weast, R.C., Lide, D. R. *Annals of Science* **1991,** *48*, 496-497.

262. Wang, H.; Liu, H.; Liu, R.-M., Gender difference in glutathione metabolism during aging in mice. *Experimental Gerontology* **2003,** *38*, 507-517.

263. Townsend, D. M.; Tew, K. D.; Tapiero, H., The importance of glutathione in human disease. *Biomedicine and Pharmacotherapy* **2003,** *57*, 145-155.

264. Okouchi, M.; Okayama, N.; Alexander, J. S.; Aw, T. Y., NRF2-dependent glutamate-L-cysteine ligase catalytic subunit expression mediates insulin protection against hyperglycemia-induced brain endothelial cell apoptosis. *Current Neurovascular Research* **2006,** *3*, 249-261.

265. Tan, K. P.; Yang, M.; Ito, S., Activation of nuclear factor (erythroid-2 like) factor 2 by toxic bile acids provokes adaptive defense responses to enhance cell survival at the emergence of oxidative stress. *Molecular Pharmacology* **2007,** *72*, 1380-1390.

266. Zhang, C. J.; Walker, L. M.; Hinson, J. A.; Mayeux, P. R., Oxidant stress in rat liver after lipopolysaccharide administration: Effect of inducible nitric-oxide synthase inhibition. *Journal of Pharmacology and Experimental Therapeutics* **2000,** *293*, 968-972.

267. Lee, T. D.; Sadda, M. R.; Mendler, M. H.; Bottiglieri, T.; Kanel, G.; Mato, J. M.; Lu, S. C., Abnormal hepatic methionine and glutathione metabolism in patients with alcoholic hepatitis. *Alcoholism-Clinical and Experimental Research* **2004,** *28*, 173-181.

268. Lu, S. C., Regulation of hepatic glutathione synthesis: current concepts and controversies. *Faseb Journal* **1999,** *13*, 1169-1183.

269. Ball, R. O.; Courtney-Martin, G.; Pencharz, P. B., The in vivo sparing of methionine by cysteine in sulfur amino acid requirements in animal models and adult humans. *Journal of Nutrition* **2006,** *136*, 1682S-1693S.

270. Wlodek, L., Beneficial and harmful effects of thiols. *Polish Journal of Pharmacology* **2002,** *54*, 215-223.

271. Maillard, J.-Y.; Hartemann, P., Silver as an antimicrobial: Facts and gaps in knowledge. *Critical Reviews in Microbiology* **2012**.

272. de Lima, R.; Seabra, A. B.; Duran, N., Silver nanoparticles: a brief review of cytotoxicity and genotoxicity of chemically and biogenically synthesized nanoparticles. *Journal of Applied Toxicology* **2012,** *32*, 867-879.

273. Hussain, S. M.; Hess, K. L.; Gearhart, J. M.; Geiss, K. T.; Schlager, J. J., In vitro toxicity of nanoparticles in BRL 3A rat liver cells. *Toxicology in Vitro* **2005,** *19*, 975-983.

274. Chairuangkitti, P.; Lawanprasert, S.; Roytrakul, S.; Aueviriyavit, S.; Phummiratch, D.; Kulthong, K.; Chanvorachote, P.; Maniratanachote, R., Silver nanoparticles induce toxicity in A549 cells via ROS-dependent and ROS-independent pathways. *Toxicology in Vitro* **2013,** *27*, 330-338.

275. Funez, A. A.; Haza, A. I.; Mateo, D.; Morales, P., *In vitro* evaluation of silver nanoparticles on human tumoral and normal cells. *Toxicology Mechanisms and Methods* **2013,** *23*, 153-160.

276. Sellers, H.; Ulman, A.; Shnidman, Y.; Eilers, J. E., Structure and binding of alkanethiolates on gold and silver surfaces - implications for self-assembled monolayers. *Journal of the American Chemical Society* **1993,** *115*, 9389-9401.

277. Yuan, X.; Tay, Y.; Dou, X.; Luo, Z.; Leong, D. T.; Xie, J., Glutathione-Protected Silver Nanoclusters as Cysteine-Selective Fluorometric and Colorimetric Probe. *Analytical Chemistry* **2012,** *85*, 1913-1919.

278. Zhang, N.; Qu, F.; Luo, H. Q.; Li, N. B., Sensitive and selective detection of biothiols based on target-induced agglomeration of silvernanoclusters. *Biosensors and Bioelectronics* **2013,** *42*, 214-218.

279. Liu, J. Y.; Wang, Z. Y.; Liu, F. D.; Kane, A. B.; Hurt, R. H., Chemical Transformations of Nanosilver in Biological Environments. *ACS Nano* **2012,** *6*, 9887-9899.

280. Xiang, Y. U.; Wu, X. C.; Liu, D. F.; Li, Z. Y.; Chu, W. G.; Feng, L. L.; Zhang, K.; Zhou, W. Y.; Xie, S. S., Gold nanorod-seeded growth of silver nanostructures: From homogeneous coating to anisotropic coating. *Langmuir* **2008,** *24*, 3465-3470.

281. Zhou, Y. T.; He, W.; Wamer, W. G.; Hu, X.; Wu, X.; Lo, Y. M.; Yin, J. J., Enzyme-mimetic effects of gold@platinum nanorods on the antioxidant activity of ascorbic acid. *Nanoscale* **2013,** *5*, 1583-91.

282. Jaeger, C. D.; Bard, A. J., Spin trapping and electron spin resonance detection of radical intermediates in the photodecomposition of water at titanium dioxide particulate systems. *The Journal of Physical Chemistry* **1979,** *83*, 3146-3152.

283. He, W. W.; Zhou, Y. T.; Wamer, W. G.; Boudreau, M. D.; Yin, J. J., Mechanisms of the pH dependent generation of hydroxyl radicals and oxygen induced by Ag nanoparticles. *Biomaterials* **2012,** *33*, 7547-7555.

284. Dikalov, S.; Skatchkov, M.; Bassenge, E., Spin trapping of superoxide radicals and peroxynitrite by 1-hydroxy-3-carboxy-pyrrolidine and 1-hydroxy-2,2,6,6-tetramethyl-4-oxo-piperidine and the stability of corresponding nitroxyl radicals towards biological reductants. *Biochemical and Biophysical Research Communications* **1997,** *231*, 701-704.

285. Gondikas, A. P.; Morris, A.; Reinsch, B. C.; Marinakos, S. M.; Lowry, G. V.; Hsu-Kim, H., Cysteine-induced modifications of zero-valent silver nanomaterials: implications for particle surface chemistry, aggregation, dissolution, and silver speciation. *Environmental Science and Technology* **2012,** *46*, 7037-7045.

286. Molyneux, P., The use of the stable free radical diphenylpicrylhydrazyl (DPPH) for estimating antioxidant activity. *Journal of Science and Technology* **2004,** *26*, 211-219.

287. Moon, J. K.; Shibamoto, T., Antioxidant Assays for Plant and Food Components. *Journal of Agricultural and Food Chemistry* **2009,** *57*, 1655-1666.

288. Pakiari, A. H.; Jamshidi, Z., Nature and Strength of M-S Bonds (M = Au, Ag, and Cu) in Binary Alloy Gold Clusters. *Journal of Physical Chemistry A* **2010,** *114*, 9212-9221.

289. Chen, Z.; He, Y. J.; Luo, S. L.; Lin, H. L.; Chen, Y. F.; Sheng, P. T.; Li, J. X.; Chen, B. B.; Liu, C. B.; Cai, Q. Y., Label-free colorimetric assay for biological thiols based on ssDNA/silver nanoparticle system by salt amplification. *Analyst* **2010,** *135*, 1066-1069.

290. Cetojevic-Simin, D. D.; Canadanovic-Brunet, J. M.; Bogdanovic, G. M.; Djilas, S. M.; Cetkovic, G. S.; Tumbas, V. T.; Stojiljkovic, B. T., Antioxidative and Antiproliferative Activities of Different Horsetail (Equisetum arvense L.) Extracts. *Journal of Medicinal Food* **2010,** *13*, 452-459.

291. Freyaldenhoven, M. A.; Lehman, P. A.; Franz, T. J.; Lloyd, R. V.; Samokyszyn, V. M., Retinoic acid-dependent stimulation of 2,2 '-azobis(2-amidinopropane)-initiated

autoxidation of linoleic acid in sodium dodecyl sulfate micelles: A novel prooxidant effect of retinoic acid. *Chemical Research in Toxicology* **1998,** *11*, 102-110.

292. Dikalov, S.; Losik, T.; Arbiser, J. L., Honokiol is a potent scavenger of superoxide and peroxyl radicals. *Biochemical Pharmacology* **2008,** *76*, 589-596.

293. Sagrista, M. L.; Garcia, A. F.; De Madariaga, M. A.; Mora, M., Antioxidant and pro-oxidant effect of the thiolic compounds N-acetyl-L-cysteine and glutathione against free radical-induced lipid peroxidation. *Free Radical Research* **2002,** *36*, 329-340.

294. Dikalov, S.; Skatchkov, M.; Fink, B.; Bassenge, E., Quantification of superoxide radicals and peroxynitrite in vascular cells using oxidation of sterically hindered hydroxylamines and electron spin resonance. *Nitric Oxide-Biology and Chemistry* **1997,** *1*, 423-431.

295. http://biotech.about.com/od/whatisbiotechnology/a/EverydayEnzymes.htm

296. Barber, J., Photosynthetic energy conversion: natural and artificial. *Chemical Society Reviews* **2009,** *38*, 185-196.

297. Tischer, W.; Wedekind, F., Immobilized Enzymes: Methods and Applications. In *Topics in Current Chemistry*, Springer: Heidelberg, **1999**; pp 95-126.

298. Gao, L.; Zhuang, J.; Nie, L.; Zhang, J.; Zhang, Y.; Gu, N.; Wang, T.; Feng, J.; Yang, D.; Perrett, S.; Yan, X., Intrinsic peroxidase-like activity of ferromagnetic nanoparticles. *Nature Nanotechnology* **2007,** *2*, 577-583.

299. Dai, Z. H.; Liu, S. H.; Bao, J. C.; Jui, H. X., Nanostructured FeS as a Mimic Peroxidase for Biocatalysis and Biosensing. *Chemistry-a European Journal* **2009,** *15*, 4321-4326.

300. He, W. W.; Jia, H. M.; Li, X. X.; Lei, Y.; Li, J.; Zhao, H. X.; Mi, L. W.; Zhang, L. Z.; Zheng, Z., Understanding the formation of CuS concave superstructures with peroxidase-like activity. *Nanoscale* **2012,** *4*, 3501-3506.

301. Song, Y. J.; Qu, K. G.; Zhao, C.; Ren, J. S.; Qu, X. G., Graphene Oxide: Intrinsic Peroxidase Catalytic Activity and Its Application to Glucose Detection. *Advanced Materials* **2010,** *22*, 2206-2210.

302. Mu, J. S.; Wang, Y.; Zhao, M.; Zhang, L., Intrinsic peroxidase-like activity and catalase-like activity of Co3O4 nanoparticles. *Chemical Communications* **2012,** *48*, 2540-2542.

303. Song, Y. J.; Wang, X. H.; Zhao, C.; Qu, K. G.; Ren, J. S.; Qu, X. G., Label-Free Colorimetric Detection of Single Nucleotide Polymorphism by Using Single-Walled

Carbon Nanotube Intrinsic Peroxidase-Like Activity. *Chemistry-a European Journal* **2010,** *16*, 3617-3621.

304. Jv, Y.; Li, B. X.; Cao, R., Positively-charged gold nanoparticles as peroxidiase mimic and their application in hydrogen peroxide and glucose detection. *Chemical Communications* **2010,** *46*, 8017-8019.

305. Wang, X. X.; Wu, Q.; Shan, Z.; Huang, Q. M., BSA-stabilized Au clusters as peroxidase mimetics for use in xanthine detection. *Biosensors and Bioelectronics* **2011,** *26*, 3614-3619.

306. Wang, S.; Chen, W.; Liu, A. L.; Hong, L.; Deng, H. H.; Lin, X. H., Comparison of the Peroxidase-Like Activity of Unmodified, Amino-Modified, and Citrate-Capped Gold Nanoparticles. *Chemphyschem* **2012,** *13*, 1199-1204.

307. Rosi, N. L.; Mirkin, C. A., Nanostructures in biodiagnostics. *Chemical Reviews* **2005,** *105*, 1547-1562.

308. Asati, A.; Santra, S.; Kaittanis, C.; Nath, S.; Perez, J. M., Oxidase-Like Activity of Polymer-Coated Cerium Oxide Nanoparticles. *Angewandte Chemie-International Edition* **2009,** *48*, 2308-2312.

309. Dong, Y. Q.; Chi, Y. W.; Lin, X. M.; Zheng, L. Y.; Chen, L. C.; Chen, G. N., Nano-sized platinum as a mimic of uricase catalyzing the oxidative degradation of uric acid. *Physical Chemistry Chemical Physics* **2011,** *13*, 6319-6324.

310. He, W.; Wu, X.; Liu, J.; Hu, X.; Zhang, K.; Hou, S.; Zhou, W.; Xie, S., Design of AgM Bimetallic Alloy Nanostructures (M = Au, Pd, Pt) with Tunable Morphology and Peroxidase-Like Activity. *Chemistry of Materials* **2010,** *22*, 2988-2994.

311. Kim, J.; Takahashi, M.; Shimizu, T.; Shirasawa, T.; Kajita, M.; Kanayama, A.; Miyamoto, Y., Effects of a potent antioxidant, platinum nanoparticle, on the lifespan of Caenorhabditis elegans. *Mechanisms of Ageing and Development* **2008,** *129*, 322-331.

312. Hamasaki, T.; Kashiwagi, T.; Imada, T.; Nakamichi, N.; Aramaki, S.; Toh, K.; Morisawa, S.; Shimakoshi, H.; Hisaeda, Y.; Shirahata, S., Kinetic analysis of superoxide anion radical-scavenging and hydroxyl radical-scavenging activities of platinum nanoparticles. *Langmuir* **2008,** *24*, 7354-7364.

313. Watanabe, A.; Kajita, M.; Kim, J.; Kanayama, A.; Takahashi, K.; Mashino, T.; Miyamoto, Y., In vitro free radical scavenging activity of platinum nanoparticles. *Nanotechnology* **2009,** *20*. Article ID 455105

314. He, W. W.; Liu, Y.; Yuan, J. S.; Yin, J. J.; Wu, X. C.; Hu, X. N.; Zhang, K.; Liu, J. B.; Chen, C. Y.; Ji, Y. L.; Guo, Y. T., Au@Pt nanostructures as oxidase and peroxidase mimetics for use in immunoassays. *Biomaterials* **2011,** *32*, 1139-1147.

315. Rimbach, G.; VIrgilli, F., French Maritime Pin Bark: Pycnogenol. In *Handbook of Antioxidants*, Cadenas, E.; Packer, L., Eds. Marcel Dekker Inc: New York, **2002**.

316. Yin, J. J.; Lao, F.; Fu, P. P.; Wamer, W. G.; Zhao, Y. L.; Wang, P. C.; Qiu, Y.; Sun, B. Y.; Xing, G. M.; Dong, J. Q.; Liang, X. J.; Chen, C. Y., The scavenging of reactive oxygen species and the potential for cell protection by functionalized fullerene materials. *Biomaterials* **2009,** *30*, 611-621.

317. Sharma, M. K.; Buettner, G. R., Interaction of vitamin-c and vitamin-E during free-radical stress in plasma - an ESR study. *Free Radical Biology and Medicine* **1993,** *14*, 649-653.

318. Duan, S. J.; Gu, L. Z.; Wang, Y. Y.; Zheng, R. B.; Lu, J. F.; Yin, J. J.; Guli, L. W.; Ball, M., Regulation of Influenza Virus-Caused Oxidative Stress by Kegan Liyan Oral Prescription, as Monitored by Ascorbyl Radical ESR Signals. *American Journal of Chinese Medicine* **2009,** *37*, 1167-1177.

319. Chen, J. Y.; Wiley, B.; Li, Z. Y.; Campbell, D.; Saeki, F.; Cang, H.; Au, L.; Lee, J.; Li, X. D.; Xia, Y. N., Gold nanocages: Engineering their structure for biomedical applications. *Advanced Materials* **2005,** *17*, 2255-2261.

320. Halliwell, B.; Gutteridge, J. M. C., The Chemistry of Oxygen Radicals and Other Oxygen-Derived Species. In *Free Radicals in Biology and Medicine*, 2nd ed.; Oxford University Press: New York, **1989**; pp 22-81.

321. Foti, M. C.; Daquino, C.; Geraci, C., Electron-transfer reaction of cinnamic acids and their methyl esters with the DPPH center dot radical in alcoholic solutions. *Journal of Organic Chemistry* **2004,** *69*, 2309-2314.

322. Shimada, Y.; Ko, S., Ascorbic Acid and Ascorbic Acid Oxidase in Vegetables. *Chugokugakuen Journal* **2008**, *7*, 7-10.

323. Munoz, J. L.; Garcia-Molina, F.; Varon, R.; Rodriguez-Lopez, J. N.; Garcia-Canovas, F.; Tudela, J., Calculating molar absorptivities for quinones: Application to the measurement of tyrosinase activity. *Analytical Biochemistry* **2006,** *351*, 128-138.

324. No, J. K.; Soung, D. Y.; Kim, Y. J.; Shim, K. H.; Jun, Y. S.; Rhee, S. H.; Yokozawa, T.; Chung, H. Y., Inhibition of tyrosinase by green tea components. *Life Sciences* **1999,** *65*, PL241-PL246.

325. Chang, T. S., An Updated Review of Tyrosinase Inhibitors. *International Journal of Molecular Sciences* **2009,** *10*, 2440-2475.

326. Bernard, P.; Berthon, J.-Y., Resveratrol: an original mechanism on tyrosinase inhibition. *International Journal of Cosmetic Science* **2000,** *22*, 219-226.

327. Rice-Evans, C. A.; Miller, N. J.; Paganga, G., Structure-antioxidant activity relationships of flavonoids and phenolic acids. *Free Radical Biology and Medicine* **1996,** *20*, 933-956.

328. Moridani, M. Y.; Scobie, H.; Jamshidzadeh, A.; Salehi, P.; O'Brien, P. J., Caffeic acid, chlorogenic acid, and dihydrocaffeic acid metabolism: Glutathione conjugate formation. *Drug Metabolism and Disposition* **2001,** *29*, 1432-1439.

329. Chen, Z. W.; Yin, J. J.; Zhou, Y. T.; Zhang, Y.; Song, L.; Song, M. J.; Hu, S. L.; Gu, N., Dual Enzyme-like activities of iron oxide nanoparticles and their implication for diminishing cytotoxicity. *ACS Nano* **2012,** *6*, 4001-4012.

330. Hu, X.; Saran, A.; Hou, S.; Wen, T.; Ji, Y.; Liu, W.; Zhang, H.; He, W.; Yin, J.-J.; Wu, X., Au@PtAg core/shell nanorods: tailoring enzyme-like activities via alloying. *RSC Advances* **2013,** *3*, 6095-6105.

331. Haghbeen, K.; Tan, E. W., Direct spectrophotometric assay of monooxygenase and oxidase activities of mushroom tyrosinase in the presence of synthetic and natural substrates. *Analytical Biochemistry* **2003,** *312*, 23-32.

332. Albarran, G.; Boggess, W.; Rassolov, V.; Schuler, R. H., Absorption Spectrum, Mass Spectrometric Properties, and Electronic Structure of 1,2-Benzoquinone. *Journal of Physical Chemistry A* **2010,** *114*, 7470-7478.

333. Espin, J. C.; Wichers, H. J., Study of the oxidation of resveratrol catalyzed by polyphenol oxidase. Effect of polyphenol oxidase, laccase and peroxidase on the antiradical capacity of resveratrol. *Journal of Food Biochemistry* **2000,** *24*, 225-250.

334. Kuchitsu, K.; Kosaka, H.; Shiga, T.; Shibuya, N., EPR evidence for generation of hydroxyl radical triggered by n-acetylchitooligosaccharide elicitor and a protein phosphatase inhibitor in suspension-cultured rice cells. *Protoplasma* **1995,** *188*, 138-142.

335. Schuchmann, M. N.; Bothe, E.; von Sonntag, J.; von Sonntag, C., Reaction of OH radicals with benzoquinone in aqueous solutions. A pulse radiolysis study. *Journal of the Chemical Society-Perkin Transactions 2* **1998**, *4*, 791-796.